Tropical Cyclone Wind Statistical Estimation

In Regions with Rare Tropical Cyclone Occurrence

Jasper Hoek

Tropical Cyclone Wind Statistical Estimation

in Regions with Rare Tropical Cyclone Occurrence

Jasper Hoek

in partial fulfilment of the requirements for the degree of

Master of Science

in Civil Engineering

Graduation Committee

Prof.dr.ir Reniers A.J.H.M.	TU Delft
Dr.ir. Morales-Nápoles O.	TU Delft
Dr.ir. Zijlema M.	TU Delft
Dr.ir. Caires S.	Deltares
Msc.ir. van Ormondt M.	Deltares

Delft University of Technology
December 12, 2017

The work in this thesis was supported by Deltares. Their cooperation is hereby gratefully acknowledged.

Summary

Tropical Cyclones (TCs) are in many regions responsible for severe damages and a great number of casualties, resulting from the severe wind speeds, rainfall, wave heights and storm surges. The recent hurricanes Harvey and Irma are examples of the great devastation that can be caused by a single event, and of the insufficient level of preparedness that is currently present to withstand the adverse effects of such an event. Even in the U.S., which suffers relatively frequently from TCs and has an extensive track record of historical events, the consequences of Harvey were unforeseen and destructive.

Difficulties in determining extreme TC conditions, whether these are rain, wind, wave or storm surge conditions, mostly come from the fact that severe adverse effects caused by TCs are very local. This is the case because the exact track, intensity and size of the storm determine to a large extent which area is affected the most and what the consequences are for the hydraulic conditions. Small variations in any of these parameters can greatly influence the conditions at any location.

This is already the case in regions which suffer relatively often from TCs. In regions that do not suffer as regularly from TCs, data scarcity makes it even more difficult to anticipate adverse consequences. In these regions TCs are nevertheless often responsible for the most severe conditions, and the effects of such events should therefore be quantified in order be able to prepare for such conditions. For extreme cyclone wave conditions specifically, there is an additional problem of feasibly determining extreme wave conditions from cyclone wind conditions.

This research presents the Tropical Cyclone Wind Statistical Estimation Tool (TC-WiSE) to determine extreme TC wind speeds and focuses on the determination of its accuracy in data scarce regions. The tool was developed by applying it in a case study in the Gulf of Mexico (GoM). Moreover a brief qualitative assessment of the available TC wave models has been performed in order to identify an adequate method to determine extreme TC wave conditions from TC wind conditions.

The tool uses the method of Empirical Track Modelling (ETM) to generate synthetic cyclones from their genesis to termination points with 6-hourly intervals. The coordinates of the cyclone eye, the heading and forward speed are the variables used to determine the cyclone track, and the maximum sustained wind speed is used to determine the intensity of the event. Changes in these variables are sampled each time step from probability distributions constructed at each cell of a spatial grid defined around the oceanic basin where the tool is applied. This results in a set of synthetic TCs with at each time step the heading, forward speed and maximum sustained wind speed.

To determine the wind speed at an exact location, the spatial wind field around the eye is computed by applying Holland's parametric wind field model (Holland et al., 2010). In order to do this, the parameters central pressure, Radius of Maximum Winds (RMW) and Radius of 35kt Wind Speeds (R35) have to be determined based on the maximum sustained wind speed. As the currently available relations to determine these parameters were deemed too deterministic, a parametric copula and empirical joint distributions were constructed to

sample these parameters from. With these parameters as input, Holland's model is applied to compute the axisymmetric spatial wind field around the eye of each synthetic TC with 1-hour intervals. This is subsequently adjusted for asymmetry introduced by the forward motion of the events and for wind inflow angle to account for the inward spiralling nature of the cyclone winds.

5000 years of synthetic events were generated to construct extreme wind speed maps in the GoM. The tool was validated by comparing estimates for return period wind speeds up to 200 years with results obtained by applying classical Extreme Value Analysis (EVA) to the historical data. Estimates made by the tool lied within 5% of estimates based on EVA for greater return periods, easily within the 95% confidence intervals and thus deemed accurate.

Accuracy of estimations in data scarce regions are determined by reducing the historical input which was used in the case study to determine extreme wind speeds in the GoM, and comparing the estimates based on the reduced input with the estimates based on all input. Input reduction has only been applied on track and intensity data. The same parametric copula and empirical joint distributions for the determination of the central pressure and wind radii were used as in the case without input reduction. The study showed that for the accuracy of the tool in data scarce regions, observed historical events in an area much larger than the direct vicinity of 200km are very important. The tool proved accurate up to 20% when at least 10 historical events were recorded within 200km of a location, and at least 45 historical events were observed in the surrounding area with similar size to the entire GoM.

To use the tool for the determination of extreme wave conditions, applying 1-dimensional numerical wave models to a large number of generated TCs would be the preferable option if there is significant computational capacity available. In case computational power is a bottleneck, empirical cyclone wave models would serve as the next best option in order to determine extreme wave conditions. These methods have however not been tested in this study and therefore this statement does come with uncertainty.

Acknowledgements

This research is done as a graduation thesis for the Master of Science in Hydraulic Engineering at the faculty of Civil Engineering at the Delft University of Technology. This research was supported by Deltares and their cooperation is gratefully acknowledged. I would like to thank my committee for their support and advice throughout my thesis. Thank you, Ad, for your interest in the subject and many critical analyses. Thank you Sofia for your continuous support and always being available for advice, for the weekly meetings and expertise on extreme value analysis and for making this thesis possible at Deltares. Thank you Oswaldo for your great enthusiasm and support, I really enjoyed our meetings. Thank you Maarten for your expertise on the subject and advice. Thank you Marcel for your critical assessments that helped me to improve my thesis.

To all of you, thank you for your help during the entire study and also for your understanding and compassion concerning my physical condition. I highly appreciate it.

Table of Contents

Nomenclature

Acronyms

AMS	Annual Maxima Series.
ATL	Atlantic Basin.
AUS	Australian basin.
BTD	Best Track Data.
CDF	Cumulative Distribution Function.
CL	Control Location.
CV	Coefficient of Variation.
ECDF	Empirical Cumulative Distribution Function.
ENP	Eastern North Pacific.
ETM	Empirical Track Model.
EVA	Extreme Value Analysis.
GEV	Generalised Extreme Value.
GoM	Gulf of Mexico.
GPD	Generalised Pareto Distribution.
IBTrACS	International Best Track Archive for Climate Stewardship.
IID	Independent and Identically Distributed.
IR	Input Reduction.
JTWC	Joint Typhoon Warning Centre.
MLE	Maximum Likelihood Estimation.
MPI	Maximum Potential Intensity.
MSE	Mean Square Error.
NA	North Atlantic.
NH	northern hemisphere.
NI	North Indian Ocean.
NMSE	Normalised Mean Square Error.
NOAA	National Oceanic and Atmospheric Administration.
PDF	Probability Density Function.
PoT	Peak over Threshold.
PWM	Probability Weighted Moments.
R100	Radius of 100kt Wind Speeds.

R35 Radius of 35kt Wind Speeds.
R64 Radius of 64kt Wind Speeds.
RI Relative Intensity.
RMSE Root Mean Square Error.
RMW Radius of Maximum Winds.
RSMC Regional Specialised Meteorological Centre.
RV Return Value.

SH southern hemisphere.
SI South Indian Ocean.
SP South Pacific.
SST Sea Surface Temperature.
STM Simple Track Model.

TC Tropical Cyclone.
TCWiSE Tropical Cyclone Wind Statistical Estimation Tool.

WNP Western North Pacific.

Latin Symbols

A	Holland's location parameter.
B	Holland's pressure profile factor.
F	Cumulative Density Function.
F_{eq}	Equivalent Fetch.
H_s	Significant Wave Height.
Hc	Higher Confidence Bound.
LC	Lower Confidence Bound.
R	Radial distance from the centre of the eye (specified by subscript).
S_n	Cramér-von Mises statistic.
T	Return Period.
V	Sustained Wind Speeds (specified by subscript).
a_x	Empirical coefficient.
b_x	Empirical coefficient.
c	Forward Speed.
f	Coriolis parameter.
g	Gravitational Acceleration.
p	Pressure (specified by subscript).
t	Time step.

Greek Symbols

Δ	Change in subsequent parameter.
Λ	Longitude.
Ω	Rotation rate of the earth.
Ψ	Latitude.
Θ	Gumbel shape parameter.
α_x	Empirical coefficient.
β_x	Empirical coefficient.
κ	Shape parameter for the Generalised Pareto Distribution.
λ	Number of events per year.
ρ	Correlation Coefficient.
ρ_a	Density of air.
θ	Heading.
ξ	Threshold parameter for the Generalised Pareto Distribution.

1 Introduction

This research presents the Tropical Cyclone Wind Statistical Estimation Tool (TCWiSE) to determine extreme Tropical Cyclone wind speeds, with the focus on regions with rare Tropical Cyclone occurrence. In this chapter the motivation for this research is given by describing the current situation and subsequently stating the problem definition accompanied by the research objective and research questions of this study. Finally, the approach to achieve this objective is outlined together with the structure of the remainder of this report.

1.1 Background

Tropical Cyclones (TCs) are natural disasters responsible for a great amount of devastation world wide. The past two centuries an average of 11,800 deaths per year were attributed to cyclones and TCs have caused an estimated 1.9 million deaths worldwide between 1980 and 2000 (Nicholls et al., 1995; United Nations Development Programme, 2004). As recent as the end of August and the beginning of September 2017, hurricane Harvey [1] made landfall in Texas and set a new record for rain associated with a TC in the continental United states. Within a week time at least 154 cm precipitation, of which 60 cm in a single day, fell in the area of Houston, which was hit hardest by Harvey (Samenow, 2017; Washington Post, 2017). To put that into perspective, the yearly rainfall in Houston varied from 60 cm to 180 cm in the period 2000 to 2016 (National Weather Service, 2017). Thus in a single day during Hurricane Harvey, there was as much precipitation as in entire years.

Besides being responsible for vast amounts of precipitation, TCs are accompanied by large pressure drops and strong winds responsible for severe storm surges and extreme wave conditions. In 2005, hurricane Katrina was responsible for storm surges of 7.5 m to 8.5 m above normal tide levels along portions of the Mississippi coast, resulting in the most costly hurricane ever recorded (NOAA Hurricane Research Division, 2016a).

Depending on the geographical region, TCs can either be a regular phenomenon which occurs on average multiple times per year, or a rare event which might occur once every year or once every few years. The Gulf of Mexico (GoM) is seen as a region with regular TC occurrence with around three events entering the region yearly, and has the longest track record of TCs going back to 1851 (IBTrACS, 2014). Even with this much historical data, the effects of Harvey were underestimated, resulting in severe damages.

In regions where TCs are not as common, they can still be responsible for extreme rainfall, wind, wave and storm surge conditions if they pass by or make landfall close

[1] In the U.S. TCs are referred to as hurricanes

enough to any location of interest. Because of lack of data, either by very rare occurrence of TCs or by inadequate measurements of the events that did happen, predictions for these extreme conditions are difficult to make. Even in regions that did suffer more regularly from such events, the predictions for extreme storm conditions by means of classical Extreme Value Analysis (EVA) are inaccurate in most areas. This is caused by data scarcity which is the result of the very local effect of cyclones and of the difficulty to obtain reliable data because of the severe weather conditions. Moreover, the exact track, intensity and size of the storm determine to a large extent which area is affected the most and what the consequences are for the hydraulic conditions. Small variations in any of these parameters can greatly influence the storm surge and wave conditions at any location.

To deal with this data scarcity problem, and the fact that small changes in the track of the cyclones can cause great variability in damages, the current trend is to generate synthetic cyclones to increase the amount of data by looking at the cyclones that could possibly occur in the future. This can be done in a very simple way, for instance by arbitrarily changing a few characteristics of historical events, or in a very elaborate way, by generating a large number of synthetic cyclones with parameters sampled from probability distributions based on characteristics of historical events by means of Monte Carlo simulation. This is however but one way to deal with this issue and possibly other methods to increase the accuracy of EVA for tropical cyclone conditions can be developed as well.

Because TCs are relatively rare phenomena by itself, determination of extreme conditions for these events at any location is arbitrary, let alone regions that relatively to other cyclone prone regions have an even smaller record of historical events. These so called regions with "rare tropical cyclone occurrence" do not suffer regularly from the effects of TCs but nonetheless experience their maximum wind speeds, surge heights and wave heights when such events occur. For these areas nonetheless estimates of the extremes are required in order to design structures that can withstand such loads or to develop evacuation plans for other purposes. Locations that have never been affected by TCs, and locations far outside the tropics are not discussed in this study.

Regarding the hydraulic conditions caused by TCs, extreme storm surge levels are much more commonly investigated than extreme wave conditions. Most likely because surge levels are more often used in risk assessment studies for insurance companies. Other possible explanations for this are the larger required computational effort for modelling waves and the smaller probability of causing floods than storm surge. Nevertheless, extreme wave conditions are of utmost importance for coastal erosion studies, the design of coastal defence structures and risk assessment of the hinterlands and therefore require more investigation to develop a feasible method for extreme wave determination.

1.2 Problem Definition

There is a scarcity of TC data for the purpose of determining extreme conditions. This is caused by the very extreme but local effects of TCs, and by the fact that in some regions there is a limited track record of historical events. This could either be because of a very low occurrence rate or, because of an inadequate collection of data. For wave data this scarcity is even more severe, as wave measurements are usually missing because during such extreme conditions, the equipment is damaged or measurements are inaccurate, whereas

other characteristics from cyclones, such as the pressure drop and coordinates of the eye, can still be measured relatively accurately. Therefore it can be concluded that extreme TC wave conditions can only be determined based on data of TC wind fields, both in regions that suffer regularly or rarely from TC occurrence.

Even when little historical data is present, a prediction for extremes is nevertheless required, even if the estimates come with great uncertainty. Having no prediction at all is unacceptable, whereas a prediction with large uncertainty, of which the uncertainty is known, can still be used for design purposes. Currently, there is the need for a tool that could be applied in data scarce regions for which the uncertainty is known for a given amount of input.

It can therefore be stated that there is lack of a tool that determines extreme wind conditions in regions with rare Tropical Cyclone occurrence, for which the accuracy is quantified for the amount input. Moreover, a guideline for what kind of wave model to apply, in order to feasibly determine extreme Tropical Cyclone wave conditions from Tropical Cyclone wind conditions is absent. This thesis aims at filling in this gap.

1.3 Research Objective and Questions

The problem definition and background information have led to the following research objective:

> *"Develop a reliable tool to determine extreme Tropical Cyclone wind speeds with special attention to regions with rare Tropical Cyclone occurrence, and to give recommendations on how the associated extreme wave conditions could be computed"*

In this study regions with rare TC occurrence are defined by having a historical record of less than 10 TCs in the direct vicinity of a location which in this study is taken as 200km, not including locations that have never been affected by TCs in the region, or locations far outside the tropics. In this case all historical cyclone events that have reached 1-minute averaged wind speeds of over 50 kt at least once during their lifetime, instead of the normal threshold of 64 kt, are used as historical events to increase the available amount of data.

The tool which is the objective of this study is called Tropical Cyclone Wind Statistical Estimation Tool (TCWiSE). To develop TCWiSE the following research questions have been formulated and should be answered:

1. What is an adequate method according to literature to:
   - **a.** deal with Tropical Cyclone data scarcity for the purpose of determining extreme wind conditions?
   - **b.** determine extreme Tropical Cyclone wave conditions from Tropical Cyclone wind data?
2. What are the main characteristics of TCWiSE?
   - **a.** How accurate, in terms of % of the error, are wind speed estimates for the 100 year return period in regions with rare cyclone occurrence?
   - **b.** What is the minimum amount of historical cyclone data that is required in order to make estimations of the 100 year extreme wind speed with a maximum error of 20%?
   - **c.** Is there a direct relation between the number of historical occurrences within 200km and the accuracy of the estimations for the 100 year return period?
   - **d.** Is there spatial variability in the accuracy of the estimation?

To answer these questions, first a literature study will be performed in which the first research question and sub-questions will be answered, and subsequently a case study is performed to test the developed tool and to answer the second research question and sub questions.

1.4 Study Approach

The first step is to perform a literature study in order to discover the existing methods to determine extreme TC conditions. Difference is made between methods to deal with TC data scarcity to determine TC wind speeds, and methods to feasibly determine wave conditions from these wind fields. In this study the developed tool for determining cyclone wind speeds is elaborated and tested for accuracy in regions with rare cyclone occurrence. An approach to determine wave fields from the computed wind fields is recommended which provides a feasible solution for determining extreme wave conditions, but applying and testing the wave model does not lie within the scope of this study. Instead of developing an entirely new method, the existing methods are combined and improved on several aspects. The focus is on developing a tool which is both feasible and reliable, for which the limitations and accuracy are known in data scarce regions, together with a quantification of the uncertainty for a given amount of input.

In order to test TCWiSE, it was applied in a case study in which extreme TC wind speeds are determined in the GoM. The GoM suffers regularly (i.e. on average multiple times per year) from TCs and has had to deal with extreme rainfall, surge and wave heights caused by the significant pressure drops and wind velocities which accompany TCs. Because the area is familiar with TCs and their destructive force, many data is gathered of historical events either from measurements or re-analysis studies. Because of the relatively large amount of data compared to other areas which suffer from TCs, the GoM makes for a suitable case study location to validate whether the developed tool is accurate or not.

1.4.1 Generating Synthetic Cyclones

After the literature review, the first step is to generate a set of synthetic cyclones for the North Atlantic (NA) basin with the use of a cyclone generator tool written in the software package MATLAB (The MathWorks, Inc, 2016). An existing tool by Rego et al. (2016), which was used for a coastal hazard assessment of Mozambique (Rego & Minns, 2016), is used as a basis for the synthetic cyclone generation part of TCWiSE. The adopted tool is improved and extended on several aspects, most importantly in terms of the functionality with limited amount of data. The tool generates storms across the entire NA with data points at a 6 hour interval containing the exact location of the storm's eye together with the maximum sustained wind speed. 5000 Years of synthetic TCs are generated with the same stochastic background as the historical cyclones, thus representing a large set of possible events that could occur in the future.

1.4.2 Determining and Validating Extreme Wind Speed Maps

In the first step of TCWiSE where the synthetic TC events are generated, only the maximum sustained wind speed and coordinate of the eye are computed at each time step. The second step is to determine the spatial wind field around the eye, for which both the maximum sustained wind speed and the pressure drop at the eye are required, together with a measure of size. In TCWiSE these parameters are determined based on relations observed in the historical data with the use of a parametric copula and empirical joint distributions.

TCWiSE determines the wind fields for each synthetic storm on a spiderweb grid by using the Holland2010 (Holland et al., 2010) wind field model with an extra wind inflow angle of 22.6° as determined by J. A. Zhang and Uhlhorn (2012) and accounting for asymmetry introduced by the translatory nature of the storms by adding 0.55 times the velocity of the storm to the wind field (Lin & Chavas, 2012). The results are further analysed in MATLAB and converted to a rectangular grid around the GoM to determine maximum wind field maps for the return periods of interest.

1.4.3 Reduction Historical Data

To verify how reliable the estimations for extreme wind speeds of TCWiSE would be in areas with less historical data, a new set of extreme wind speed maps is determined, but now based on less historical data. The new sets are compared to the original set to determine a measure of accuracy for predictions in regions with less available historical cyclone data. By doing this for different portions of historical data, a relation between the uncertainty of the estimations, and the amount of available historical was sought which quantifies the reliability of the tool in data scarce regions.

1.5 Report Structure

The literature review in Chapter 2 provides a theoretical background for the models and relations used throughout this study and investigates the most feasible and reliable method to deal with data scarcity and to determine extreme cyclone wave conditions from wind conditions. In Chapter 3 the case study in which TCWiSE is applied is further elaborated, together with the study area and the data acquisition. Chapter 4 describes and validates the cyclone generator component of the tool as used in this study. Chapter 5 discusses the spatial wind field model to determine the spatial wind field around the eye, together with the determination of the pressure and wind radii which are necessary as input. Subsequently the determination of extreme wind speed maps from the spatial wind field distribution of separate TCs is treated together with the validation of the extreme wind speed maps obtained with TCWiSE. Chapter 6 reduces the historical input of the model to test the accuracy of the tool in data scarce regions and to quantify the uncertainty of the estimates for the amount of data used as input. In Chapter 7 the findings in this study are discussed together with the limitations of TCWiSE and in Chapter 8 the conclusions of this study are stated together with recommendations for further research.

2 Literature Review

This chapter describes the background information related to the various aspects of this study. The reliability and feasibility of the currently available methods to deal with Tropical Cyclone (TC) wind data scarcity, and to determine extreme TC wave conditions from TC wind data are investigated.

First some background is given on the definition and existence of TCs. The main characteristics that define a TC are discussed and the various parameters that represent these characteristics are treated. Next, the current methods to overcome TC data scarcity are discussed together with the available cyclone wave models to determine extreme TC wave conditions. Afterwards, the focus is on synthetic cyclone simulation, which is a method to deal with data scarcity with a strong statistical background, where the different aspects of cyclone generation such as the track, intensity and spatial wind field are all treated together with a brief overview of the different methods.

2.1 Tropical Cyclone Definition

Tropical cyclones are rotating low-pressure weather systems that develop over the warm waters of the oceans, typically between the latitudes of 30°N and 30°S (Malilay, 1997). Cyclonic storms with 1-minute averaged maximum wind speeds measured at the standard measuring height of 10m of over 64kt are referred to as Tropical Cyclones (Schott et al., 2012). Whether a cyclone is rotating clockwise or counter-clockwise, depends on whether the cyclone is located on the northern hemisphere (NH) or southern hemisphere (SH).

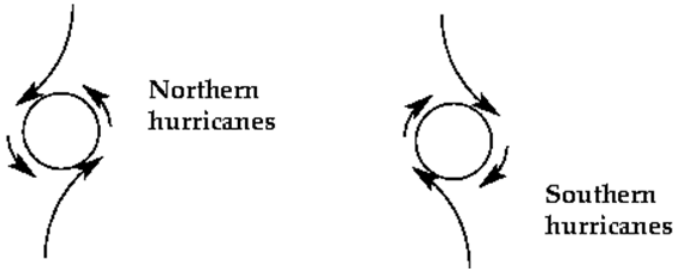

Figure 2.1 – Effect of Coriolis on tropical cyclones. Adapted from (Francis, 2011)

Because TCs are low-pressure weather systems, there is a pressure gradient between the eye and the surrounding atmosphere causing air to flow from the outside to the centre. This airflow is then diverted to the right in the NH and to the left in the SH by the Coriolis force, a force generated by the rotation of the earth. Consequently this causes cyclones in

the NH to rotate counter-clockwise and cyclones in the SH to rotate clockwise. A simple schematic of the effect of Coriolis on cyclones is given in Figure 2.1.

The strength of TCs is generally classified by the use of the Saffir-Simpson scale which divides them in categories 1 to 5 depending on intensity. The corresponding wind speeds and consequences are shown in Table 2.1. When wind speeds are below 64kt the event is referred to as a tropical storm and when wind speeds reach below 34kt one speaks of a tropical depression. A map with the tracks of the global historical TCs and their category according to the Saffir-Simpson scale is given in Figure 2.2.

Table 2.1 – Saffir-Simpson scale. Adapted from (Schott et al., 2012)

Category	Consequence	Wind speeds			
		m/s	kt	mph	km/h
1	Some damage	33-42	64-82	74-95	119-153
2	Extensive damage	43-49	83-95	96-110	154-177
3	Devastating damage	50-58	96-112	111-129	178-208
4	Catastrophic damage	58-70	113-136	130-156	209-251
5	Catastrophic damage	>70	>136	>156	>251

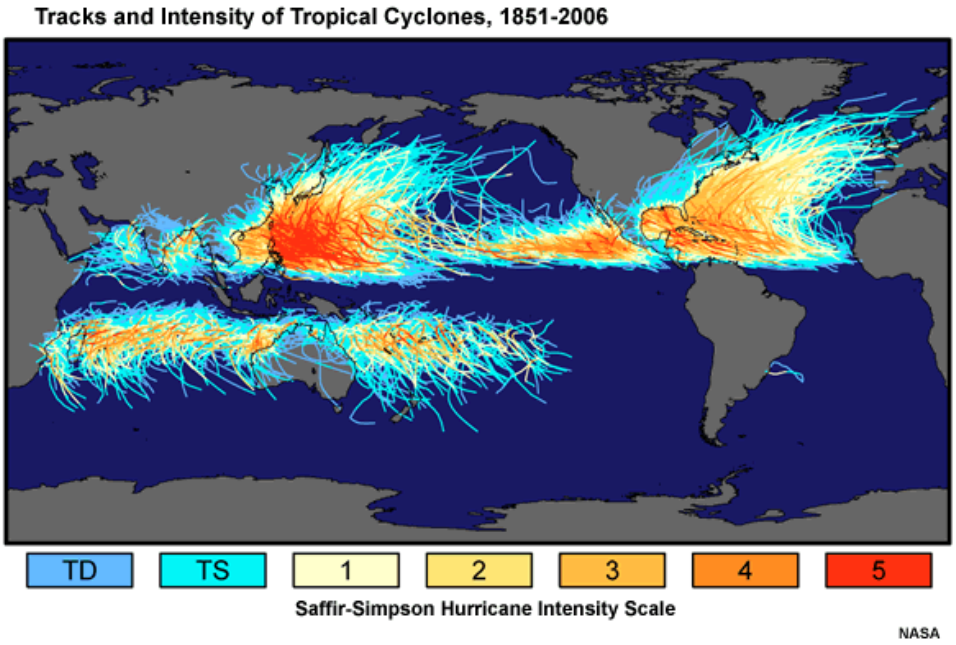

Figure 2.2 – Historic global tropical cyclone tracks colour coded based on the Saffir-Simpson scale (Laing, 2011)

2.1.1 Global Tropical Cyclone Occurrence & Nomenclature

The world's oceans can be divided into 7 basins which refer differently to TCs depending on the basin. In the Atlantic Basin (ATL), which comprises the North Atlantic (NA), the

Caribbean and the Gulf of Mexico (GoM), and in the Eastern North Pacific (ENP), TCs are referred to as "hurricanes"; In the Western North Pacific (WNP) TCs are referred to as "typhoons" and in the North Indian Ocean (NI) and South Indian Ocean (SI), Australian basin (AUS) and South Pacific (SP) they are referred to as "cyclones" (Malilay, 1997; Camargo et al., 2005). All of these terms have the same definition and therefore the scientific name Tropical Cyclone (TC) will be used throughout this document.

The yearly number of cyclones differs per basin, and also within basins TCs are more likely to occur or make landfall in specific regions. In Table 2.2 the number of yearly observed cyclones are given per basin. Nearly 70% of all cyclones occur on the NH and a large part of that in the WNP near the coast of Japan, the Philippines and China. Also the GoM and the Carribean Sea, which are part of the Atlantic basin, suffer frequently from TCs.

Table 2.2 – Yearly number of tropical storms and cyclones per basin based on data from 1981/1982-2010/2011 for northern/southern hemisphere showing the maximum and minimum number of events ever recorded in a single year together with the average. Adapted from NOAA Hurricane Research Division (2016b)

Tropical Storm or stronger (greater than 34 kt sustained winds)				Tropical Cyclone (greater than 64 kt sustained winds)			
Basin	**Most**	**Least**	**Average**	**Most**	**Least**	**Average**	**%**
Atlantic [1]	28	4	12.1	15	2	6.4	13.6
NE/Central Pacific [2]	28	8	16.6	16	3	8.9	19.0
NW Pacific	39	14	26.0	26	5	16.5	35.2
N Indian	10	2	4.8	5	0	1.5	3.2
SW Indian	14	4	9.3	8	1	5.0	10.7
Aus SE Indian	16	3	7.5	8	1	3.6	7.7
Aus SW Pacific	20	4	9.9	12	1	5.2	11.1
Globally	102	69	86	59	34	46.9	100.0

[1] Note that the data includes subtropical storms in the Atlantic basin.
[2] Note that the data includes storms and hurricanes that formed in the Central Pacific.

2.1.2 Anatomy

As mentioned, TCs are rotating storms around a central eye with very low pressure. The rotational behaviour of cyclones is caused by the Coriolis force which is caused by the rotation of the earth. Cyclones are usually around 320km in diameter and have three specific parts which can be identified namely the eye, eyewall and rainbands (Graham & Riebeek, 2006).

The eye is the inner most centre of the storm which is typically 30-60 km in diameter. This is the calmest area of the storm with moderate winds but with the lowest pressure. For very intense storm this pressure can get as low as 880 mbar or hPa which is considerably low in comparison with the usual average of around 1000 mbar. The air temperature is generally somewhat higher than in the rest of the storm and usually free of clouds (Zehnder, 2015).

The eyewall surrounds the eye and is the most destructive part of the storm where the rainfall is highest and the wind is strongest. The eyewall stretches from 15-30 km to about 30-50km from the storm centre. The winds are strongest at a height of about 300m because at lower altitudes they are slowed down by friction with the surface and at higher altitudes they are driven by a smaller pressure gradient force(Zehnder, 2015).

Rainbands are the outer most part of TC and can extend to about 160 km from the storm centre. Rainbands are secondary convective cells arranged around the centre which spiral into the centre of the storm. They can either stay stationary around the centre or spiral around it. Rotating rainbands are usually associated with wobbling of the storm track causing the cyclone to change its direction and possibly making landfall at an entirely different position than was forecast (Zehnder, 2015).

2.1.3 Tropical Cyclone Phases

There are three different phases to distinct during the lifetime of a cyclone. First, the cyclone is generated, which is called cyclone genesis, then the cyclone propagates, and finally the cyclone is terminated. The different phases are described briefly below.

2.1.3.1 Cyclone Genesis

TCs form in regions with high humidity, light winds and warm Sea Surface Temperature (SST), usually above 26.5 °C. The first sign of cyclone genesis is usually a cluster of thunder storms called a tropical disturbance, which can form in three ways all related to the convergence of surface-winds (Graham & Riebeek, 2006). The first trigger is the meeting of the NH and SH easterly trade winds which causes multiple thunderstorms every day. From time to time a cluster of thunderstorms will break away, and form a more unified storm system which can eventually turn into a TC. The second possible trigger is uplifting of warm moist air by denser cold air along a boundary between two masses of warm and cold air which could form a thunderstorm. The third trigger responsible for cyclone genesis is the African easterly wave, which is an area of disturbed weather which travels across

the Atlantic from East to West. Convergence of winds on the east of this wave triggers the formation of thunderstorms which can eventually turn into a TC (Graham & Riebeek, 2006).

Under the right conditions, the tropical disturbance can take a more organised structure which causes a pressure drop around the storm and consequentially wind blowing in a circular motion around the storm by the Coriolis force as explained earlier. The pressure drop is caused by the condensation of water vapour which releases energy into the area of the tropical disturbance. The heat pushes the air upwards which is compensated by sinking of the surrounding air which is then compressed and pushed further outwards causing a pressure drop in the centre. The more this happens, the stronger the winds and the more heat is drawn from the ocean. The ocean's heat and moisture functions as fuel for the TC and is therefore the driving force behind cyclone formation (Zehnder, 2015).

2.1.3.2 Cyclone Propagation

After genesis, a TC travels in a certain direction with a certain translation speed with a certain size and maximum wind speed. As the cyclone feeds on the energy from the ocean, it constantly changes in intensity and direction based on environmental parameters. The exact physics behind how a storm intensifies and which direction it will take is very complex. Since the Coriolis force is one of the forces which drives a cyclone, they will become weaker when getting closer to the equator as the Coriolis force approaches zero. This can clearly be seen in Figure 2.2 as there are no paths which cross the equator. The longest TC track ever observed lasted 31 days and travelled 13,000km. On the other hand, many storms have been observed which only classified as a TC for less than 12 hours (Scowcroft et al., 2015).

2.1.3.3 Cyclone Weakening and Termination

Cyclone termination, or lysis, can happen rather fast when the energy source for cyclones is depleted, for instance when the storm crosses over cold water or land. Another possibility is when the winds at high altitude disperse the heat which increases the surface pressure. Cyclones can also cause their own downfall by stirring up deeper colder water and thus removing their own energy source (Zehnder, 2015).

When cyclones move into higher latitudes they also enter cooler water and thus lose strength. This usually causes the pressure deficit to decrease and the storm to increase in size and turning into a extra-tropical cyclone. These storms are recognised by their V-shape instead of circular shape and usually dissipate within a few days (Zehnder, 2015).

2.2 Determination of Extreme Conditions for Tropical Cyclones

Non-cyclonic extreme conditions, either for waves, wind, storm surge or rainfall, are generally determined based on a classical way of performing Extreme Value Analysis (EVA), an explanation of which is given in Appendix B. This analysis can only be deemed accurate if it is based on a sufficient number of maxima. As mentioned for extreme wind or wave

conditions caused by TCs, there usually is a lack of data which causes the direct application of EVA to become inadequate. For cyclone wind speeds the problem is that there is insufficient cyclone data in general to perform an analysis on, but for waves specifically there is also the problem of going from cyclone wind data to cyclone wave data in an efficient matter which can be used to determine extreme conditions. In this section the current methods do deal with both of theses issues are discussed. From the methods to overcome wind data scarcity one is selected which will serve as a basis for this study.

2.2.1 Overcoming Data Scarcity

Worldwide the length of TC track records vary from approximately 30 years to more than 150 years. The accuracy of the track records however varies as well and has gotten significantly better over time. These track records usually include a coordinate of the eye, a maximum sustained wind speed, the pressure drop at the eye and recently also a measure for TC size. Depending on the region however, the number of events recorded in the direct vicinity of a location varies significantly, from less than a handful to over a 100. Depending on the available cyclone data and the number of historical cyclones, different methods have been applied to try and overcome this scarcity problem to be able to make an estimate for extreme conditions.

2.2.1.1 Hindcasting Wave Heights with Wave Models Based on Cyclone Wind Data

In case there is only wave data scarcity, but not TC wind data scarcity, these wind measurements can be used to generate wave heights for these historical events. If these span an extensive period and contain enough data points, they can be directly used in EVA to determine the design conditions for a specific location. Studies like this have been performed in the Gulf of Mexico and the Caribbean Sea as these are hurricane prone regions with enough measurements. Wilson (1957) studied the hurricanes in the GoM between 1900 and 1949 and computed the wave statistics and probability of occurrence of future hurricanes by means of graphical moving fetch techniques. A more modern approach is using full spectral wave models combined with hydraulic models as done by Calverley et al. (2005) who studied the wave climate in the Caribbean Sea by hindcasting the TCs from 1921 to 1999. In regions that also have wind data scarcity this method would still not provide a large enough database of wave heights to perform reliable EVA on and therefore this method is not suitable for this study.

2.2.1.2 Generating Synthetic Cyclones by Altering Historical Cyclones

Since cyclones follow a specific track, the damages they cause can be very location specific. Small changes in heading or size could cause very different wave and storm surge fields. A possibility to investigate the possible effects of future TCs is therefore to slightly alter historical cyclones by changing certain parameters. If for instance there have been 10 cyclones in the region under investigation, but all had a slightly different heading or intensity or size, one can imagine that future cyclones could possibly be a combination of these parameters or an interpolation of parameters.

Smith Warner International ltd. and Deltares (2012) applied such a technique to determine wave heights at the Virgin Islands in the Caribbean Sea. To determine the possible impact of future hurricanes, the historical observed events were altered in terms of direction, intensity and spatial offset and modelled in terms of wave height and storm surge levels. This method proved helpful for estimating possible wave heights and storm surge levels for specific locations.

A clear disadvantage of this method is the lack of insight in the probabilities of these obtained cyclones. This method only gives information about what could happen, but does not help in determining design levels for wind speeds or wave heights for specific return periods. The different combinations of parameters were selected without connecting them to how often, or to how likely it is that these combinations would actually occur. Therefore this method to overcome data scarcity is not of use for this study unless a probability would be linked to each of these combinations.

2.2.1.3 Simulate Synthetic Cyclones by Means of Monte Carlo Simulation Based on Characteristics of Historical Cyclones

The state of the art technique, and also the most elaborate one to overcome TC data scarcity, is the simulation of synthetic cyclones by means of randomly sampling TC characteristics from probability distributions constructed with the characteristics of the historical cyclone events. By doing this, the important characteristics at landfall or the propagation and intensity changes along the entire track can be modelled. The approach assumes that each cyclone is an independent realisation of the same stochastic process which allows thousands of years of synthetic cyclones to be modelled which can be used to determine the extreme TC conditions for greater return periods (James & Mason, 2005).

Various research has been done on synthetic cyclone simulation which has lead to different variations of these models, each with different level of detail or focus (Georgiou et al., 1983; Vickery et al., 2000; Emanuel et al., 2006). There are multiple components to the entire simulation. For each components multiple models or main variables can be used depending on the preference. All methods have in common firstly that they use a Monte Carlo based approach for randomly sampling different characteristics, and secondly that the distributions that are sampled from are based on historical events.

Since this approach has a very profound probabilistic basis it seems suitable for determining extreme conditions. As this is in line with the objective of this study, the idea of simulating synthetic events based on historical characteristics will be adopted for this study and in the next section the different components, characteristics and methods used in synthetic cyclone simulation are further elaborated on.

2.2.2 Cyclone Wave Models

Once extreme TC wind conditions have been determined, one would need to combine this data with a cyclone wave model in order to be able to determine extreme TC wave conditions. This model can be either an extensive numerical full spectral wave and hydrodynamic model, or a more simple parametric model. Within the numerical models a distinction can be made between fully coupled atmosphere-wave-ocean models (Chen & Curcic, 2016; Liu et al., 2011), or models that are driven by a predefined wind field (Alves et al., 2005;

Dietrich et al., 2011; Meza-Padilla et al., 2015). These models have been used in both forecasting and hindcasting studies. These three different types of models mentioned will be elaborated further.

2.2.2.1 Coupled wave-atmosphere-ocean models

These models describe the behaviour of ocean surface waves generated by TCs in great detail, and also the effect the waves have on the wind field and atmosphere. The effect of ocean currents are included as well which leads to three separate components of the model being the atmosphere model, the ocean surface wave model and the ocean circulation model (Chen & Curcic, 2016). In the model by Chen and Curcic, the atmospheric model passes the wind profile and air density to the wave model, and radiative heat fluxes and precipitation rate to the ocean circulation model. The surface wave model passes vectorial atmosphere stress to the atmosphere model and vectorial ocean stress to the ocean circulation model. The circulation model passes sea surface temperature to the atmosphere model and surface current field and water density to the wave model. In this way the three components are coupled and the behaviour of a TCs can be forecast a couple of days in advance.

As one can imagine, models like this are perfect for predicting the behaviour of a specific cyclone, but modelling this behaviour will be very computationally intensive. Using such a strategy to compute wave heights for multiple events is not realistic and therefore this method is inappropriate for determining a set of wave conditions which could be used to determine extreme conditions. Therefore this method is not regarded as a feasible method which could be used to determine extreme TC wave conditions.

2.2.2.2 Numerical models driven by predefined wind fields

In contrast to the coupled wave-atmosphere-ocean models, where wind and wave fields are computed simultaneously, for models that are driven by predefined wind fields, first the entire wind fields should be known as a function of location and time, and subsequently the hydrodynamic conditions, being wave and flow conditions, can be modelled. Therefore there will be no feedback from the waves to the wind field, or coupling with oceanic circulations. These models can be either just spectral wave models such as SWAN, WAVEWATCH and WAM, or one or more of these models coupled with flow models that can resolve the resulting currents and storm surges. If one is interested in a very high level of detail, various different flow and wave models can be coupled such as deep water wave models, steady state models and near shore wave models as done in Dietrich et al. (2011). Storm surge can have a significant effect on the waves, especially in shallower waters, and waves can also influence storm surge levels by means of wave set-up and radiation stress.

In principle this method is less computationally intensive than the fully coupled wave-atmosphere-ocean model. However, this method can be quite heavy as well. Depending on the level of detail that one is interested in, and therefore the grid size, time step and other processes that are included, the time required to run the model could vary greatly. Since a significant number of storm conditions should be modelled to define a set of wave heights that can be used to determine extreme conditions, the computational time of each condition is of importance for the feasibility of the method. Therefore a trade-off must be made between the level of detail versus the computational effort when using this model.

Most feasible would be applying 1-dimensional wave models to the computed wave models, or low resolution 2-dimensional wave models. Another option would be to reduce the number of wind conditions by making a selection of the conditions which together represent the same probability distribution as all cyclone conditions. This is however not an easy process, and most likely requires making more assumptions that will reduce the accuracy of this method. Therefore the feasibility and accuracy of this method greatly depends on the available computational power. Another option would be to use the determined extreme wind speeds and combine them with assumptions for direction and location, and subsequently use 2-dimensional wave models to determine extreme wave conditions.

2.2.2.3 Parametric cyclone wave models

In general the generation of waves can be quite well described with the use of parametric wave models, although the level of detail will never be as high as for fully spectral wave models. For TCs, the wind field can be described relatively well in simple parametric wind field models, but the wave field in TCs is more complex. For non cyclone parametric wave models, the wind is assumed to blow in a specific direction, for a specific duration over a specific length or fetch, resulting in duration or fetch limited wave generation (Holthuijsen, 2007). Because of the forward velocity of the TCs, the wind field can move together with the wave field it has generated and, in cases where the wave field remains in high wind regions of the cyclone, this can cause for a so called "Extended" or "Trapped" Fetch (Young & Vinoth, 2013). The waves that are located in this wave containment quadrant have the potential for extreme growth and yet these waves are not preceded by leading swell (Bowyer & MacAfee, 2005). Based on field measurements, numerical models and satellite data, parametric models such as Young (1988) and Bowyer and MacAfee (2005) have been developed to deal with this extended fetch, but have been limited by the available data. Young and Vinoth (2013) optimised these models by using altimeter data of 440 TCs. They noticed a bias in previous parametric models compared to the altimeter data as a function of the maximum wind speeds and translational speed of the TCs which they reduced by optimisation techniques.

These parametric cyclone wave models use the JONSWAP fetch limited growth relationship for the generation of surface waves by wind (Hasselmann et al., 1973):

$$\frac{gH_{smax}}{V_{max}^2} = 0.0016\sqrt{\frac{gF_{eq}}{V_{max}^2}} \tag{2.1}$$

Where:

g = Acceleration due to gravity
H_{smax} = Maximum significant wave height
V_{max} = Maximum wind speed
F = Equivalent fetch

In regular wind fields the fetch is defined by a stationary wind field, but because of the moving nature of cyclones, a different expression for this equivalent fetch is required. In Young (1988) the equivalent fetch is defined as follows and others use a similar expression:

$$\frac{F_{eq}}{R'} = a_1 V_{max}^2 + a_2 V_{max} + a_3 c^2 + a_4 V_{max} + a_5 c + a_6 \tag{2.2}$$

Where:

R' = Empirical function of the Radius of Maximum Winds
c = Translation Velocity or forward speed of the tropical cyclone
$a_1 - a_6$ = Empirical coefficients

As can be seen, the equivalent fetch and therefore the significant wave height depend only on the wind speed, forward velocity of the TC and the Radius of Maximum Winds (RMW). The parametric model assumes a straight cyclone track as those will result in the longest wave entrapment and is therefore in a lesser extend applicable to very curved tracks. The parametric model is also only suitable for wave determination in the direction the cyclone is travelling. As the theory behind the equivalent fetch is based on the difference between the propagation speed of the cyclone and the group velocity of the waves it is generating, this method only applies to waves propagating in the same direction as the cyclone. In many cases TCs will not make landfall at or travel exactly in the direction of the location of interest and therefore determining the wave height at specific locations will remain dubious. However, since wave-growth is by far the greatest if the waves remain in the wave containment quadrant, and waves that travel perpendicular to the cyclone propagation speed will only have limited wave-growth, the parametric model seems appropriate for determining extreme wave conditions.

A great advantage of using parametric models is the fact that even for computing the wave heights for a database of 5000 years of cyclone events, the computational time will be relatively short as no complicated numerical models are involved. Therefore a parametric model could serve as a feasible option for determining extreme wave heights.

2.3 Synthetic Cyclone Simulation

This section elaborates on the method of synthetic cyclone simulation which was selected as an adequate method to deal with TC data scarcity for the purpose of determining extreme cyclone conditions in this study. Synthetic cyclone simulation is currently the state of the art in dealing with data scarcity of TCs. Many research has been done on the method by various institutes and researchers. The method is widely used in the U.S. banking and insurance industries to determine insurance rates based on simulated extreme wind speed maps. The wind speed maps are also used to drive storm surge models to set flood insurance rates and minimal floor levels along the hurricane prone U.S. coast (Vickery et al., 2009). In this section the different techniques and methods will be explained as well as the different variables that are used to represent the storm characteristics, together with the different phases or components of the modelling process.

2.3.1 Available simulation methods

Basically there are two different types of models available for synthetic cyclone generation. These are the Simple Track Model (STM) and the Empirical Track Model (ETM). Within these models various researchers have come up with different approaches which could be used. Both types will be discussed briefly below including some of the variations used within the models.

2.3.1.1 Simple Track Modelling

STM was the first method developed to generate synthetic cyclones. The basic idea is that specific cyclone characteristics such as wind speed, central pressure deficit, RMW, heading, translation speed, coast crossing position or distance closest to the coast and others are obtained and used to construct probability distributions. Next, these characteristics are sampled from their distributions by means of Monte Carlo Simulation and passed along a straight track in the sampled heading, while keeping all other sampled parameters constant. Once the cyclone makes landfall the intensity decays using a filling rate model (Vickery et al., 2009).

The method was first developed by Russel (1968) and subsequently elaborated by among others Tryggvason et al. (1976), Batts et al. (1980), Georgiou (1983) and Vickery and Twisdale (1995). The models mostly differ in the physical models used such as the filling and wind field models and in probability distributions fitted to the characteristics. Other differences were related to whether either central pressure deficit or maximum sustained wind speeds were used to quantify the intensity of the cyclones.

The method is very site specific as all parameters are gathered for a single area or coastline. Therefore it is not possible to apply the method on a larger area. Some other disadvantages as stated by Nguyen (2015) to the method are the assumption of a straight track and constant intensity until landfall. Also the fact that the different parameters are sampled independently may lead to incoherent values which would never occur in reality.

2.3.1.2 Empirical Track Modelling

ETM is in principle the evolution of STM. It uses the same technique of gathering the statistics and then sampling them by means of Monte Carlo Simulation. Instead of sampling all parameters once and assuming a straight track and constant intensity, the characteristics are sampled at the genesis location of the cyclone and subsequently modelled for its entire lifetime by randomly sampling the change in its characteristics every time step, usually six hours.

Within ETM there are two distinct types of methods for modelling both the track and intensity. These are auto-regressive models and Markov models. Auto-regressive models use a process where its output depends linearly on its previous values plus a random term. The number of previous time steps used depends on the order of the model. The first ETM as introduced by Vickery et al. (2000) was an auto-regressive model where the changes in heading and translation speed were computed based on the heading and translation speed of the previous time step, plus a random error term ε as can be seen in the equations:

$$\Delta \ln c = a_1 + a_2\Psi + a_3\Lambda + a_4 \ln c_t + a_5\theta_t + \varepsilon \tag{2.3}$$

$$\Delta \ln \theta = b_1 + b_2\Psi + b_3\Lambda + b_4 c_t + b_5\theta_t + b_6\theta_{t-1} + \varepsilon \tag{2.4}$$

Where c is the translational velocity or forward speed of the TC, θ the heading, $a_1 - a_2$ and $b_1 - b_2$ are constants specifically developed per grid cell by means of linear regression analysis, Ψ and Λ are respectively the latitude and longitude of the storm's centre and t represents the current time step. The random error term is independently sampled each time step from identical stochastic distributions based on the model residuals (S. Zhang & Nishijima, 2012).

Markov models describe a series in which the next state solely depends on the previous state, thus displaying the so called "Markov Property" (Brzeźniak & Zastawniak, 2000). Markov processes where the states are discrete are called Markov Chains. The change of both heading and translation speed are sampled from discrete Probability Density Functions (PDFs) depending on the values at the current time step and the location (Powell et al., 2005; Emanuel et al., 2006). The following probabilities are therefore necessary at each time step and grid point:

$$P(\Delta c_{t+1}|c_t, \Psi, \Lambda, S) \tag{2.5}$$
$$P(\Delta \theta_{t+1}|\theta_t, \Psi, \Lambda, S) \tag{2.6}$$

In this case S represents the time of the season but the exact parameters that the process depends on differs per model. The PDFs are constructed per spatial grid cell separated with a distance in the order of one latitudinal and longitudinal degree. The radius around these points in which data points contribute to the PDF depends on the required distance to obtain a robust PDF required for the quantity of interest.

2.3.2 Components

In the case of ETM, several components can be distinguished which together form the simulation of a synthetic TCs. For STM these components are of less importance as all characteristics are kept constant. These components are all treated below.

2.3.2.1 Track

Naturally the track of a TC is extremely important in determining the effects it will have at a specific location. Whether the eye passes straight over a city or a bay or passes 500km away from it will make all the difference with respect to damage and casualties suffered. The track consists of its genesis location, the track propagation during its lifetime and the termination point.

As explained earlier, there are multiple triggers for TCs to form and depending on the exact geographical location, cyclone genesis will be likely or not. This likeliness is specified in spatially-varying PDFs which represent the annual occurrence at a specific location, usually a grid cell of a specific shape (rectangular, triangular, hexagonal, etc.) with a length in the order of one to five degrees of latitude (one degree equals approximately 111km) (Nguyen, 2015).

The track propagation of a TC is mainly defined by the heading (θ) and the translation velocity (c) of the eye. In case of STM the track can either be predefined or straight, however with ETM it is determined by randomly sampling the change in c and θ at every time step from predetermined distributions.

The termination point, if not predefined, usually depends on two factors. The first one is a minimum intensity the TC should have, in this case defined by the maximum sustained wind speed V_{max}. If the TC reduces strength and V_{max} goes below this threshold, the TC is terminated. The second one is a maximum predefined time-span the TC can exist. This is not a physical process, however based on studying actual TCs a duration can be determined which will most definitely not be exceeded. If a synthetic cyclone has

not stopped before that, it will automatically be terminated. Other studies have used different criteria for track termination such as using a PDF similar to the one for genesis or termination when searches at multiple space-time resolutions fail to provide evidence for a transition (Emanuel et al., 2006).

As mentioned, in many models all aspects of the track determination are based on spatially and time-varying PDFs. These PDFs of course have to be based on actual data of TCs. This data is gathered by many meteorological institutes around the globe which all collect cyclone data for different oceanic basins. An overview of which institute collects data in which basin is given in Figure 2.3. This data is assessed and processed into a

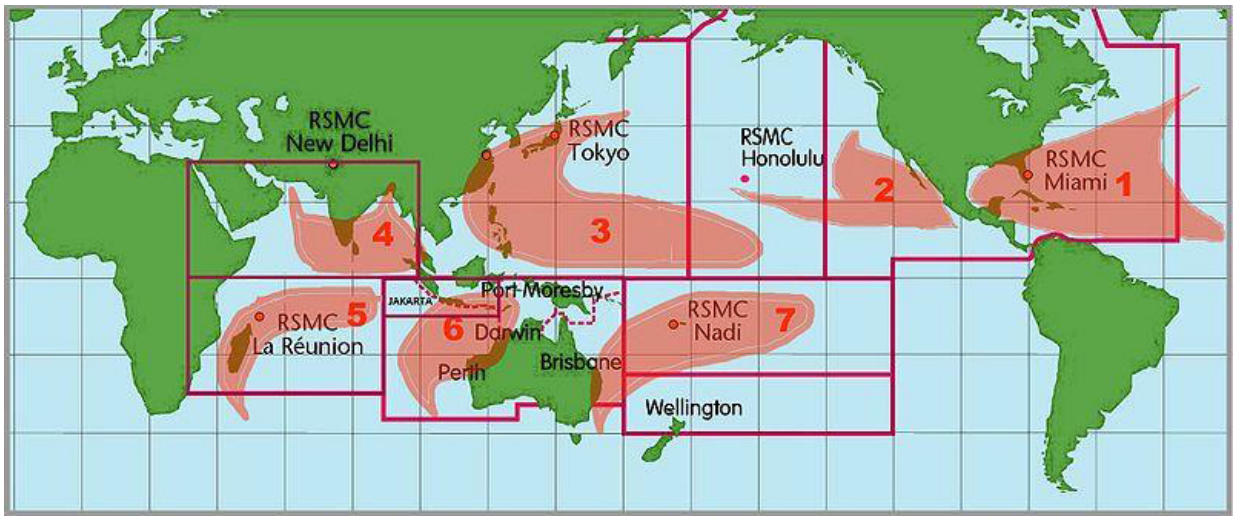

Figure 2.3 – Overview of which institute records tropical cyclone data in each basin (NOAA, 2014)

smoothened representation of the TC location and intensity during its lifetime. This "Best Track Data (BTD)" is stored in the International Best Track Archive for Climate Stewardship (IBTrACS) (2014) which is freely accessible. Both storm positions and intensities are stored in 6-hourly intervals with the variables latitude, longitude, minimum central pressure and maximum sustained surface winds. Surface winds implies wind speed at a standard 10 m elevation over clear, flat terrain. Maximum sustained wind speed data from the NA uses a 1 minute averaging whereas other institutes might use a 10 minute averaging. These values can be converted to one another by applying conversion factors, by definition lower than 1 when converting to a longer time averaging period.

2.3.2.2 Intensity

Similar to the propagation of the track, the propagation of the intensity is extremely defining for the effects of the TC. The two parameters that express the storm's intensity are the maximum sustained wind speed V_{max} and the central pressure p_c. Instead of the central pressure, also the central pressure deficit Δp is often used which is equal to an environmental pressure p_n far away from the eye, minus the central pressure. Because the number of measurements of these two parameters are usually not equal, it is wise to use only one of them. Although V_{max} gives a better representation of the damage potential, Δp gives a more reliable representation of the storm intensity for three reasons (Nguyen,

2015). Firstly, pressure measurements are more reliable because they are more easily done as the anemometers are more easily influenced by the strong winds whereas the barometers remain reliable. Second, the wind speeds in the BTD are rounded to the nearest 5kt where the pressure is rounded to the nearest hPa which is much more accurate. Thirdly, V_{max} is not consistent for a given p_c which makes p_c the only parameter to distinguish different TCs from one another. Moreover, the location of the eye and location of V_{max} do not normally coincide where the eye and p_c do. This is because the translation velocity of the TC causes the wind speed to no longer be axisymmetric around the eye, and the fact that V_{max} occurs at a certain distance from the eye, called the RMW or R_{max}, which therefore is a measurement for the storm size. The exact shape of the radial wind profile around the eye is described by spatial wind field models which will be treated further on in this section.

As explained earlier, TCs obtain their energy from warm surface waters. To define this dependency on warm surface waters as an energy supply, a relative intensity parameter was introduced by Emanuel (1988) which linked the central pressure to the maximum possible latent heat input from ocean to atmosphere and a thermodynamic efficiency proportional to the temperature difference between the sea-surface and lower stratosphere. This Relative Intensity (RI) was therefore a measurement for the current intensity compared to the Maximum Potential Intensity (MPI) expressed as a dimensionless parameter. To introduce a more physical meaning to the modelling of the central pressure in synthetic cyclones, Emanuel's parameter was first used by Darling (1991) in his methods for estimating hurricane wind speeds. A problem which is encountered when using the notion of relative intensity is that TCs that move out of the tropics, even though their potential intensity is zero, have still caused severe damage in the past (Emanuel et al., 2006).

2.3.2.3 Filling rate Model

As storms can still be devastating after making landfall, it can be interesting to model the intensity behaviour after landfall. This might be of less interest for the generation of waves and storm surge, but is still important for the overall damage caused by a cyclone. After a TC makes landfall its intensity usually decreases rather quickly as the storm fills or weakens. Filling is not the same as a decrease in strength caused by additional friction over land (Vickery et al., 2009). Typically a filling, or decay model, is an exponential function as a function of time since landfall combined with specific empirically derived decay constant in the form of:

$$\Delta p(t) = \Delta p_0 e^{-at} \tag{2.7}$$

Where $\Delta p(t)$ is the central pressure deficit as a function of time after landfall in hours, Δp_0 the central pressure deficit at landfall and a the empirically derived decay constant. The coefficient a can be modelled as a function of the pressure deficit, forward speed and size of the cyclone by:

$$a \sim \frac{c\Delta p_0}{RMW} \tag{2.8}$$

which are readily defined TC characteristics which makes it easier to apply (Vickery, 2005). When V_{max} is used the same form of decay model can be used but with V_{max} instead of Δp as in DeMaria et al. (2005). DeMaria et al. also introduced a factor F which represents the

fraction of the TC which is located above land which leads to a decay model of the form:

$$V_{max}(t) = V_b + \big(V_{max}(t-1) - V_b\big)e^{-Fa} \tag{2.9}$$

Where V_b represents a background intensity which can be maintained by a storm above land.

Georgiou (1983) was the only one to replace time dependence for distance dependence after landfall but this approach was rarely used in further studies.

2.3.2.4 Spatial Wind Field

The spatial wind field around a TC is of great importance for the determination extreme wind speeds at specific locations. BTD only contains the location of the eye and intensity of the storm, and the spatial wind field model is therefore an important aspect of cyclone modelling to determine the surrounding wind field. Several complicated and computationally intensive methods have been developed to determine the spatial wind field such as kinematic analysis wind approaches, steady-state slab Planetary Boundary Layer models, a combination of both or mesoscale weather models (Nguyen, 2015). The most common method however and also the one which is easiest to apply, is the parametric spatial wind field model. In this method modifications of the Rankine combined Vortex formulae are used, which describe the fundamental profile of cyclones where pressure drops exponentially towards the eye, and wind speed first increases exponentially until it reaches its maximum at the eyewall, and then decreases to calm conditions within the eye of the cyclone. Multiple adaptations of the parametric model have been developed but in this study only the models by Holland (2010; 1980) referred to as the Holland1980 and Holland2010 models respectively are described in Appendix A.

Holland's method causes the cyclones to be axisymmetric, which in reality is never the case. The surface wind field is in fact the sum of an axisymmetric wind field as described by Holland et al. (2010) and a background wind field of the environment which is related to the motion of the storm. This is replicated in different studies by adding the motion vector of the storm to the symmetric wind field. Lin and Chavas (2012) however found that adding the full motion vector to the wind field results on average in an incorrect wind field. Instead, a reduction of the motion vector by a factor of 0.55 and a counter-clockwise rotation of 20° should be applied first, before adding it to the symmetric wind field.

Another adaptation which should be made to the axisymmetric wind field is the addition of a wind inflow angle of 22.6° which accounts for the inward spiralling nature of TCs (J. A. Zhang & Uhlhorn, 2012) . Without accounting for this, the winds are blowing perpendicular to the storm's eye while in fact the winds are blowing slightly inwards towards the eye because of the pressure drop in the centre.

To apply the Holland1980 model one would only require the three observable quantities V_{max}, Δp and R_{max}, and for the Holland2010 model any additional radii of certain wind speeds (usually the Radius of 35kt Wind Speeds (R35), Radius of 64kt Wind Speeds (R64) or Radius of 100kt Wind Speeds (R100)) could also be used. In synthetic cyclone simulation, usually only one intensity parameter, either V_{max} or Δp, is sampled by the model at each time step. Sampling both would require conditional sampling at each time step because both are very dependent. Therefore after generating the storms with just one intensity

parameter, the other parameter still has to be determined, together with at least the RMW to determine the size, and preferably also the R35 or R64.

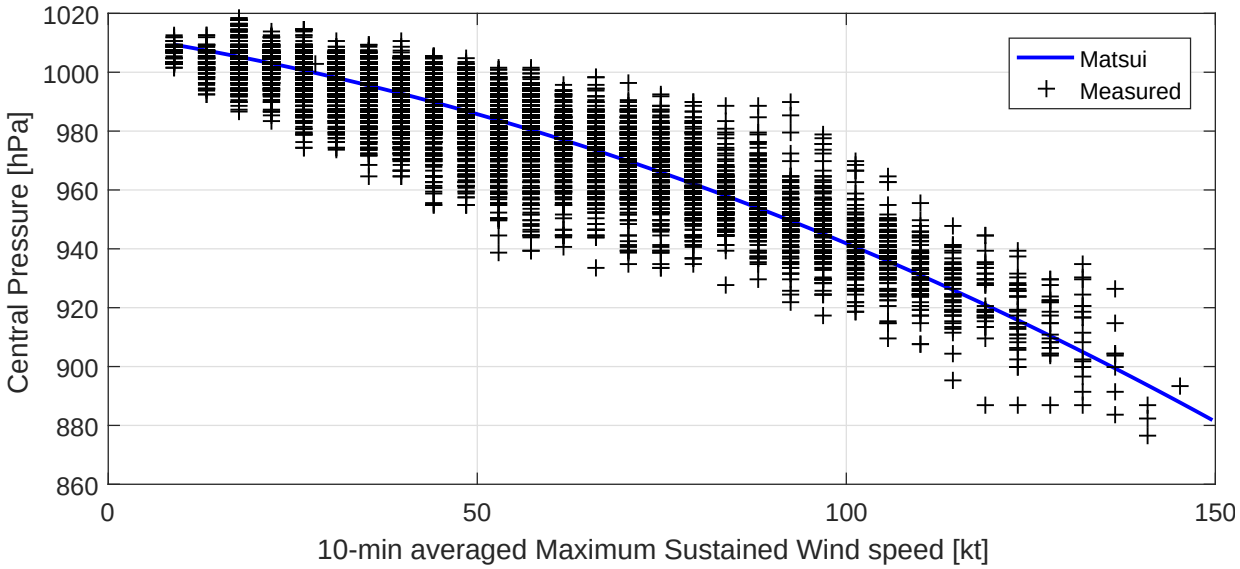

Figure 2.4 – Relation between V_{max} and p_c for the Gulf of Mexico as found by Matsui et al. (2011) plotted together with measured data

Either p_c or V_{max} are usually determined by means of an empirical relation between the two which was investigated by many different researchers. The relation between the two is also dependent on the geographic location and therefore usually separate relations are found for each oceanic basin. The relation between V_{max} and p_c as found by Matsui et al. (2011), which was determined based on TC data in the North Atlantic, is shown in Figure 2.4. As can be seen the relation follows the data relatively well, but the measured data nonetheless shows a clear spread around the relation. Using a relation like this will give a deterministic relation between the two parameters and does not allow for any other combinations of the two which are in fact possible as can be seen in the plot.

A similar relation is found between R_{max} and Δp. In most locations around the world latitude is also included in this relation, but according to Vickery and Wadhera (2008) this relation is independent of the latitude in the GoM. This relation, together with observed values is shown in Figure 2.5. As can be seen there, is a very large spread around the found relation. For large pressure drops, which usually coincide with high wind speeds, the size is determined to be very small while there have been observations in the past of much larger sizes for very strong events. Therefore applying such relations in synthetic cyclone simulation might lead to an underestimation of storm size for strong events which would in turn cause one to underestimate the wind speed at specific location for large return periods. Nonetheless many researchers are still applying these deterministic relations to determine the storm size.

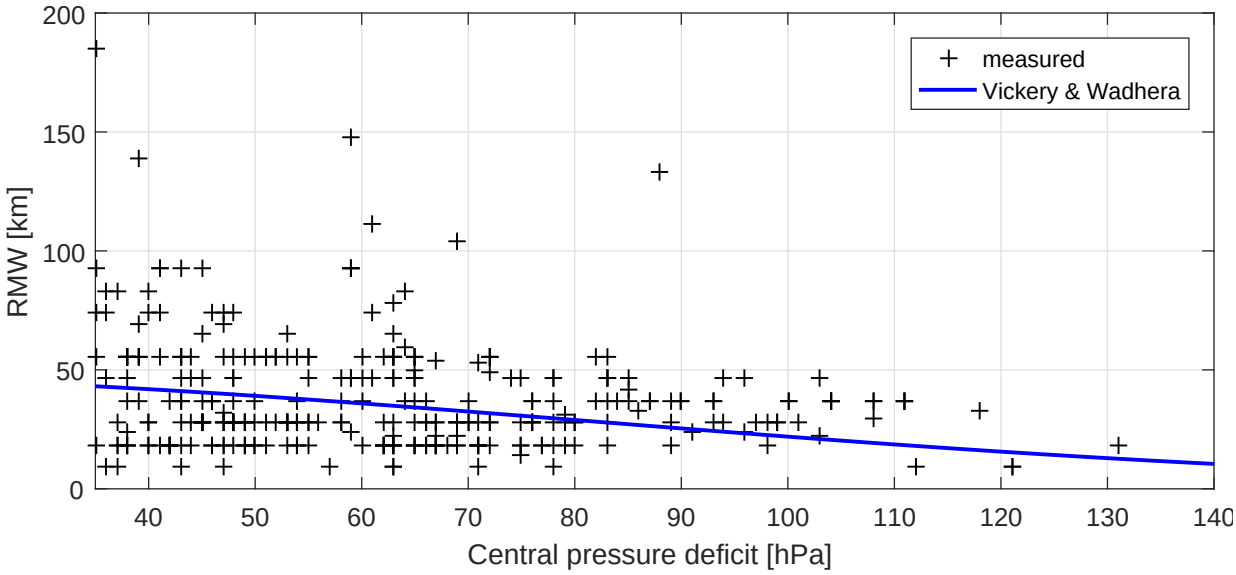

Figure 2.5 – Relation between Δp and RMW for the Gulf of Mexico as found by Vickery and Wadhera (2008) plotted together with measured data

3 Case Study Set Up

From the literature study, simulating synthetic cyclones was determined to be an adequate method to deal with Tropical Cyclone (TC) data scarcity. This method is therefore applied in the Tropical Cyclone Wind Statistical Estimation Tool (TCWiSE) and further developed and investigated by means of a case study. In this chapter the model domain is further specified together with the motivation for choosing this specific area. Also the data used for this study is further specified, together with an analysis of this data.

3.1 Study Domain

The objective of this study is to develop the tool TCWiSE to determine extreme TC wind speeds, and moreover to determine its accuracy in regions that suffer from rare cyclone occurrence where little data is available for input. Since in these regions there is very limited data to serve as a basis for an analysis, it is very difficult to say anything about the accuracy of the method which was used for this estimation. To be able to say anything about the reliability of the developed method, it is necessary to validate that predictions based on a limited amount of data, are in line with the same predictions based on a more extensive set of historical data. Because this is not possible for regions with rare cyclone occurrence, these regions are not proper areas for the development of the method. Instead, an area which has a much more extensive historical record of TCs would be more suitable as a study location. For this area it is important that there is regular cyclone occurrence and moreover that all of these events have been properly recorded.

The United States have been front runners in the field of hurricane research and have obtained a significant record of TC data over the years. Especially the United States Gulf Coast has suffered severely from hurricanes in the past which have caused a significant number of casualties and damages. For instance the Galvestone Hurricane in 1900 and the San Felipe-Okeechobee Hurricane in 1928 were responsible for 8,000 and 1836 deaths respectively in the U.S. alone (NOAA Hurricane Research Division, 2016a). Events like these gave the need for thorough investigation of hurricanes to be able to better forecast future events and to protect the inhabitants of the coastal region. After several hurricane warning services in the early 1900s and hurricane research projects in the 1950s, this has eventually lead to the existence of the National Hurricane Center. By performing many reanalysis studies on a wide range of old data and observations, they have managed to create a database of all TCs in the area from 1851 until now (McAdie et al., 2009).

Because of the combined fact that TCs at the Gulf Coast are so well recorded, and that they have a relatively frequent occurrence, the Gulf of Mexico (GoM) is chosen as the model

domain for this study. The geographical location of the study area is shown in Figure 3.1. Hurricanes affecting the GoM often originate near the west coast of the African continent and travel across the North Atlantic and the Caribbean Sea before making landfall at the United States Gulf Coast or making a steep turn heading past the east coast in the direction of the United Kingdom before losing strength and disappearing. Therefore all storms that are generated in the Atlantic basin are used as input for the purpose of this study.

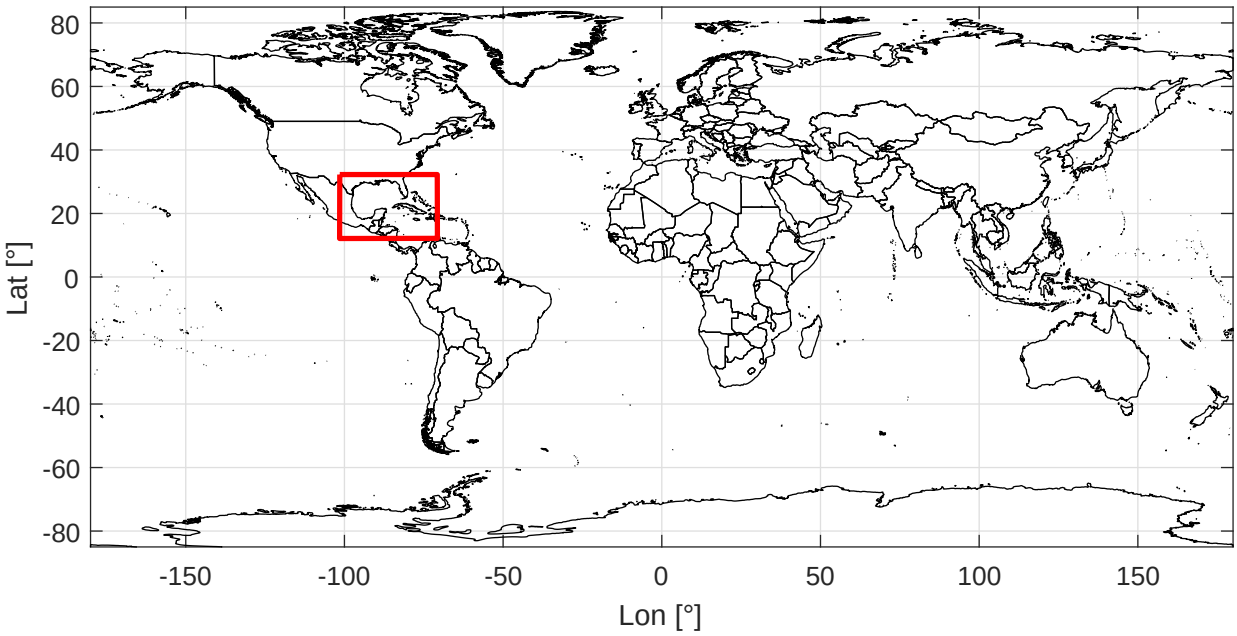

Figure 3.1 – Geographical location of the Gulf of Mexico

For the purpose of this study, only the events that have affected the GoM are selected for further research. This selection is done by taking all synthetic events that have come within a certain range of the GoM. This range is specified by a buffer zone around the area, reaching 5 nautical degrees (∼550km) seaward and 1 nautical degree land inwards (∼110km). The difference in distance from land and sea comes from the fact that once TCs make landfall, they reduce significantly in strength and moreover that extreme winds further offshore could also generate waves that affect the area of interest. The buffer zone around the GoM in which TCs are affecting the study area is shown in Figure 3.2.

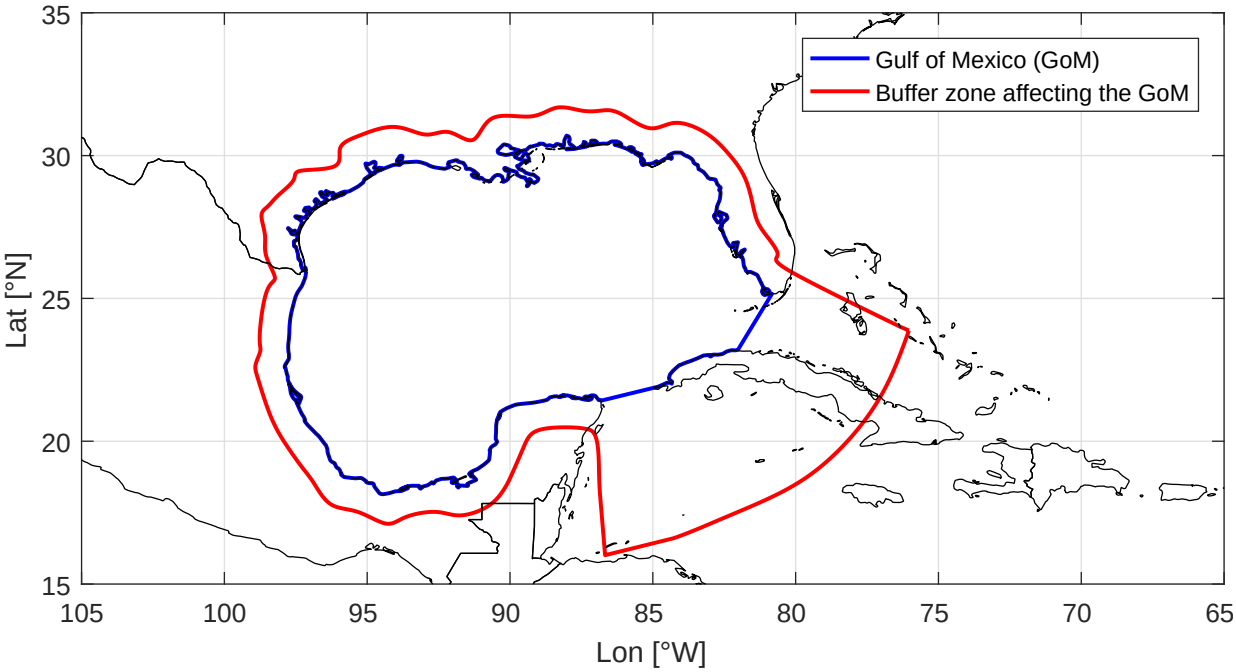

Figure 3.2 – Buffer zone around the study domain in which TCs affect the Gulf of Mexico

3.2 Study Data

TC data is gathered by many different parties world wide such as various Regional Specialised Meteorological Centres (RSMCs) and Joint Typhoon Warning Centres (JTWCs) for data at different ocean basins and some other individual meteorological offices around the world. International Best Track Archive for Climate Stewardship (IBTrACS) collects the data from all these institutes and merges them into one global best track database which contains the data for all the sources. The data can be filtered depending on which area one is interested in. This is done by only importing data that occurred in a specific oceanic basin and by only importing data from a specific source. For this study naturally all data observed in the Atlantic basin is selected and the source of the data is RSMC Miami in Florida, U.S., also known as the National Hurricane Center of the National Oceanic and Atmospheric Administration (NOAA). Hurricane data has been gathered under the HURDAT-reanalysis project which has lead to an extensive data set of historical TCs.

The data is available from as far back as 1851. For the purpose of this study however only data observed from 1886 is included. This is because from 1886 the accuracy in measurements of the maximum sustained wind speeds has increased from 10 kt to 5 kt (Landsea et al., 2014). All storms in the database that at some point have reached 1 minute averaged maximum sustained wind speeds of over 50 kt are included in this study instead of wind speeds of over 64 kt which is the official boundary for TCs. This is done to increase the amount of historical storms and therefore have a better picture of the behaviour of the storms along the track. The original data is 1 minute averaged wind speed and therefore all references made to the maximum sustained wind speed or V_{max} in this document are 1 minute averaged unless mentioned otherwise. An overview of the historical cyclone tracks used for this study and the genesis and termination points of each track is shown in Figure

3.3.

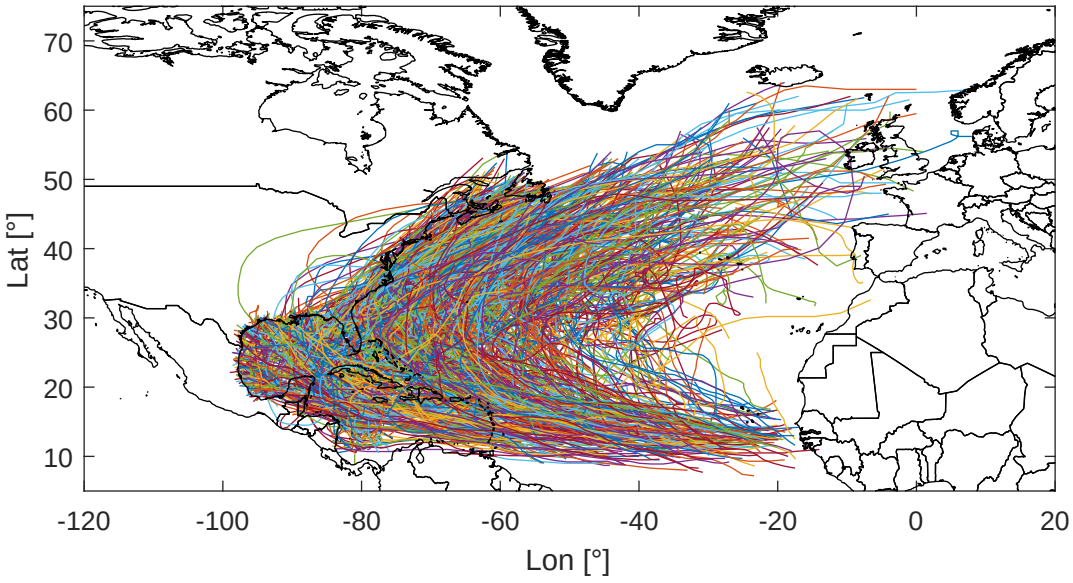

(a) Cyclone tracks

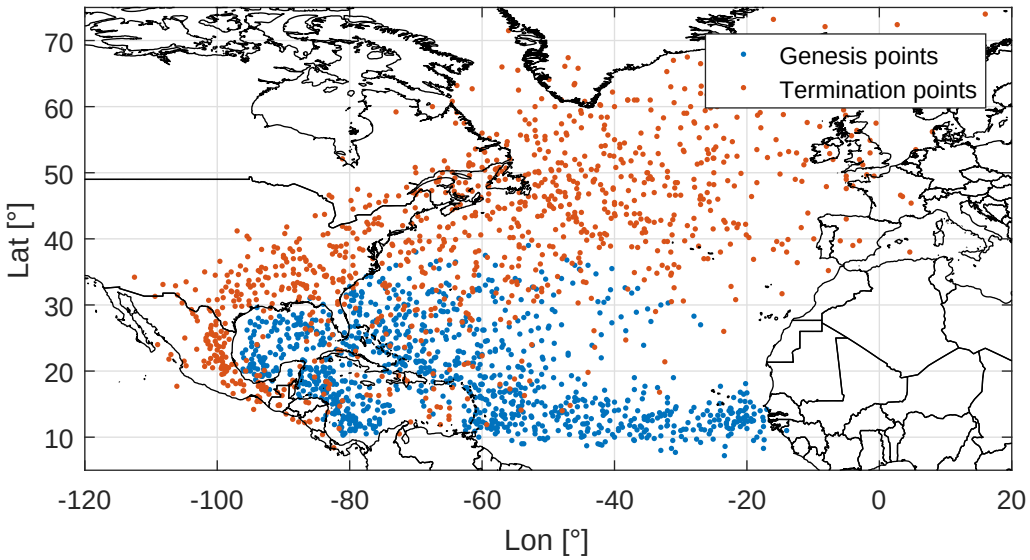

(b) Cyclone genesis and termination points

Figure 3.3 – Historic cyclone data used in this study

As can be seen from both figures, many of the cyclones affecting the GoM generate in the middle of the North Atlantic (NA) between 10° and 20° latitude and between -60° and -20 ° longitude. They generally start heading west and travel towards the GoM before heading east again. By doing this, more than a few storms cross one of the many islands surrounding the Caribbean sea. This has as a consequence that many measurements of maximum sustained winds are missing at the locations where storms cross these islands as can be seen in Figure 3.4. This causes for an incomplete time series of V_{max} which in turn will result in incorrect behaviour of synthetic cyclones in this region. As this is the case for over 30% of the historical tracks, this missing data has to be estimated. Luckily, in 97%

of these cases only one consecutive 6 hour data point is missing. Therefore it is justified to interpolate the missing data points from their previous and consecutive values. Many data points are also missing at the time around landfall in the U.S. but since in this study there is less interest in the behaviour of TCs after leaving the GoM, these missing values are less critical. These missing values are however also interpolated.

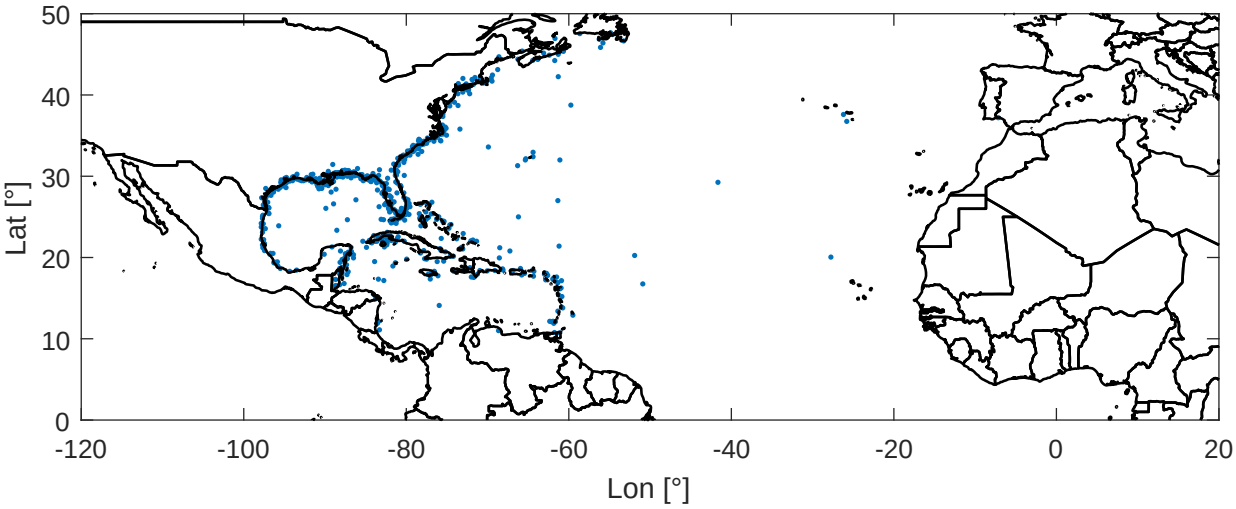

Figure 3.4 – Missing values in the wind field

High Sea Surface Temperature (SST) is the driving force behind TC genesis and without it, TCs cannot occur as was found in Section 2.1.3.1. Therefore, the obtained data from the IBTrACS database is subjected to an extra check where all genesis locations are overlain with a SST map to check whether these conditions could have lead to a TC genesis. Usually, water temperatures around 26.5 °C are seen as a minimum for TC formation, but for this purpose the boundary of 24 °C is taken as the limit below which TC genesis is seen as impossible. This has been done as the SST map used for this purpose (International Research Institute, Columbia University, 2017) is a monthly average of the month which has seen the most frequent cyclone occurrence for the basin of interest, which is September for the NA. Since it is a monthly average, it might have been possible that the local temperature at the time of genesis was higher than the average and therefore suitable for TC genesis. By taking a lower bound of 24 °C these mistakes are avoided. Figure 3.5 shows the genesis events in the data set together with a plot of the SST.

Several events which are circled in red, were observed in the data set while SST conditions could in principle not have caused for TC genesis. These are either the result of incorrect measurements, or possibly already existing events which were only tracked from this location onward. In both cases, including these genesis locations in the statistics for simulating synthetic events would result in unrealistic genesis locations. Besides genesis locations, all TC data recorded with SSTs of less than 10 °C were removed from the data set. Under these circumstances the events can no longer be considered tropical, which changes their behaviour and makes them not of interest for the purpose of this study.

After interpolating the missing values and removing events that started in low SST locations, the total number of storms observed that had at least one data point with maximum sustained winds greater than 50 kt is 1054 in 130 years of data from 1886 to

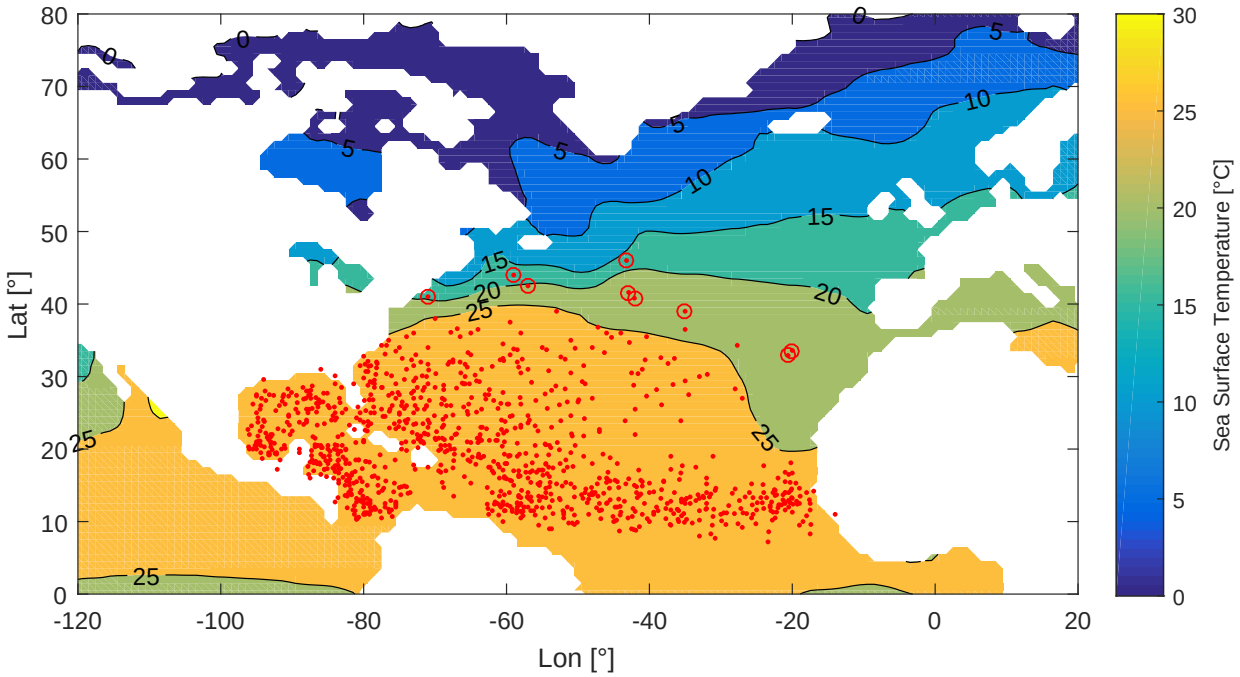

Figure 3.5 – Genesis locations overlain with a the average SST map of the month September, with a circle around the genesis events in the data set that were observed with low SST

2015. This is an average of 8.11 events per year although historically, there can be much variation in the number of storms per year as can be seen in Figure 3.6 which shows the number of occurred events per year together with the average number of events per month.

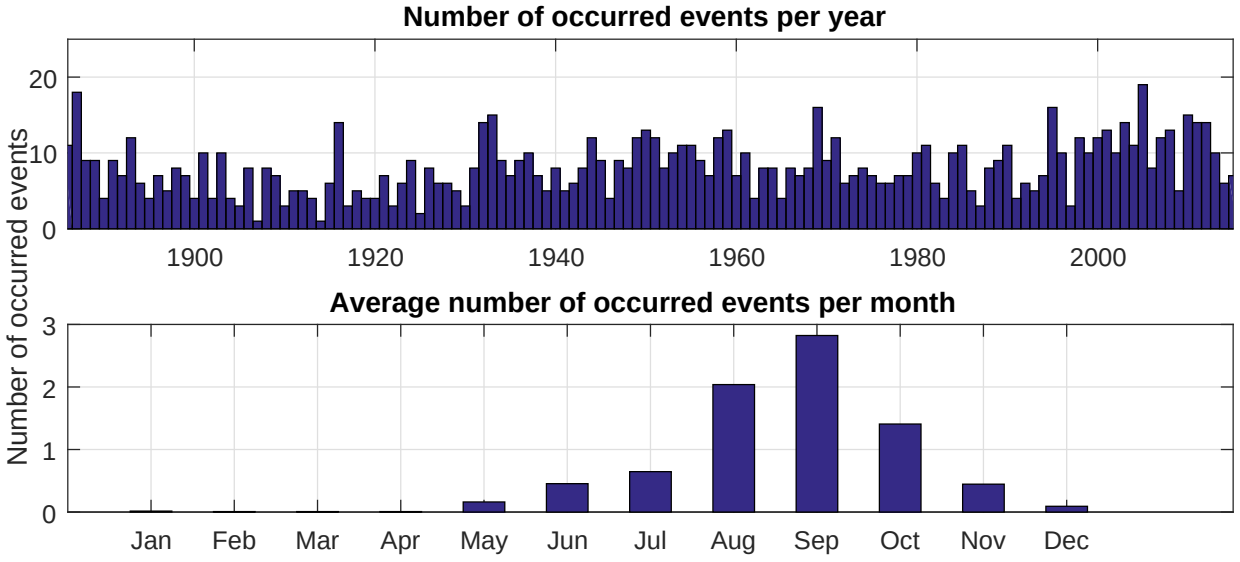

Figure 3.6 – Histograms of thr number of events per year with maximum sustained winds greater than 50 kt and of the average number of events per month

In the historical data set there have only been 2 years where only 1 event surpassed the 50 kt threshold which were 1907 and 1914. The year that contains the maximum number of events that met the 50 kt threshold is 2005 when 19 events had maximum sustained

wind speeds greater than the threshold. There is an increasing trend present in the annual occurrence but since it is pure speculation whether this trend will continue, no change in annual occurrence is accounted for during the simulation of synthetic events.

From the monthly variation in occurrence a very clear hurricane season can be observed starting in May/June and ending in November/December with a clear peak in August and September. In both months over 2 TCs are recorded on average every year. In this study the monthly occurrence data is used to determine the SST. The month with the most occurrences most likely also has the highest SST, and therefore the highest probability of TC genesis. The SST map that belongs to this month is subsequently used to determine whether the conditions for historical cyclone genesis were realistic.

4 Synthetic Track Generation

The first part of Tropical Cyclone Wind Statistical Estimation Tool (TCWiSE) is the generation of the synthetic cyclones. For this purpose use is made of a cyclone generator tool written in MATLAB (The MathWorks, Inc, 2016). An already functioning tool written by Rego et al. (2016) for a coastal flooding hazard assessment of Mozambique was used for this study and adapted in several aspects to better serve the objective of this study. Significant adaptations to the tool are highlighted with a grey text box. This chapter treats the different aspects of the cyclone track generation with special attention to the aspects that were modified. The tool is used to generate 5000 years of synthetic track data for the Gulf of Mexico (GoM). The generated tracks are analysed and compared with the historical data to verify the validity of the synthetic data set. This is done both qualitatively and quantitatively.

4.1 Description of the model

As mentioned in the literature review in Section 2.3.1 there are various methods that have been used for the generation of synthetic cyclones. The method in this study is that of the Empirical Track Model (ETM) where the changes in track and intensity are modelled by means of Monte Carlo Simulation with 6-hourly intervals. The model is set up as a Markov model where the values of the next time step solely depend on that of the previous time step similar to the methods developed by (Emanuel et al., 2006) and (Powell et al., 2005). The three main parameters that represent the synthetic events are shown in Table 4.1, together with the modelled dependency of each parameter.

Table 4.1 – Characteristic parameters of the synthetic TCs representing the track propagation and intensity, together with the modelled dependency of each parameter. $t-1$ represents the previous time step.

Parameter	Symbol	Dependency
Maximum sustained wind speed	V_{max}	$V_{max\,t-1}$
Forward speed	c	c_{t-1} & θ_{t-1}
Heading	θ	c_{t-1} & θ_{t-1}

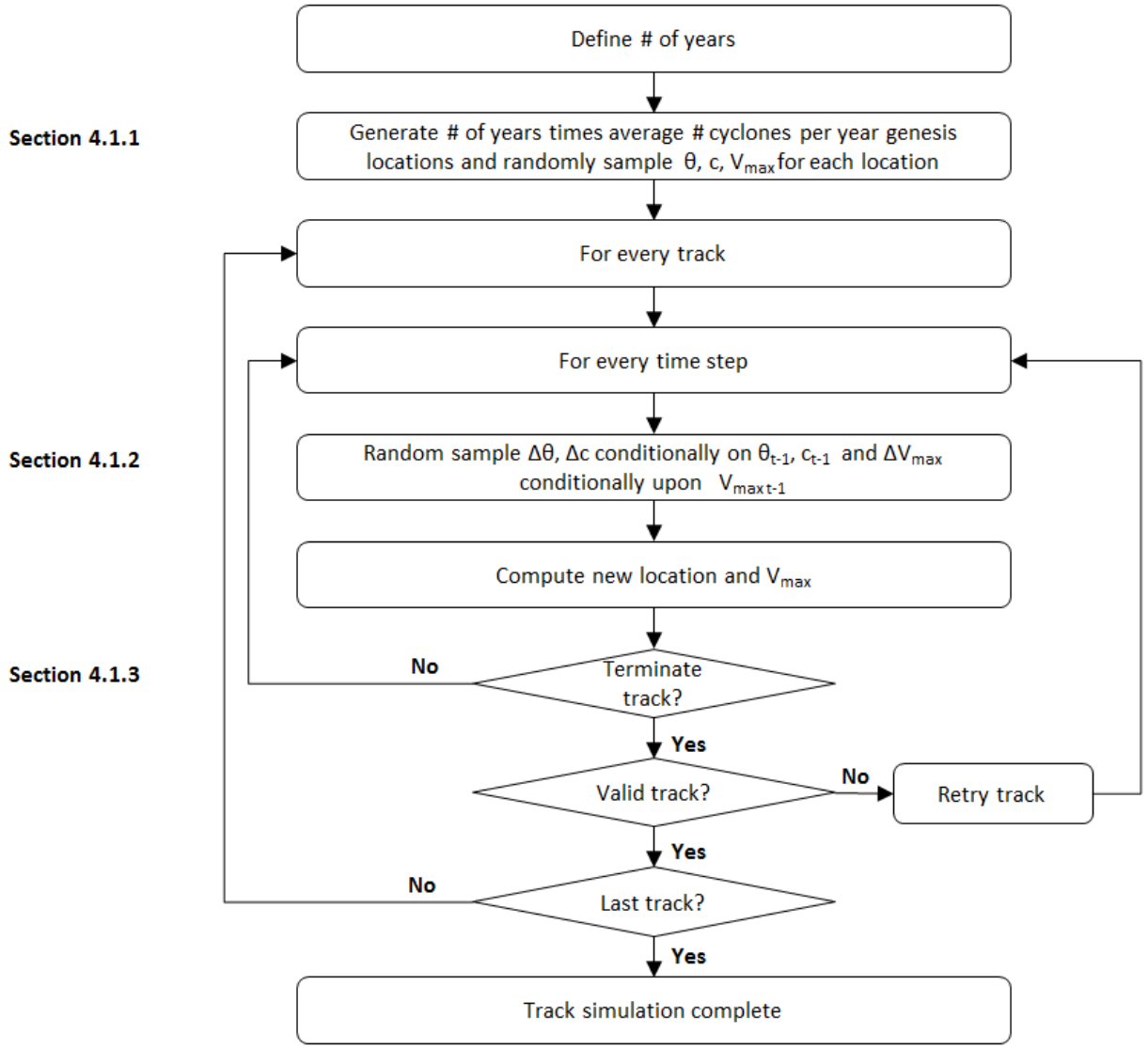

Figure 4.1 – Flowchart of the track modelling procedure

A compact flowchart of the method which is used to generate the synthetic tracks is shown in Figure 4.1. The user specifies the number of years which are to be simulated. The tool then computes the number of storms to be generated by taking the average number of storms observed per year within the oceanic basin of interest and multiplying them by the number of years. For every track its genesis location is determined after which the evolution of the track propagation and intensity is sampled on a 6 hour interval until termination. The tool which was adapted for this study uses the maximum sustained winds V_{max} as the main intensity parameter which is sampled at every time step. A more detailed description of the track initialisation, track & intensity evolution and termination is stated below.

4.1.1 Track initialisation

The track initialisation is done through randomly sampling the genesis locations for each track from a spatial Probability Density Function (PDF) constructed based on the historical

input data. Only the spatial occurrence of the genesis locations is sampled as no temporal variability of genesis locations and parameters is modelled.

The spatial PDF used to sample the genesis locations was constructed by first drawing a 1° rectangular grid around all historical events under consideration. For each grid point all genesis locations within a 200 km distance were counted and normalised with the total number of counted genesis points to obtain the genesis density at each grid point. In this way the summed density over all grid points is equal to one. The obtained PDF is plotted in Figure 4.2.

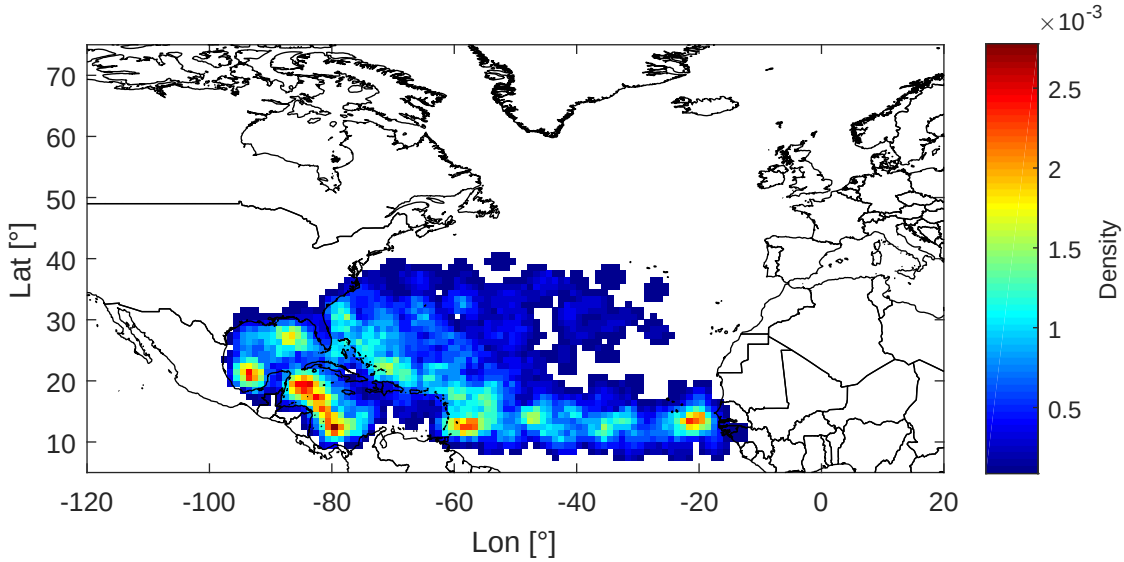

Figure 4.2 – Probability Density Function of the historical genesis locations

As was mentioned before, just off the west coast of the African continent there is a hot spot for cyclone genesis. Also just east of the Caribbean Islands and in the western part of the Caribbean many cyclones are generated. Even within the GoM there are areas that show cyclone genesis. Cyclone genesis in this study is taken as the first point of a Tropical Cyclone (TC) that is obtained in the International Best Track Archive for Climate Stewardship (IBTrACS) database, which means it is the point from where meteorological institutes started tracking the storm. Although Figure 4.2 shows some genesis density over land, genesis events sampled over land are not accepted and re-sampled until all events start over water.

After generating the genesis locations, the intensity and track propagation (heading & translation velocity) at the moment of genesis are determined. The intensity, heading and translation velocity of the TC at the genesis location are determined by randomly sampling from all the historical occurrences at genesis within the search range. This search range however is different from the one used for determining the genesis probability and will be explained in Section 4.1.2.

Sampling of the genesis parameters is done differently than in the original tool. The original tool applied the average V_{max} at genesis to all storms generated at that location, and sampled the forward speed and heading out of all historical occurrences within the search range. In the new tool this has been adapted to sampling from historical

occurrences for all three parameters, and only from occurrences at genesis instead of from all data points within the search range. This has been done to allow more variation in intensity and to account for differences in heading between storms that are crossing a location or are generated at a location.

4.1.2 Track & intensity evolution

After generation of the genesis location and parameters, the evolution of the track and intensity is modelled during it's lifetime in 6 hourly intervals. The propagation is modelled by sampling the change in direction ($\Delta\theta$), translation velocity or forward speed (Δc) and intensity (ΔV_{max}) for each time step.

4.1.2.1 Search range

The PDFs that are sampled from are constructed for each grid point based on historical data points within a specific search range. This search range is defined by a rectangular box of $1^\circ \times 1^\circ$ around the point of interest. The minimum number of data points required within the search range is 80 data points. As a rule of thumb generally 30 data points are considered as the required number of points to construct a robust PDF, but because these points are subdivided in multiple bins a higher number is required. Using a number much higher would be pointless as there are not that many total data points. If less than 80 points are located within the search range, the search range is increased until more points are found.

Originally, the tool only expanded its search range in longitudinal direction. The difference in Sea Surface Temperature (SST) which drives TCs is much larger in latitudinal direction as one goes out of the tropics. Therefore incorporating data points that lie further away in latitudinal direction might lead to discrepancies in the behaviour of the synthetic storms. This tool setting was changed nonetheless to a search range expansion in all directions, as having enough data at a single point is more important than the slight differences that might be observed when looking along the same latitude. From the initial box of $1^\circ \times 1^\circ$ the search range in all four directions is increased with 0.5° until the maxima of $8^\circ \times 10^\circ$ in longitudinal and latitudinal direction are reached or the minimum of 80 data points have been found.

4.1.2.2 Track

The change in track propagation, which includes direction and forward speed, is sampled independently from the intensity evolution. It is done in three different ways, depending on the availability of data. If there is no historical data obtained through the first method, the second option is tried, and if this still does not yield any result, the last method is tried. The three methods are stated below.

1. Both $\Delta\theta$ and Δc are sampled from PDFs constructed conditionally dependent on c_{t-1} and θ_{t-1}, where t represents the current time step and thus $t-1$ the previous time step. To construct these PDFs, θ_{t-1} has been divided into 18 equally large bins of

20° and c_{t-1} has been divided into 8 bins of 10 kt. Most of the TCs have a forward speed between 0 and 40 kt, but since there have also been recordings of faster moving TCs the bins have been extended up to 80 kt. Synthetic events with a forward speed over 80kt are seen as non-physical and therefore terminated. For each forward speed bin, only occurrences that fall directly inside that bin are used to construct the PDF. However for the heading, all occurrences that fall within 45° of the centre of that bin are used. This results in $8 \times 18 = 144$ discrete PDFs with the historical occurrences of Δc and $\Delta\theta$ conditional on c_{t-1} and θ_{t-1} per grid cell.

2. If no occurrences are found in a specific bin, the bins for Δc are made conditionally only upon c_{t-1}, and the bins for $\Delta\theta$ are made conditionally only upon θ_{t-1}. This is done to avoid having empty bins to sample from.

3. If this bin still does not contain any historical occurrences, the changes are still sampled from occurrences within this specific bin, but now from occurrences observed at all grid cells along the same latitude instead of only within the search area of the specific grid cell. This behaviour to deal with completely empty bins was incorporated in the original tool and has not been adapted as it serves as a proper solution for data sparse areas and conditions not often observed.

For each bin, a PDF is constructed by using a kernel function, which smoothens the discrete PDF obtained from the occurrences. The tool originally sampled directly from the historical occurrences. This however leads to very little possibilities in bins with only a couple of historical occurrences, especially in regions with less historical occurrences. This would lead to a bias of the synthetic tracks and therefore inaccurate estimates of extreme conditions. During simulation the changes in heading and forward speed are sampled from the continuous PDF constructed for the specific bin the current heading and forward speed are in.

4.1.2.3 Intensity

The change in maximum sustained wind speed ΔV_{max} is sampled in the same manner as $\Delta\theta$ and Δc but instead of depending on θ_{t-1} and c_{t-1}, it depends only on $V_{max\,t-1}$. $V_{max\,t-1}$ has been divided into 7 equal bins of 20 kt and 1 bin with all speeds over 140 kt resulting in 8 continuous PDFs per grid cell. Therefore for ΔV_{max} there are only two options to obtain data:

1. ΔV_{max} is sampled from the PDF of the corresponding $V_{max\,t-1}$ bin, constructed with the occurrences within the search range of the closest grid cell.

2. Similar as for the forward speed and heading, if a bin of $V_{max\,t-1}$ does not contain any occurrences at a specific grid cell, ΔV_{max} is sampled from the PDF of all occurrences in that bin along the same latitude.

In both cases the PDFs that are sampled from are constructed by means of smoothening the discrete PDF by applying Kernel density estimators.

The historical observations of V_{max} are only accurate up to 5kt and will therefore only result in values for ΔV_{max} of 5kt or a multiple of that. To prevent that from happening, all historical observations are corrected by adding a random uniform error between -2.5 kt and +2.5 kt. This removes the discreteness of the historical data which allows for more realistic changes in sustained wind speed for the synthetic events.

As has been explained in Section 2.3, the evolution of track intensity greatly depends on whether the TC is located above land or water. When the eye of the TC is located over land, in ETM, the intensity evolution is generally modelled with the use of a land decay model. These models are usually exponential depending on the time since landfall and the intensity at landfall. The generator tool which was adopted for this study however does not use such an exponential decay model. Instead it uses a constant decay of 5 kt per time step if a data point is located above land. For the purpose of this study this has been copied without adaptation. The reason behind this is because the behaviour after landfall is not of interest for this study, and any reduction in intensity which might occur when a TC comes near small islands in the Caribbean is also represented in the PDF of ΔV_{max} at that geographical location.

To check whether an event is located above land or water, a landmask with a grid of $0.05^\circ \times 0.05^\circ$ is used which determines landfall with approximately 5km accuracy. This accuracy is accepted as the affected areas of cyclones is generally much greater than 5km.

Besides intensity evolution over land or water, the generator tool incorporates a few other mechanisms that influence the intensity that are listed below.

- Physically it is not possible for TCs to cross the equator as the Coriolis force reduces to zero. However, because the synthetic storms are generated based on the statistical aspects and not the physical aspects, cyclone generator tools tend to overestimate the number of TCs approaching the equator. In the adopted generator tool the strength of the synthetic TCs is reduced by 10 kt if a TC is located within 10° of latitude and heading towards the equator. This method however results in too many TCs losing too much strength and terminating near the equator. Instead, when TCs are located within 10° of latitude and moving towards the equator, changes in track direction are only accepted if they turn the TC away from the equator. If the sampled $\Delta\theta$ will not turn them away, $\Delta\theta$ is re-sampled.

- As mentioned in the literature review in Section 2.3, there is a physical limit to the maximum intensity a TC can attain which depends on the SST. In ETM, this limit is usually modelled by modelling the Relative Intensity (RI) as a function of the Maximum Potential Intensity (MPI). In the adopted tool however no such limit is applied and only synthetic TCs that reach a V_{max} of over 180 kt are seen as being not physically possible and are regenerated. This method has been adopted for the purpose of this study and has not been altered. This is done because of a lack of MPI data and optimising every aspect of the tool lies beyond the objective of this study.

4.1.3 Track Termination

In the original tool track termination is triggered by two factors. The first one is a maximum lifetime of 30 days and the second one is when V_{max} drops below 20 kt. After a track is terminated, it is checked whether the event has attained a maximum sustained wind speed of 50 kt at least once during it's lifetime. If this is not the case, the event is rejected and regenerated. This method would only allow very weak events to be terminated. According to the historical data, events can terminate suddenly with nearly any wind speed, although generally between 20-40kt. The original behaviour of the tool would therefore drastically overestimate track duration, and therefore track occurrence.

It was therefore opted to change this behaviour by sampling at every time step whether a track should terminate or not. This was done with a method adopted from Emanuel et al. (2006), which determined the probability of termination by dividing all termination events by all non-termination events within the vicinity of a grid cell. This was done conditionally upon track duration and maximum sustained wind speed. Track duration t was divided into equal bins of less than 80 h, between 80 and 160 h, between 160 and 240 h and more than 240 h. V_{max} was divided into bins of less than 40kt and greater than 40kt. For the purpose of this study these bin widths were adopted from Fearon (2014) to avoid extra steps of calibration. A minimum of 30 points was determined sufficient for a robust termination probability but no events further away than 1100km ($\sim 10°$) from a grid cell were included. If no observation were made for a grid cell, the probability of termination is one. It is still checked whether the event has reached at least 50 kt wind speed once during it's lifetime, if not, the track is regenerated. Figure 4.3 shows a schematic of the original and adapted termination behaviour of the tool

where P_x represents the probability of termination as computed for each bin.

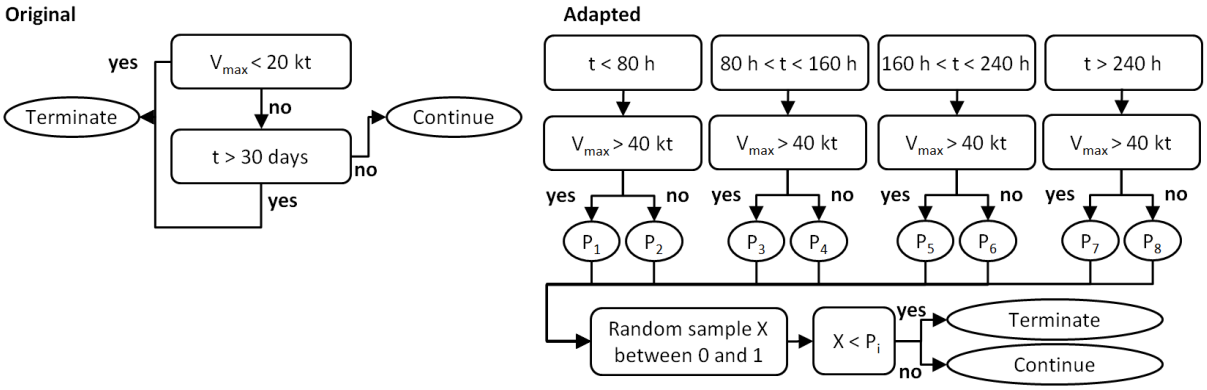

Figure 4.3 – Flowchart of the termination procedure for the original cyclone generator tool and the adapted tool as used for this study

4.2 Model results and validation

The track generator tool is validated both qualitatively and quantitatively by means of visual inspection and certain test statistics. Visual inspection is done on certain aspects such as the shape of the tracks, the locations of the genesis or termination points as well as on colour maps of average occurrence rates. Quantitative inspection is done at specific locations defined within the GoM and is done by comparing Cumulative Distribution Functions (CDFs) of certain variables for the historical and simulated data. The validation is done based on 5000 years of generated synthetic tracks which are compared with the input data spanning 130 years from 1886-2015. All historical and synthetic events that at least once during their lifetime have reached a maximum sustained wind speed of 50 kt are considered and counted as TCs in this study.

4.2.1 Qualitative validation

The first and most simple inspection which shows whether the synthetic TCs resemble the historical TCs is by looking at the propagation of the historical tracks versus that of the synthetic tracks. Figure 4.4 shows the historical tracks together with the same number of synthetic tracks randomly selected from 5000 years of synthetic tracks. The simulated tracks resemble the historical tracks quite well. One can clearly observe the same trend of tracks generated west of the African continent which travel further west towards the US and then back east again in the direction of Europe. As for this study there is no interest in cyclone propagation above land, both the synthetic and historical tracks are cut off 12 hours after landfall in both plots. They are only shown for a longer duration over land if they return back to water afterwards. About the same amount of synthetic and historical events reach the European coast and a few more synthetic events appear to reach the African continent. Overall the occurrence of TCs making landfall in Europe or Africa appears to be slightly overestimated by the synthetic events. This might have to do with

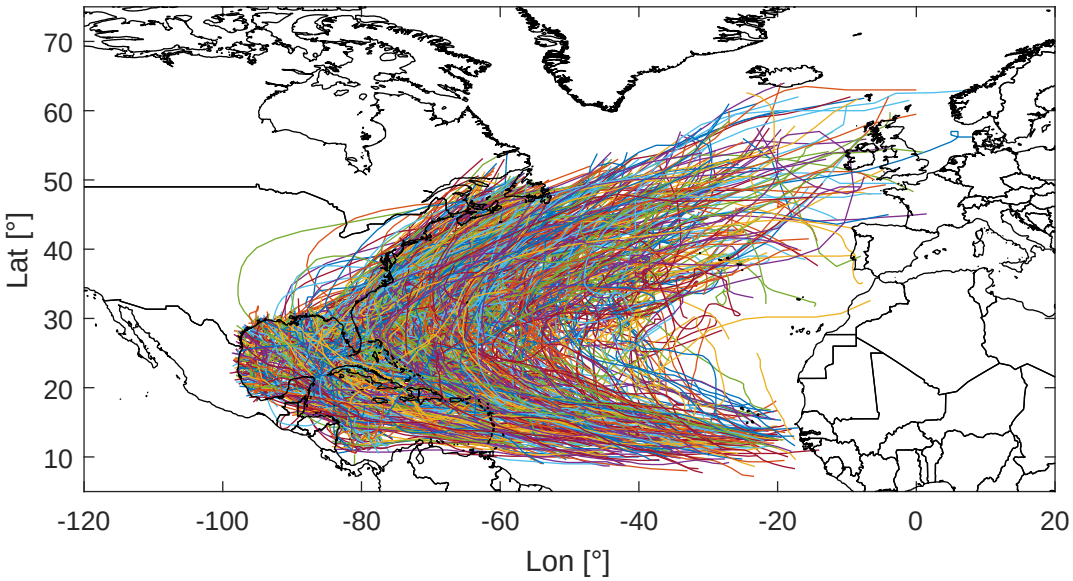

(a) Historic cyclone tracks

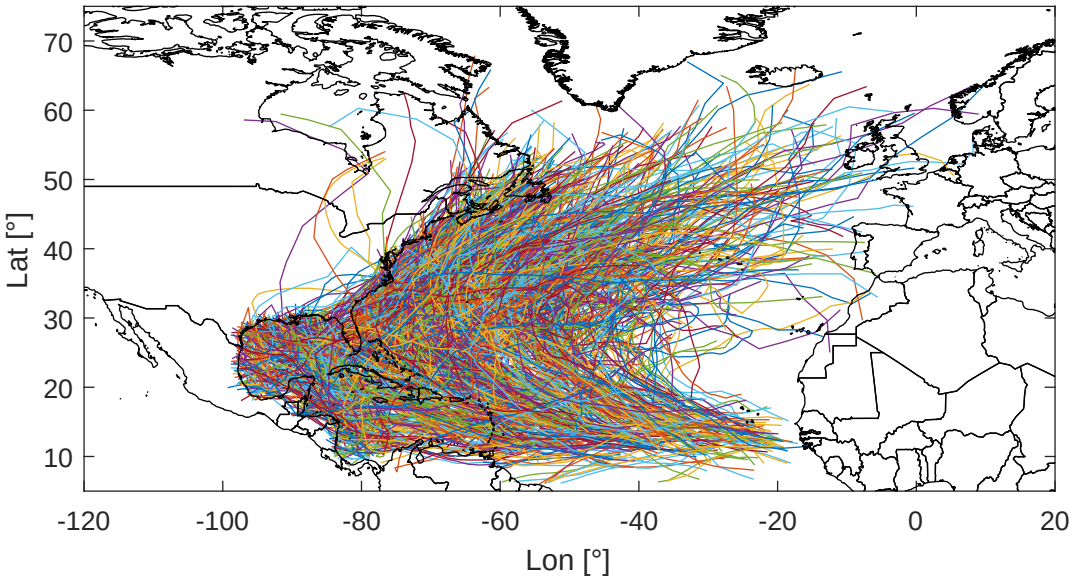

(b) Synthetic cyclone tracks

Figure 4.4 – Tracks of 130 years of historical TC data together with 130 years of randomly selected synthetic tracks

the fact that very little physical constraints are applied to the results and therefore most events that are statistically possible, even the ones that might not physically be possible, can be generated by the tool.

Another aspect that says a lot about the propagation of the tracks is a comparison of the historical and simulated genesis and termination points which are shown in Figure 4.5. These show the genesis and termination locations of the historical events together with those of the same amount of synthetic events. The simulated genesis locations match the historical genesis locations perfectly. This is as expected as the probability that an event

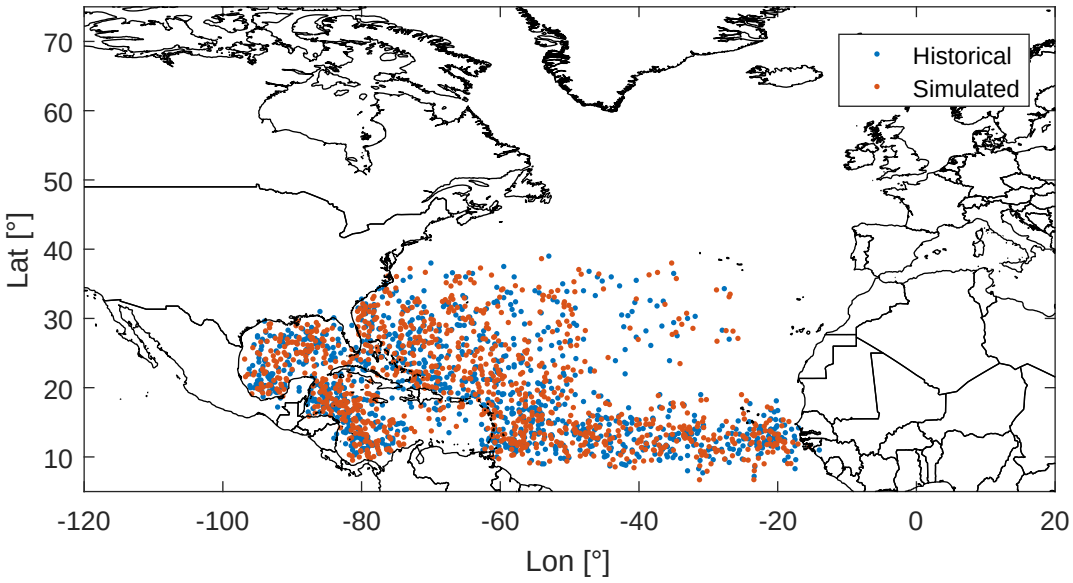

(a) Genesis locations

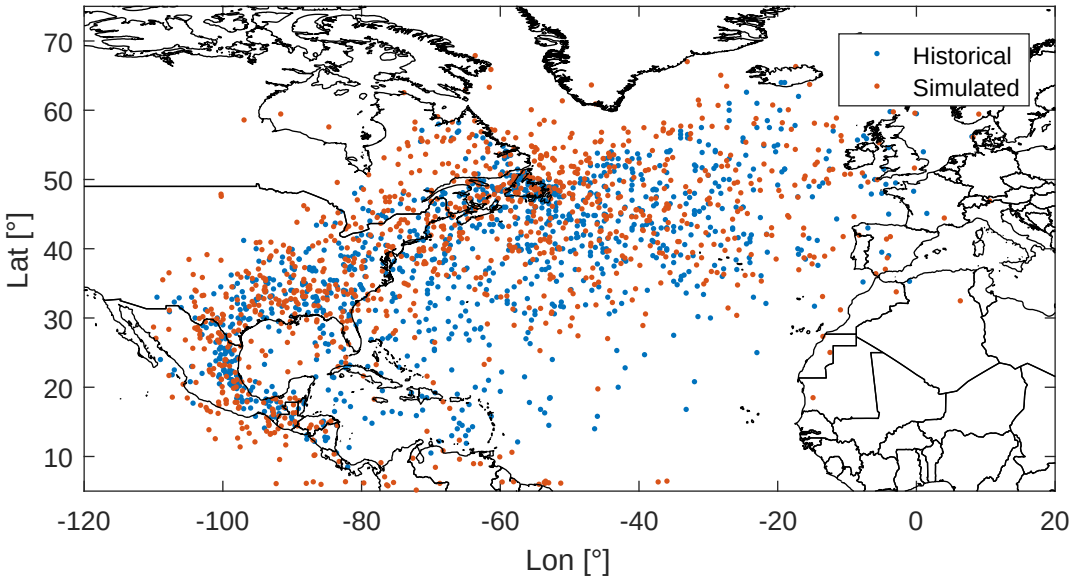

(b) Termination locations

Figure 4.5 – Genesis and termination points of 130 years of historical TC data together with 130 years of randomly selected synthetic tracks

is generated at a specific location is directly related to that of the historical events.

For termination locations however, the simulated locations differ more from the historical locations. Although the probability of termination is directly related to the historical probability of termination, the probability of synthetic events being in the vicinity of historical termination locations with the same characteristics (duration and intensity) is not directly related to historical termination locations but to the functionality of the entire tool. Because the actual number of termination events at a specific location is a function of both termination probability and the number of events subjected to this probability, the

synthetic termination locations do not match the historical termination locations as well as the synthetic and historical genesis locations match each other.

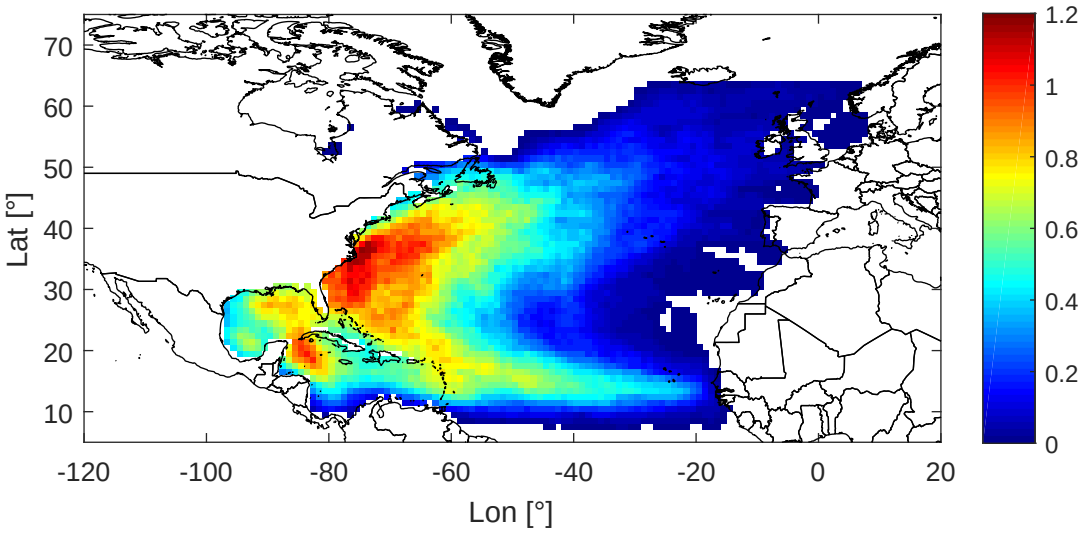

(a) Historic cyclone data

(b) Synthetic cyclone data

Figure 4.6 – Plot of average occurrence of historical and simulated TCs within 200km per grid cell for historical TCs from 1886-2015 and 5000 years of simulated events

A better measure of the functionality of the tool is the number of average observed cyclones within a specific range per grid point as shown in Figure 4.6. 200 km has been chosen for this purpose as this is generally the distance in which a location is severely affected by at TC. The plot for the synthetic storms is based on the full 5000 years of synthetic storms and therefore colour changes are much smoother than for the historical events which only span 130 years. The very straight cut-off on the southern and northern side of the plot are the result of the grid which was drawn in a rectangle around the historical events, and therefore all synthetic events that go outside are cut off. Also the fact that the synthetic events discover much more possibilities of future events results in

small probabilities of occurrence in very remote locations. A C-like shape is present in both plots with its peak at the East coast of the U.S. and also the increased occurrence south east of Cuba and in the GoM along the coast of Florida, Alabama and Mississippi is clear in both the historical and synthetic statistics. Altogether The Generator Tool seems to work well, especially in the area of interest, however it is difficult to exactly tell how much the simulated and historical events compare based on visual inspection alone. Therefore quantitative inspection will have to determine how well the tool is functioning.

4.2.2 Quantitative validation

The quantitative inspection is done at 12 Control Locations (CLs) within the GoM shown in Figure 4.7. The CLs are placed more closely together in the east where TC characteristics are expected to change more rapidly over short distances. Locations 9 and 10 are mostly passed by tracks that have crossed land and therefore differences between historical and synthetic data at these locations will give information about the functionality of the land decay function incorporated in the cyclone generator component of TCWiSE.

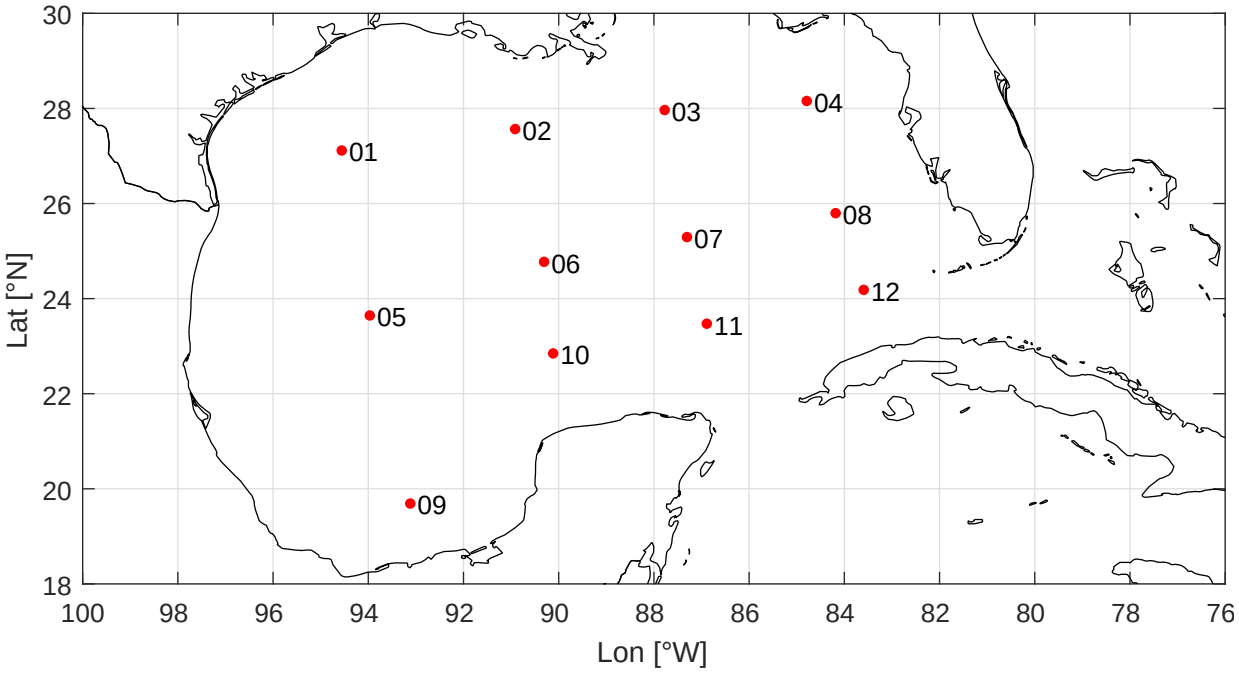

Figure 4.7 – Control Locations

The generation of synthetic TCs yields 3 distinct parameters which can be compared for the historical and synthetic tracks namely V_{max}, c and θ. Comparison is done by constructing CDFs for V_{max} and c and PDFs for θ at each of the 12 CLs of all observations within a 200 km radius. This is done for both the 130 years of historical data and 5000 years of synthetic data. Both functions are compared visually, which gives a first implication of the resemblance, but they are also compared by means of the Kolmogorov-Smirnov test (K-S test), which tests the null hypothesis that both samples are sampled from the same population (Scheff, 2016). The K-S test is given by:

$$D_n = \sup |F_n(x) - F(x)| \tag{4.1}$$

Where sup is the supremum or least upper bound of the set differences. The null hypothesis is rejected if D_n is larger than the critical value which can be obtained from tables available in MATLAB (The MathWorks, Inc, 2016) which is used for the K-S test. Table 4.2 shows the K-S statistic for the three variables under investigations for all CLs together with whether the null hypothesis is rejected or not. The CDFs of V_{max} and c and the PDFs of θ for both the historical and synthetic data for all 12 locations are shown in Figure 4.8, 4.9 and 4.10 respectively. The CDFs of the historical data include the 95% confidence intervals, these are not shown for the synthetic data as the number of synthetic events caused the confidence interval to be very small and therefore to visually coincide with the best estimate. The results are analysed per variable in the following subsections.

Table 4.2 – K-S statistic and test for V_{max}, c and θ. A 0 indicates that the null hypothesis that both samples come from the same population is not rejected and a 1 that the null hypothesis is rejected.

Control Location	1	2	3	4	5	6	7	8	9	10	11	12
ksvmax	0.14	0.07	0.11	0.09	0.08	0.13	0.10	0.04	0.11	0.13	0.11	0.09
	1	0	1	1	0	1	1	0	1	1	1	1
ksc	0.09	0.10	0.11	0.07	0.10	0.07	0.11	0.08	0.19	0.11	0.10	0.10
	1	1	1	0	1	0	1	1	1	1	1	1
kstheta	0.07	0.09	0.07	0.06	0.11	0.07	0.07	0.11	0.06	0.08	0.08	0.13
	0	1	0	0	1	0	0	1	0	0	1	1

4.2.2.1 Maximum Sustained Wind Speed

First the CDFs of V_{max} will be compared shown in Figure 4.8. At first glance one could say that in general the CDFs of the historical and synthetic data compare quite well and look relatively similar. In a third of the locations the CDFs of the simulated data lies within the confidence bounds of the historical data. There appears to be a small bias towards lower values of V_{max} in the synthetic data. Only in location 9 the synthetic data clearly shows more probability for higher values of V_{max} than the synthetic data. This is most likely the effect of the constant decay per time step applied over land in the generator tool instead of an exponential decay. The land decay model could also explain the slight underestimation of V_{max} in several other locations. Because most storms that affect the GoM come from the North Atlantic (NA), they either pass closely by, or cross one of the many small islands along the way. Landfall, or being very close to land, eliminates or at least reduces the energy source that TCs thrive on and therefore reduces the intensity of the storm. Therefore, it is very likely that in this specific case, a reduction of intensity or at least the influence of landfall is included in the historical cyclone data. Therefore applying an additional reduction in intensity by means of a decay function, whether this one is constant or exponential, overestimates the reduction in intensity compared to what would occur in reality. This of course is a hypothesis and not necessarily the reason for the slight differences in V_{max} between the historical and synthetic data.

From the K-S statistic in Table 4.2 it can be seen that for V_{max} for all but three locations the null hypothesis is rejected and the statistic lies between 0.07 and 0.14 for all locations. However, this does not mean that the tool is not producing reliable results. This is the case because the large deviations can be explained by how the K-S test works, which makes it very aggressive in rejecting a hypothesis. Because the K-S test only looks at the maximum difference between the two CDFs, it is very sensitive and therefore quick in rejecting the null hypothesis. Nevertheless, the K-S tests rejects the hypothesis for most locations which implies that the tool is not perfect in replicating historical events. This is however accepted as the overall similarities of the input and output are great, and comparison of CDFs of all data does not necessarily give information about the predictions of extremes which are the objective of this study.

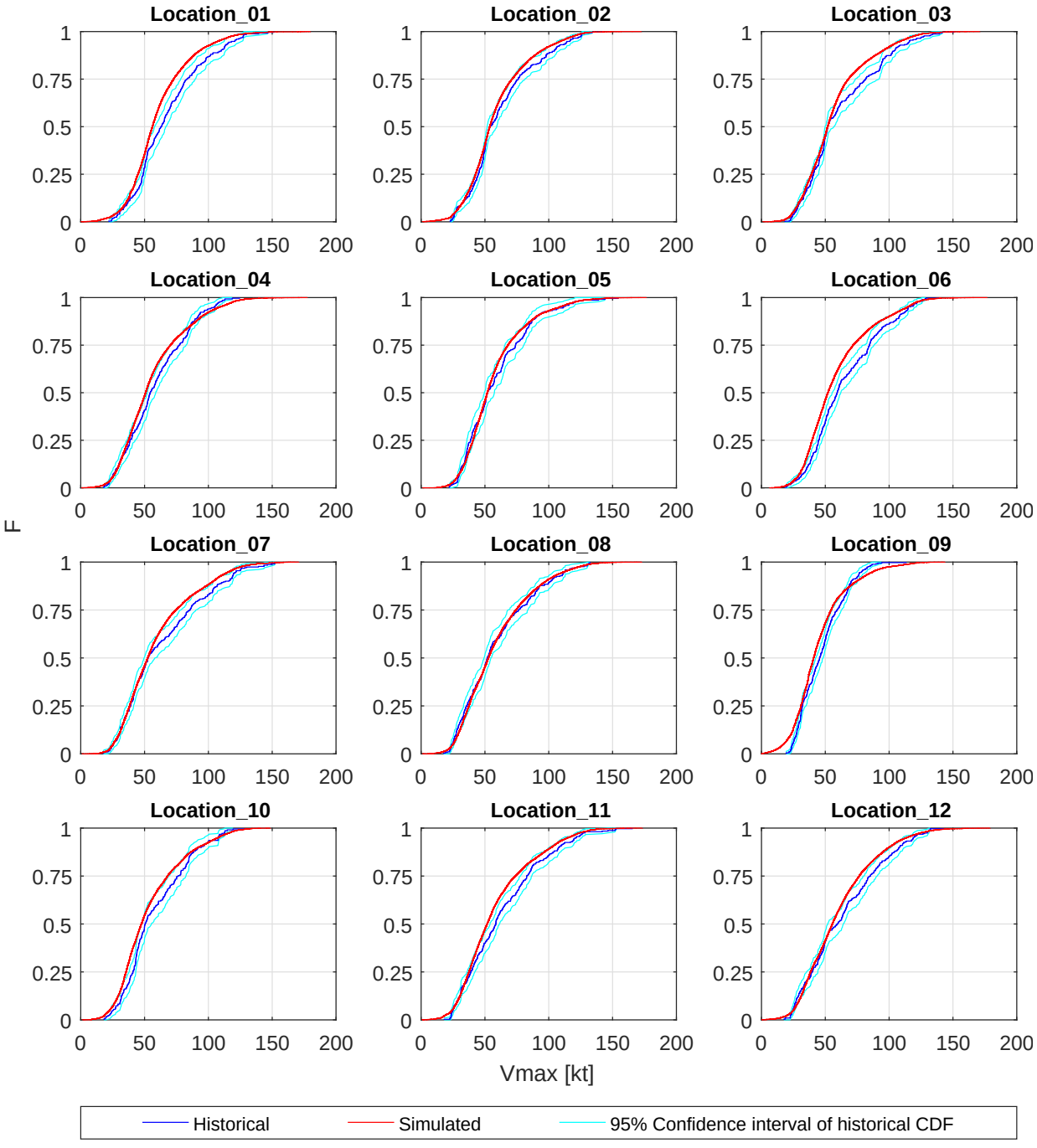

Figure 4.8 – CDFs of V_{max} for 130 years of historical TC data and 5000 years of synthetic TC data at 12 control locations with the 95% confidence intervals for the historical data

Reasons for why some locations show a better comparison than others are not entirely clear or easily found. Locations 8, 2, 5 and 4 show the most agreement and 1, 6 and 10 show the most deviation. Proximity to land does not appear to be a main influence as location 5 is furthest away from any land whereas 4 and 8 are both quite close. Also distance covered after crossing land like Cuba does not seem to have a major influence as both locations 8 and 11 would be reached approximately simultaneously after a TC has crossed Cuba and have a large difference in accuracy. Although possibly the accuracy might be related to this distance, as this property has not specifically been investigated.

Since there is no clear explanation between the difference in comparison of the CDFs of V_{max} at each location, and it appears to be somewhat random which location compares better, it might very well be that there is no apparent aspect or component of the tool that is responsible for these differences. The CDFs of the synthetic data are mostly within the confidence bounds or very close to them and are therefore deemed satisfying for further use in this study.

4.2.2.2 Forward Speed

Figure 4.9 shows the CDFs for the translation velocity or forward speed of the historical and synthetic cyclones. When compared to those of V_{max}, these appear to fit more closely. A first reason would be that both the historical and synthetic values are nearly continuous and not discrete, and therefore no artificial error had to be applied to the historical data to make it continuous. This is because the forward speed was determined based on the traversed distance during a 6 hour time step, and the location of the eye for each time step is measured with a high accuracy. Another reason is the fact that the change in forward speed is only dependent on the historical data, and no extra models such as the land decay model for V_{max} are involved.

At every location the forward speed varies from approximately 0 to 30 kt, and also the shapes of the CDFs are very similar. Therefore it appears that there is not a clear correlation between the exact location of a storm and the forward speed. This is most likely also a reason why the tool is better at producing synthetic tracks with the same distribution of translation velocity as the historical tracks, than at producing the same distribution of maximum sustained wind speed or heading as these parameters show much more spatial variability.

The K-S statistic does not reject the null hypothesis for locations 4 and 6, but does reject it for the other locations. The statistics for all locations lies between 0.07 and 0.11 except for location 9 which has a K-S statistic of 0.19. Reasons for why this location does not match as well as the other locations are unknown. Visually it is difficult to discern any differences in measure of comparison between the locations that are not rejected versus those that are rejected. Based on the K-S statistic alone one might say that the generator tool does not yield satisfying results. However, because of the strict nature of the K-S test and the fact that visual inspection clearly shows good results, the results are satisfying nonetheless.

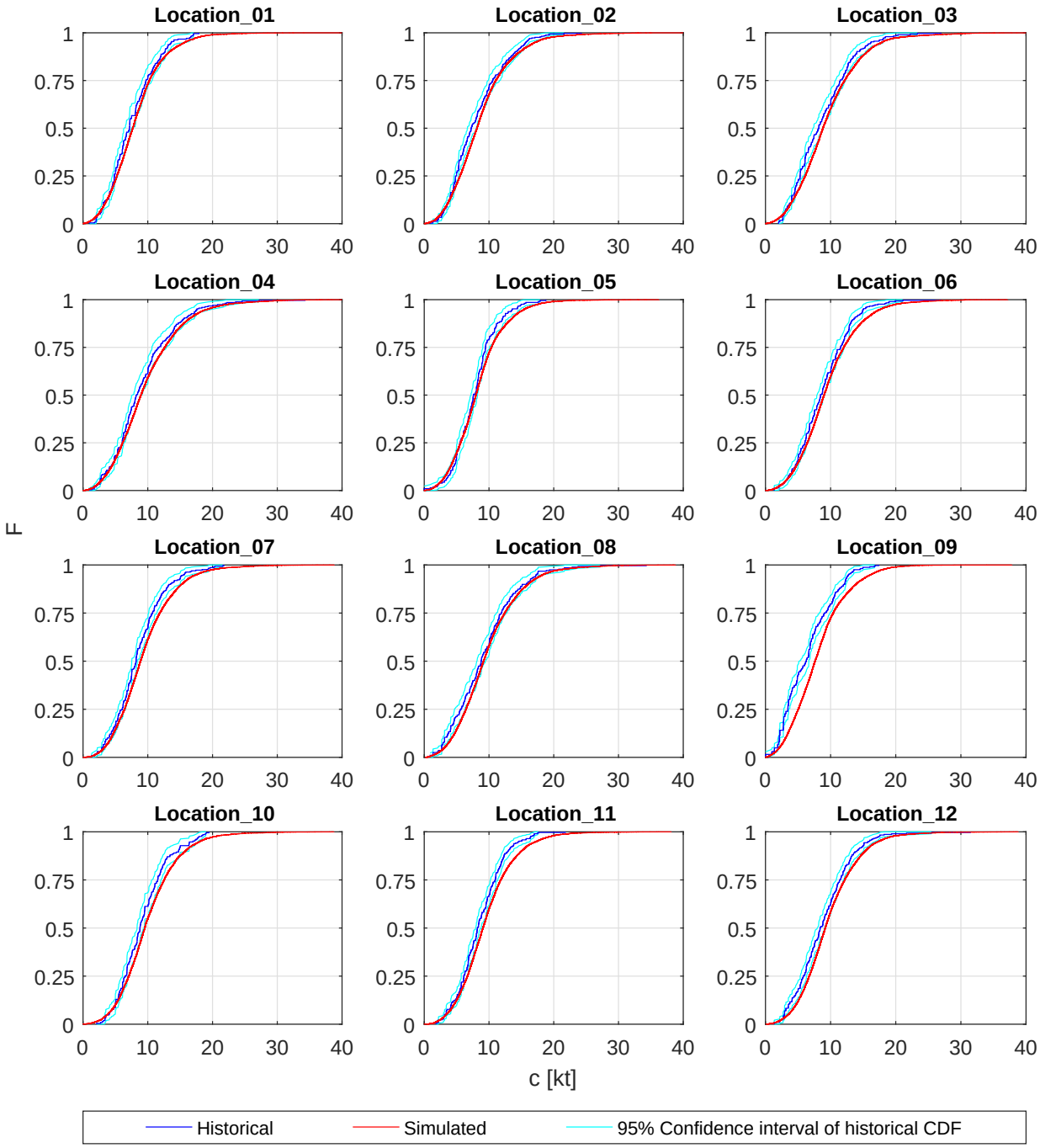

Figure 4.9 – CDFs of the forward speed for 130 years of historical TC data and 5000 years of synthetic TC data at 12 control locations with the 95% confidence intervals for the historical data

4.2.2.3 Heading

Figure 4.10 shows the PDFs for the heading, measuring clockwise from the North, for the historical and synthetic cyclones. Some of the locations are a near perfect match but for other locations the comparison seems quite poor. The CDFs depict a slight distorted picture as the x-axis in this case is a loop since heading describes a circle, and therefore it was opted to display the PDF instead of the CDF to compare the distribution of the synthetic data to that of the historical data.

In general the PDFs of the synthetic data are much smoother as is expected. All small bumps in the PDFs of the historical data are smoothed out and replaced by a single line passing through them as is clearly visible at locations 1, 2, 5, 7, 9 and 11. At every location both the historical and synthetic cyclones are generally heading north and not south, with a few exceptions. Whether cyclones head either north east or north west is very location specific and the clear observable difference at location 12 between the historical and synthetic events is most likely a result of the nature of this location. TCs in the Atlantic basin that pass within 200 km of location 12, either head towards the coast of Texas or Mexico, or they are making a turn and are heading past or across Florida along the East coast of the U.S.. Because location 12 is exactly on the fork of these two headings, specific details of how the tool defines the PDF of $\Delta\theta$ might result in an incorrect or at least slightly deviated picture at this exact location.

The tool gathers data for this location within a 100 km square box, but since more data is most likely required, this box is expanded in both directions. For this location specifically, the change in heading of TCs is very dependent on the exact location, as to the west of this locations most storms are heading north west, and to the east most storms are heading north east. Because the tool gathers data from a larger area, changes in characteristics that occur on a small spatial scale are not perfectly replicated. In general TCWiSE will still produce tracks similar to the historical ones, only the exact location of this fork is slightly different and therefore the picture painted at this control location is slightly deviated.

This phenomenon becomes more clear if one compares the PDF at location 11 with that of location 12. It can be seen that at location 11 nearly all storms are heading north west, whereas at location 12 they are evenly spread between a north western and north eastern heading. Even though the two locations are only a few hundred kilometres apart, the heading has drastically changed. The heading of the synthetic tracks also shows much less deviation from the historical tracks at location 11 compared to location 12. Because the general behaviour of the historical tracks changes very rapidly over a short distance, and the tool gathers data per grid cell over a larger area, the tool is not capable of reproducing this behaviour exactly at this location. On a larger scale the behaviour is still accurate, as the tool has time to adjust for very local changes.

The K-S statistic for the heading rejects the hypothesis at 5 out of 12 locations. These most likely are all affected by the phenomenon just explained and are therefore rejected. Overall the tool appears to reproduce the variability in heading quite well and the tracks are therefore deemed suitable for the purpose of this study.

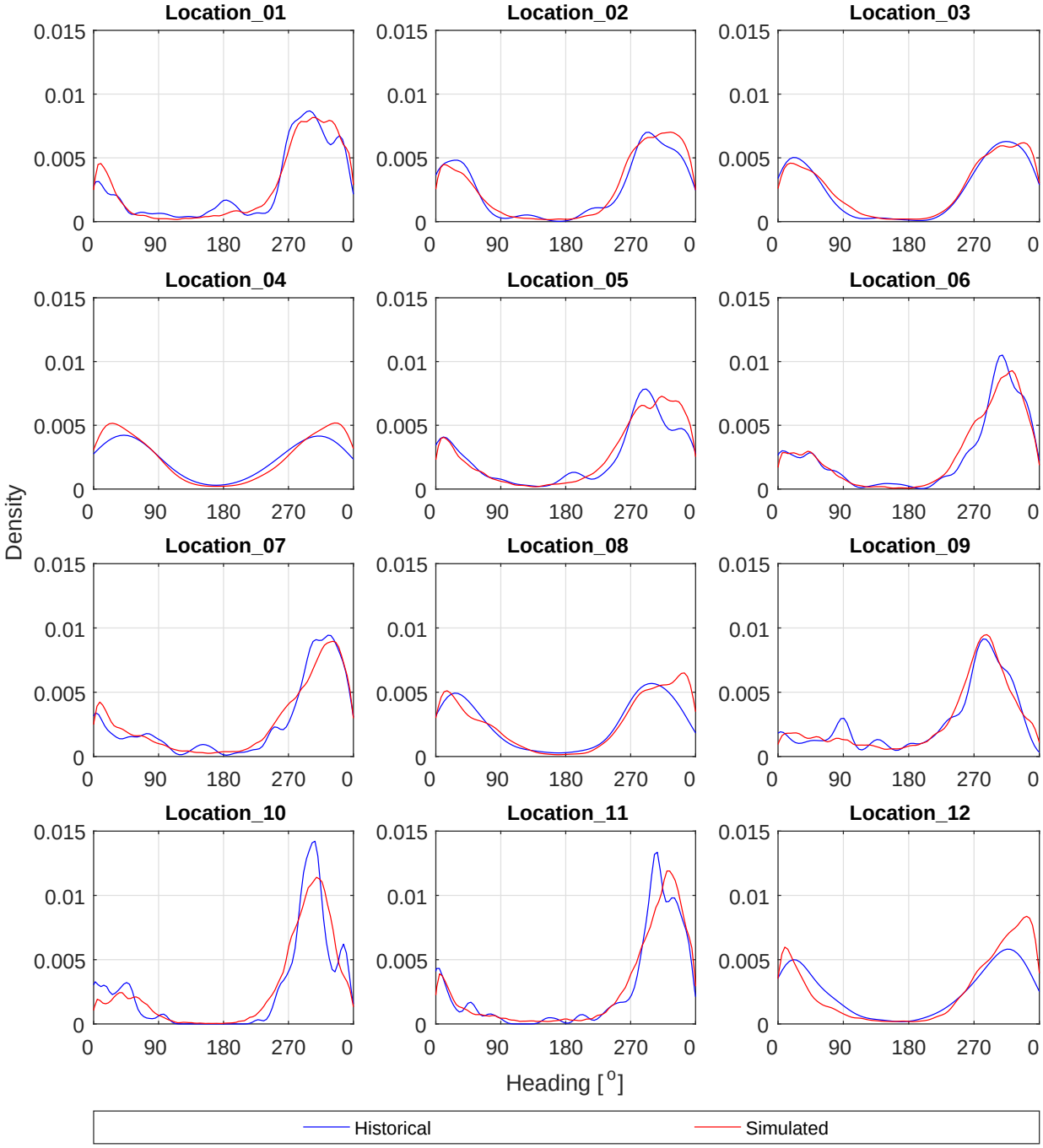

Figure 4.10 – Kernel smoothed PDFs of θ for 130 years of historical TC data and 5000 years of synthetic TC data at 12 control locations

5 Extreme Wind Speed Map Determination

This chapter elaborates the process of obtaining extreme wind speed maps from the synthetic set of Tropical Cyclones (TCs) as applied in the Tropical Cyclone Wind Statistical Estimation Tool (TCWiSE). First, the used spatial wind field model is described together with the additional conditions applied to account for several factors such as asymmetry and wind inflow angle. Subsequently, the determination of the yet unknown, but required parameters for the application of the spatial wind field model is treated. The process of constructing extreme wind speed maps from the spatial wind fields of the individual events is described next. These are then validated by comparing them with extreme wind speed maps which are constructed by applying classical Extreme Value Analysis (EVA) on the historical events, assuming that the 130 years of historical events in the Gulf of Mexico (GoM) provide sufficient data for an accurate estimate of greater return period values by means of EVA.

5.1 Spatial Wind Field Model

The synthetic events produced by the cyclone generation component of TCWiSE so far only contain the location of the eye at each time step together with the corresponding maximum sustained wind speed V_{max}. The location of V_{max} however does not coincide with the location of the eye, but also depends on the size of the storm and on the forward speed of the storm which introduces asymmetry in the wind field. To produce the entire spatial wind field around the eye, one requires a spatial wind field model which can compute V_{max} around the eye at every location as a function of distance and angle from the eye as explained in the literature in Section 2.3.2.4.

The Holland2010 (Holland et al., 2010) parametric spatial wind field model has been adopted for the purpose of this study with several adaptations. This model was preferred over the earlier Holland1980 model (Holland, 1980) because of the consistent overestimation of the wind speed further away from the eye of the Holland1980 model. The Holland2010 model was applied by using the Radius of 35kt Wind Speeds (R35) as additional input for storms with a V_{max} of over 35kt, next to the other parameters V_{max}, p_c and the Radius of Maximum Winds (RMW). For events with lower wind speed the Holland2010 model reduces to the Holland1980 model in absence of the R35 value. For a description of the wind field model by Holland et al. the reader is referred to Appendix A. The theory by Lin and Chavas (2012) has been adopted to account for asymmetry in the wind field introduced by the translatory nature of the TC, which adds the forward speed c multiplied by a factor of 0.55 and a rotation of 20° counter-clockwise to the sustained wind speeds. Also a wind

inflow angle of 22.6° is introduced which accounts for the inward spiralling nature of the cyclone winds as was determined by J. A. Zhang and Uhlhorn (2012).

5.1.1 Spatial Wind Field Parameter Determination

To compute the spatial wind field one requires at least both V_{max}, p_c and RMW as was mentioned earlier. Because of the application of the Holland2010 model instead of the Holland1980 model, at least one additional wind radius is required. Since there is more data available on lower wind speed radii it was opted to use the R35 instead of higher wind speed radii. Since only V_{max} is determined for the synthetic events so far, the parameters p_c, RMW and R35 still have to be determined. The most common way to model this relation is to directly link p_c to V_{max} and RMW to p_c as mentioned in Section 2.3.2.4 and shown in Figures 2.4 and 2.5. As can be seen from these two figures, both relations do follow the data, but complete remove the large variability that is present. Therefore using these relation directly for all synthetic events would lead to a very different picture of the resulting wind fields as the size of the cyclone has a lot of influence on return period values for specific locations. Moreover, no such relation have yet been determined for the R35 and therefore a different method is deemed necessary for modelling p_c, RMW and R35 to achieve the same variability in the parameters as what occurs in reality. An overview of the characteristic variables of the synthetic TCs together with which parameters they depend on in TCWiSE is given in Table 5.1.

Table 5.1 – Characteristic parameters of the synthetic TCs in TCWiSE, required for the determination of the spatial wind field, together with the modelled dependency of each parameter. $t-1$ represents the previous time step.

Parameter	Symbol	Dependency
Maximum Sustained Wind Speed	V_{max}	$V_{max\,t-1}$
Central Pressure	p_c	V_{max}
Radius of Maximum Winds	R_{max}	V_{max}
Radius of 35 kt Wind Speeds	$R35$	V_{max} & R_{max}
Translation Velocity	c	c_{t-1} & θ_{t-1}
Heading	θ	c_{t-1} & θ_{t-1}

This is done differently for each variable. This has to do with the data availability of data and also on the difference in dependence on location for each variable. Central pressure data is available from as early as 1888 whereas best track data for wind radii is only available from 2004 and some raw data going back to 1988. Also, central pressure data shows the same trend throughout the entire North Atlantic and the GoM, whereas wind radii data for the GoM differs significantly from the rest of the Atlantic basin. This implies that there is much more data available to determine a relationship between V_{max} and p_c than there is to determine a relationship between V_{max} and wind radii. Another factor which influences the selection of the method used to determine a specific parameter, is the dependence of that parameter on other parameters. Ideally, a joint distribution would be constructed between all four parameters, which would allow for dependence between all variables. This

could be done by constructing a multidimensional copula (Chi & Goodwin, 2012), or by using vine copulas which model the dependence between variables by constructing a vine, or a set of nested trees, between the variables and subsequently fitting copulas to each of the edges between the variables (Jäger & Morales-Nápoles, 2016). Both methods however are complex and time consuming, especially with the limited amount of data available. Therefore for the purpose of this study both p_c and RMW are determined solely based on V_{max} and only R35 is modelled dependent on both V_{max} and RMW. This is done because large values for RMW would by definition result in large values for R35 and also the fact that large values for V_{max} would result in larger values for R35 because of the large difference in wind speed between the two radii. The determination of p_c, RMW and R35 are treated separately in the following subsections.

5.1.1.1 Central Pressure Determination

The central pressure is determined by constructing a parametric copula which represents the joint distribution between V_{max} and p_c. This copula is then used to sample p_c every time step which allows for a realistic representation of the spread in p_c in the synthetic data set.

Copulas are defined as functions that represent the joint distribution of two or more random variables of which the marginal distributions are uniform. They can show the dependence between two or more variables without knowing anything about the probabilistic distribution of the separate variables. Copulas were first introduced by Sklar (1959) who stated in Sklar's theorem that any multivariate distribution can be written in terms of the marginal distribution functions of each variable and the copula which describes the dependence between the variables. According to Sklar the cumulative distribution $H(x, y)$ of any pair (X, Y) of continuous random variables can be written as:

$$H(x, y) = C\{F(x), G(y)\} \qquad x, y \in \mathbb{R} \tag{5.1}$$

Where $F(x), G(y)$ are the marginal distributions and $C : [0, 1]^2 \rightarrow [0, 1]$ is the copula (Genest & Favre, 2007). Thus for a complete description of the distribution of two random variables and their joint behaviour, one requires the marginal distributions of both and the copula that models the joint behaviour. With respect to the joint distribution of p_c and V_{max}, both the marginal distribution of p_c and the copula still have to be determined. The marginal distribution of V_{max} follows as result of the synthetic cyclone generation and therefore does not have to be determined.

There a many different Copula families which are used to model the joint behaviour of random variables, but in this study only 5 have been tested as these are common and the used programming language Matlab (The MathWorks, Inc, 2016) currently has these 5 Copulas readily available. These are the Gaussian, Gumbel, Clayton, t and Frank Copula. These are commonly fitted by means of correlation estimators such as Kendall's tau, Spearman's rho or Pearson's linear correlation coefficient. In this study Pearson's linear correlation coefficient is used which is a measure of dependence and defined in the interval $[-1, 1]$ with [-1,0] implying negative correlation and [0,1] implying positive correlation which for samples is defined by (Anderson, 1984):

$$\rho = \frac{\sum_{i=1}^{n}(x_i - \overline{x})(y_i - \overline{y})}{\sqrt{\sum_{i=1}^{n}(x_i - \overline{x})^2}\sqrt{\sum_{i=1}^{n}(y_i - \overline{y})^2}} \tag{5.2}$$

An important distinction between copula families is the level of tail dependence which describes the dependence between extremes. In case of positive correlation, which implies that higher values of one parameter usually coincide with higher values of the other parameter, upper tail dependence implies an increased density in the upper right quadrant and lower tail dependence implies extra density in the lower left quadrant. A better way to show this is by plotting the density functions of the three copulas Gaussian, Gumbel and Clayton which respectively have no, upper and lower tail behaviour with Spearman's rho of $\rho_s = 0.9$ as shown in Figure 5.1.

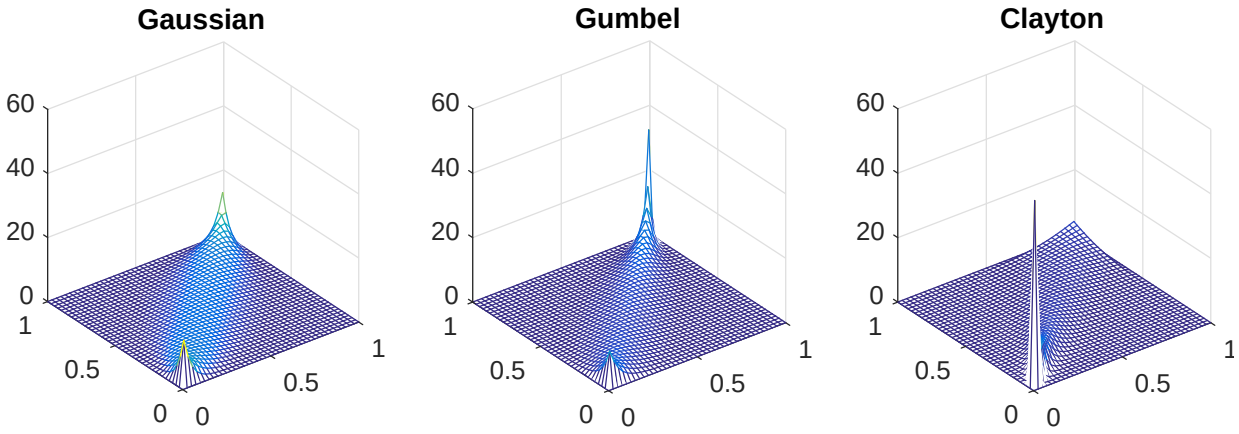

Figure 5.1 – Density function of the Gaussian, Gumbel and Clayton copula for Spearman's rho of $\rho_s = 0.9$

Fitting of the 5 copula families is done by estimating the parameters belonging to the respective copula families by using maximum likelihood. The first step is to obtain the rank of both variables by ranking the variables from lowest to highest and then assigning them a rank by their position and then normalising by dividing by the number of observations plus one. The found empirical copula is then transformed to standard normal space which means they are transformed to a Gaussian distribution having a mean of $\mu = 0$ and a standard deviation of $\sigma = 1$ to better observe the dependence per quadrant which would imply tail dependence. In Figure 5.2 the resulting plot for both the observed data and the Gumbel copula fitted to the data is shown. As can be seen there is a very clear negative correlation with a Pearson's linear correlation coefficient of $\rho = 0.88$. Because the Gumbel copula can only show positive correlation, the observed ranks of the central pressure are mirrored by taking $R_i = 1 - R_i$ where R_i is the normalised rank of each observed value. By doing this a positive correlation, instead of a negative correlation is observed in the data to which the Gumbel copula can be fitted. After having fit to the mirrored rank of p_c one can sample from the copula and subsequently mirror the sampled normalised ranks of p_c again to obtain a negative correlation as was present in the original data.

For the Clayton copula the same technique was used but now the normalised ranks of V_{max} were mirrored instead of the normalised ranks of p_c. The observed data appears to show dependence in the lower right or south east quadrant, and since the Clayton copula has lower tail dependence, the observed data should be mirrored in the x-axis to make sure the tail dependency of the Clayton copula occurs in the same quadrant as for the observed data. The Gaussian, Frank and t copula do not require positive correlation to be fit and therefore do not require any special altercations before fitting to the data.

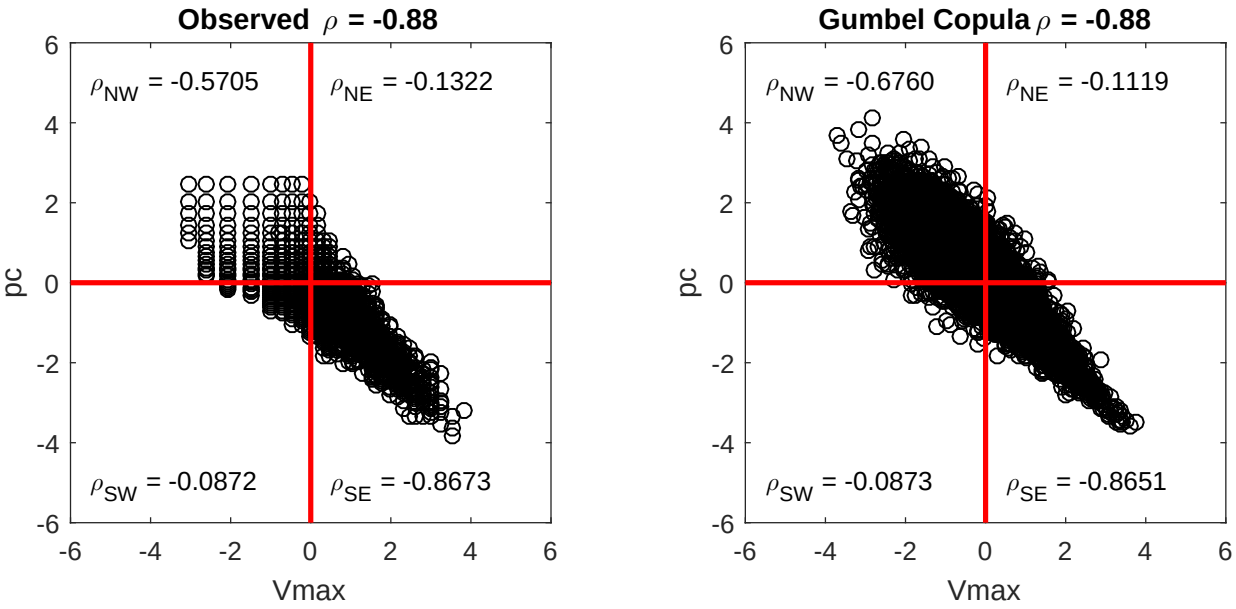

Figure 5.2 – Normalised ranks of observed data transformed to standard normal space and the same number of samples of the Gumbel copula fitted to the observed data transformed to standard normal space together with the linear correlation coefficients per quadrant

The best fitting copula is determined based on 2 criteria. The first criterion is the value of Pearson's linear correlation coefficient per quadrant or semi-correlation, which was already presented for the observed data and the Gumbel copula in Figure 5.2. A clear difference in correlation between the south east and north west quadrant would imply tail dependency in case of a negative overall correlation. The second criterion is the sum of square differences based on the Cramér-von Mises statistic which is defined as (Genest & Favre, 2007):

$$S_n = \sum_{i=1}^{n} \left\{ C_n\left(\frac{R_i}{n+1}, \frac{S_i}{n+1}\right) - C_{\Theta_n}\left(\frac{R_i}{n+1}, \frac{S_i}{n+1}\right) \right\}^2 \tag{5.3}$$

Where C_n is the empirical copula and C_{Θ_n} the fitted parametric copula. The lower the value of the statistic the better is the fit of the parametric copula. The resulting linear correlations ρ for each quadrant and the sum of square differences based on the Cramér-von Mises statistic S_n for the observed data and for the different copula families are given in Table 5.2

As can be seen from the semi-correlations of the north west and south east quadrant of the observed data, the data shows tail dependence as $\rho_{nw} = -0.57$ is significantly smaller in absolute sense than $\rho_{se} = -0.87$. From that fact alone it would already give a preference to either the Gumbel or the Clayton copula as those are the two that show tail behaviour where the Gaussian, t and Frank do not. From the semi-correlations of the Clayton copula of $\rho_{nw} = -0.34$ and $\rho_{se} = -0.91$ it is clear that the copula shows a high tail dependence with the semi correlation in the south east quadrant even being higher in absolute sense than the total correlation of the data. The semi-correlation in the north west quadrant also shows much less correlation than the observed data does. The Gumbel copula, just like the Clayton copula, also shows tail dependence with the same semi-correlation in the

Table 5.2 – Pearson's linear correlation coefficient per quadrant ρ and the sum of square differences based on the Cramér-von Mises statistic S_n for the fitted parametric copula families to the empirical copula of V_{max} and p_c

Parameter	Observed	Gaussian	Clayton	Gumbel	t	Frank
ρ_{nw}	-0.57	-0.74	-0.34	-0.67	-0.79	-0.63
ρ_{ne}	-0.13	-0.17	-0.12	-0.07	0.05	-0.06
ρ_{se}	-0.87	-0.74	-0.91	-0.87	-0.79	-0.65
ρ_{sw}	-0.09	-0.19	-0.11	-0.04	-0.01	-0.15
S_n	-	0.63	0.80	0.50	0.54	0.53

south east quadrant as the observed data and slightly more correlation in the north west quadrant. Therefore based on the first criterion the Gumbel copula is clearly the best fitting copula to the observed data.

The second criterion also rules in favour of the Gumbel copula as the sum of square differences based on the Cramér-von Mises statistic is lowest for this copula, although both t and Frank copulas nearly have the same statistic. Based on these two tests it can therefore be reliably concluded that the Gumbel copula with the parameter of $\Theta = 3.53$ is the most suitable copula among the tested copulas to model the joint behaviour of maximum sustained wind speeds and central pressure of a TC.

To use the Gumbel copula to sample central pressure values based on observed or simulated maximum sustained wind speed values, firstly, the sustained wind speed needs to be converted to the interval [0,1] by taking the normalised rank. Subsequently one needs to sample p_c conditionally upon the rank which is done by solving the inverse conditional Gumbel copula. The conditional Gumbel copula is given in equation 5.4 (Leontaris et al., 2016) and the inverse is found using a numerical bisection method which is modelled in Matlab (The MathWorks, Inc, 2016) with the Gumbel inverse function written by Patton (2003).

$$C(v_t|u_t;\theta) = u_t^{-1} \exp\left\{ -\left[x^\theta + y^\theta\right]^{\frac{1}{\theta}} \right\} \cdot \left[1 + (y/x)^\theta\right]^{\frac{1}{\theta}-1} \tag{5.4}$$

Where $x = -\ln u_t$ and $y = -\ln v_t$ with u_t representing the normalised rank of the known V_{max} values and v_t representing the normalised ranks of the p_c values of interest.

After sampling conditionally from the copula, the normalised ranks of p_c are known but still have to be inverted back to their margins to end up with actual central pressure values. This could be done the easiest by inverting back with the empirical margins which can be readily obtained from the data. However by doing this, obtaining values of central pressure outside the observed range is not possible. Since simulating many years of synthetic cyclones will most definitely result in maximum sustained wind speeds not yet observed, and the strong correlation between V_{max} and p_c, it is safe to assume there is a high probability that there should also be central pressure values in the synthetic data set which are beyond the yet observed range. Therefore one first has to fit a probability distribution to the margins of p_c, and then transform back over those margins. This is done by fitting the parametric distributions Generalised Extreme Value (GEV),Generalised Pareto Distribution (GPD), Gumbel, Lognormal, Gaussian, Rayleigh and Weibul to the central pressure deficit.

Because the only difference between the central pressure and the pressure deficit (Δp) is the subtraction from the ambient air pressure, the probability distribution of both will be identical and therefore the distributions can be fit on either although fitting on Δp is more convenient as the values of interest in this case are maxima. These distributions are then compared visually with one minus the empirical Cumulative Distribution Function (CDF) of the data in semi-log scale to better observe the behaviour of extremes in Figure 5.3.

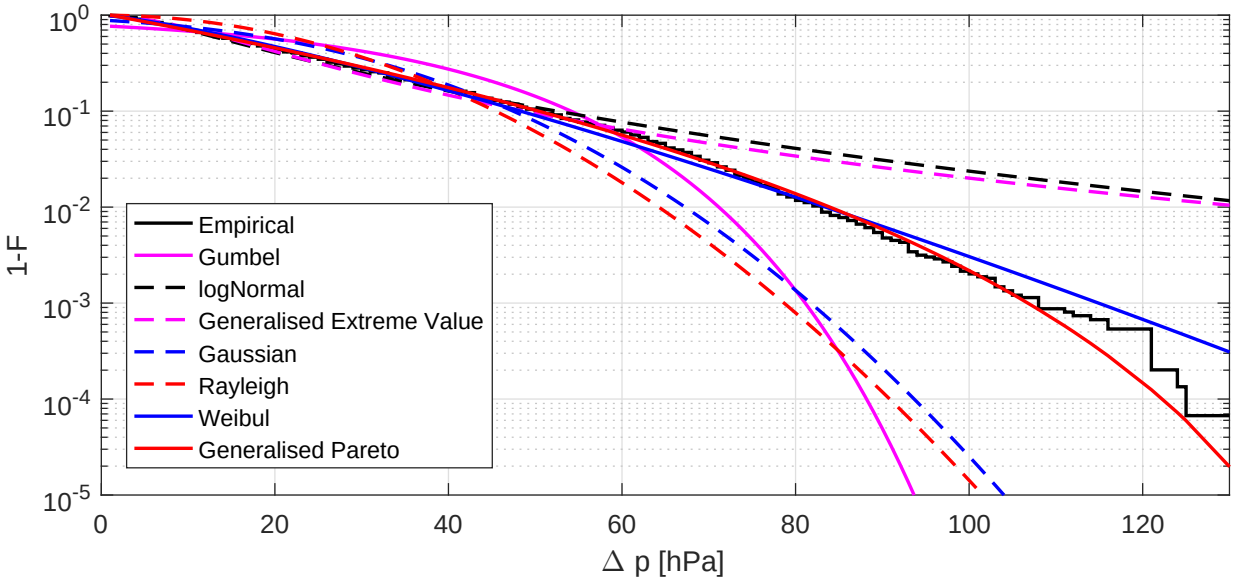

Figure 5.3 – One minus the empirical CDF of the margins of Δp together with the fit of 7 probabilistic distributions

Besides visual inspection, the distributions are also compared by taking the Root Mean Square Error (RMSE) of each distribution which is given by:

$$RMSE = \sqrt{\frac{\sum_{i=1}^{n}(\hat{y}_i - y_i)^2}{n}} \tag{5.5}$$

where $\hat{y}_i$ are the obtained values of the parametric distributions and y_i the values of the empirical distribution. A lower RMSE implies a better fit of the parametric distribution. The values are given in Table 5.3.

Table 5.3 – RMSE of 7 fitted probabilistic distributions to the margins of Δp

Distribution	GEV	GPD	Gumbel	Lognormal	Gaussian	Rayleigh	Weibul
RMSE	0.0208	0.0098	0.0823	0.0565	0.0207	0.0897	0.0164

From visual inspection of Figure 5.3 combined with the RMSE values it is clear that the GPD is the best fit for the data. The Weibul distribution also represents the margins very well, however the GPD is preferred as the Weibul distribution would over estimate the probability of the extremes which can be seen by the nearly straight line (in semi-log

scale) the distribution has for the larger values. On the other hand the GPD shows a clear downward curve which implies a certain maxima the pressure deficit could attain. The behaviour of the GPD is in line with the physical behaviour as the pressure deficit is bound to a certain maxima which is determined by among others the Sea Surface Temperature (SST) and humidity (Emanuel, 1988). The definition of the GPD is given in Appendix B in equations B.1, B.2 and B.3. The obtained parameters belonging to the fitted GPD were determined as a shape parameter of $\kappa = 0.17$, a scale parameter of $\alpha = 25.86$ and a threshold of $\xi = 1$.

All components that are required to sample central pressure values for a simulated value of maximum sustained wind speed have now been determined. First the simulated values for V_{max} are transformed to their normalised ranks, which are then used to conditionally sample normalised ranks of p_c with the obtained Gumbel copula. The obtain ranks are then transformed back to their margins by using the determined GPD. The historical observations of p_c vs v_{max} are plotted together with the same amount of randomly selected observations of 5000 years of simulated TC events in Figure 5.4.

As can be seen from the Figure, the sampled data resembles the historical data very well, with perhaps a little more tail dependence than is present in the historical data. It should be mentioned that twice as many observations with $V_{max} > 120kt$ are present in the historical compared to the sampled data in this plot which partially explains the smaller spread in the tail of the sampled observations.

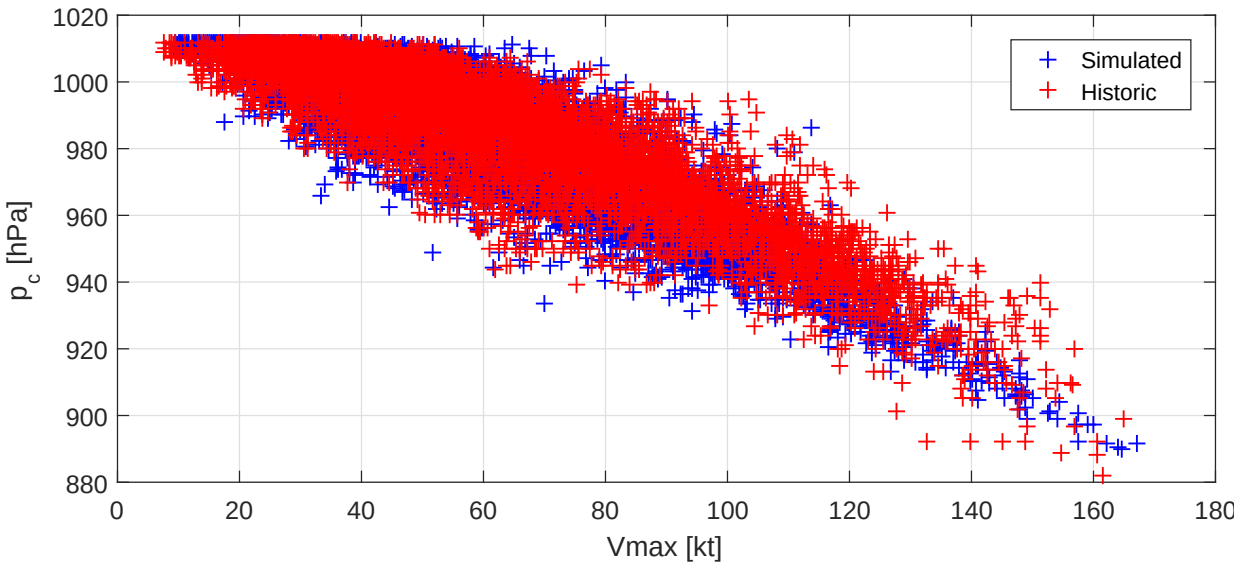

Figure 5.4 – Historic observations of p_c vs v_{max} plotted together with the same amount of randomly selected observations of 1000 years of simulated TC events

5.1.1.2 RMW Determination

As mentioned earlier, RMW is not determined by using parametric copulas as was done for the determination of p_c. This was done because of the limited amount of data available for RMW and because of the time constraints tied to this study. As finding the best possible representation of RMW is not the object of this study, it was opted to take a different,

less time consuming approach, which would still represent the variation of TC size and the dependence on intensity.

Data for RMW is not present in the IBTrACS (2014) data used for the generation of TCs and therefore data obtained from two other sources was used to define a relation between RMW and the intensity. These sources are the Extended Best Track Data Set (DeMaria et al., 2015) and data obtained directly from the NOAA Automated Tropical Cyclone Forecast archive(NOAA, 2016). Conflicts in the two sources, i.e. data points measured for the same event which did not match, were removed from the data. From this data only observations within the GoM were used to define a relation between RMW and the intensity, as there was a clear difference in relation between data obtained in the entire NA and data obtained solely in the GoM.

RMW is sampled conditionally upon V_{max} and not on p_c or Δp which is done in most other studies. This is done because the RMW data showed a clear correlation with both p_c and V_{max}, and because V_{max} is the intensity parameter simulated by the track generator, the V_{max} data is more reliable than the p_c data which is also determined conditionally on V_{max}. The conditional sampling is done by using an empirical joint distribution which was obtained by dividing V_{max} in 6 equal bins of 20kt from 0-120kt and a single bin for all observations greater than 120kt, and making an empirical Probability Density Function (PDF) of the RMW data in each bin. For each bin this data is subsequently smoothed using a kernel density estimator to obtain smooth PDFs which allow for sampling of values not yet observed. The historical observations of RMW vs V_{max} are plotted together with the same amount of randomly selected simulated observations of 5000 years of simulated TC events in Figure 5.5.

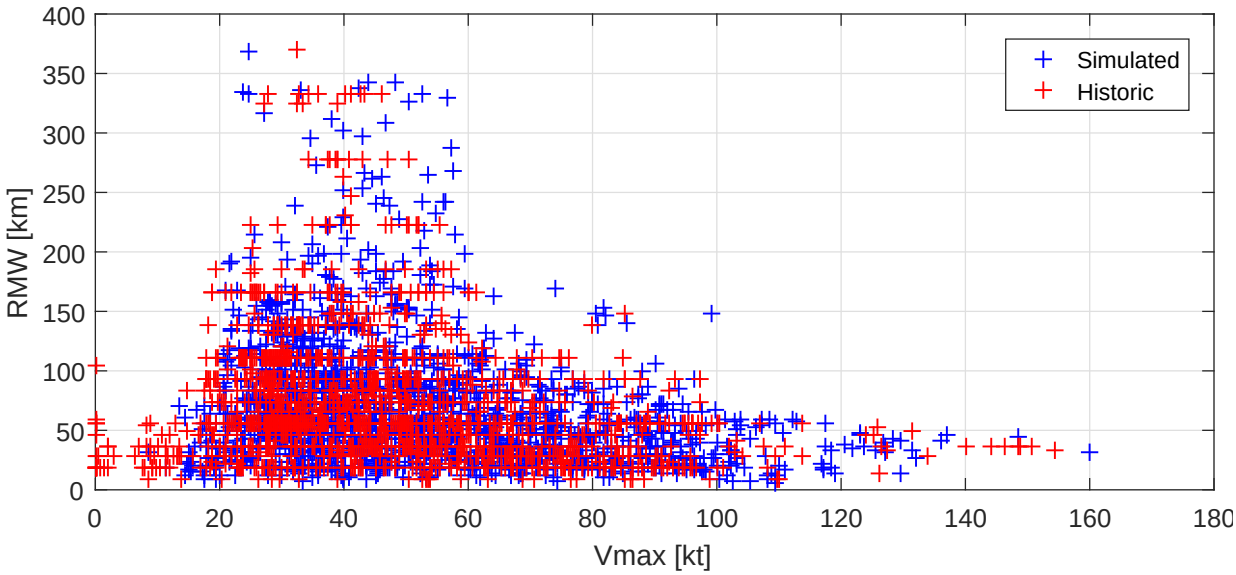

Figure 5.5 – Historic observations of RMW vs V_{max} plotted together with the same amount of randomly selected observations of 5000 years of simulated TC events

As can be seen the simulated data follows the behaviour of the observed data. Table 5.4 displays Pearson's linear correlation for each quadrant for the observed and fitted joint distributions of V_{max} and RMW. The table shows near identical correlations for each quadrant thus confirming the goodness of fit of the empirical joint distribution. By using the kernel

density estimator, RMW values that lie between or just beyond observed RMW are also sampled which results in a near replication of the observed events, but more smoothened. As very little data is available for high values of V_{max}, no negative trend is present in the sampled data for higher observations of V_{max}. As mentioned in Section 2.3.2.4, different studies generally observed a negative trend in RMW for higher V_{max}, and therefore the used approach might possibly result in a slight overestimation of RMW for high intensities. However, since TCs of such intensity have not been observed yet this cannot be stated with certainty. An overestimation of size could lead to a slight overestimation of extreme wind speeds. For engineering design applications a conservative estimate of extreme conditions is often preferred. If a deterministic relation as found for instance by Vickery and Wadhera (2008) would have been used, TCs with a high intensity would by definition be very small in size which would most likely lead to an underestimation of extreme conditions. Therefore the presented methods is deemed more suitable for the determination of extreme conditions for design purposes.

5.1.1.3 R35 Determination

In Figure A.2 in Section 2.3.2.4, it was clear that the Holland1980 model overestimated the wind speeds at distances from the eye greater than RMW. Therefore it was opted to apply the Holland2010 model, which fits the spatial wind field at radii greater than RMW to an extra wind radius observation. The model therefore requires at least one extra wind speed radius. The R35 was selected for this purpose as it had the most data available for the determination of a realistic relationship and since it is a relatively low wind speed, making it very effective for defining a maximum size up to where a TC could be damaging. The determination of R35 is done similarly to the determination of RMW with using an empirical joint distribution, except that instead of sampling conditionally on V_{max} alone, it is also sampled conditionally on RMW. This is done by dividing V_{max} in

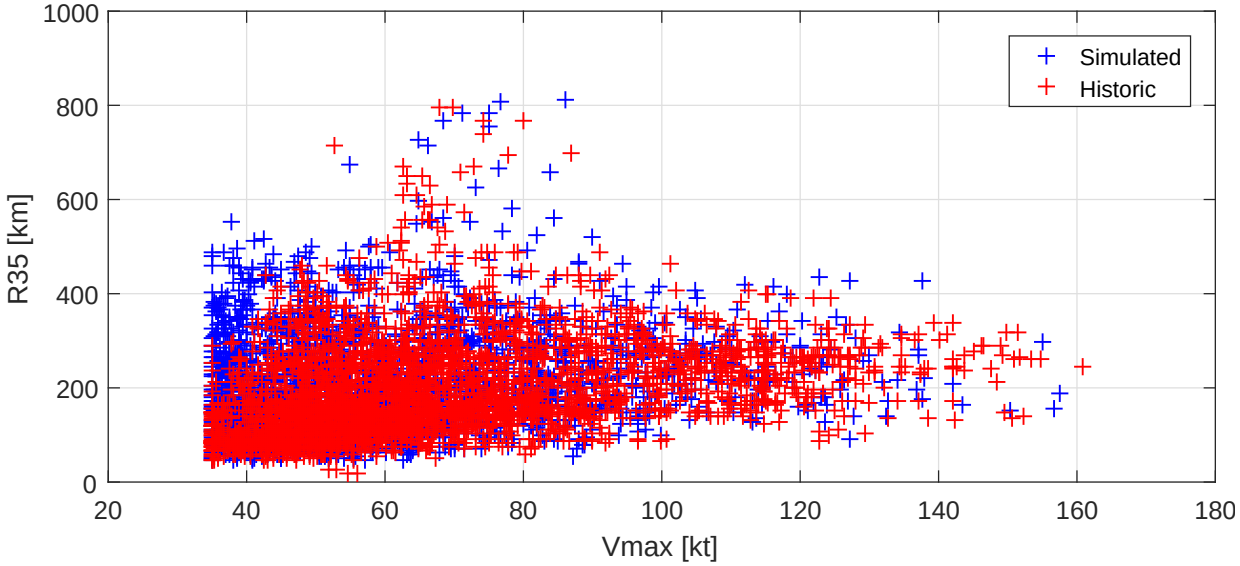

Figure 5.6 – Historic observations of R35 vs V_{max} plotted together with the same amount of randomly selected simulated observations of 5000 years of simulated TC events

bins of 0-63kt, 64-99kt and greater than 100kt wind speeds, and RMW in four equal bins of 50km and one bin for radii greater than 200km. For each of the 15 bins an empirical PDF of the observations is constructed which is subsequently smoothened using a kernel density estimator. If bins do not contain any observations, but a combination of V_{max} and RMW does lead to sampling from that bin, it is sampled from a bin with the same V_{max} category, but with a smaller RMW. This is done as the dependence on intensity is deemed more important, as this way it is avoided that extreme wind speeds occur at a very large distance from the eye.

The historical observations of R35 vs V_{max} are plotted together with the same amount of randomly selected simulated observations of 5000 years of simulated TC events in Figure 5.6. The simulated observations resemble the historical observations quite clearly. Both sets show the same trend of increasing minimum of R35 for increasing V_{max} and an upper bound of 400-500 km for $V_{max} > 100$kt. Sizes can get extremely large for wind speeds between 64 and 100kt, but this trend is also observed in the historical data and therefore accepted. From the correlations per quadrant in Table 5.4 it can also be seen that the observed and fitted distributions have similar correlations for each quadrant for both pairs of variables. Only the south western quadrants for both pairs seem to differ notably. For the pair of V_{max} and R35 the south western quadrant represents low intensity events which are small in size, and therefore not of interest for extreme values. For the pair of RMW and R35 the south western quadrant also mostly represents small and low intensity events, as high intensity events generally have a large R35 by definition. Therefore the differences in correlation in these quadrants are considered acceptable and not of influence for the determination of extreme wind speeds.

Table 5.4 – Pearson's linear correlation coefficient ρ per quadrant for observed joint distributions and fitted empirical joint distributions of V_{max} & RMW, V_{max} & R35 and RMW & R35

Parameter	V_{max} & RMW		V_{max} & R35		RMW & R35	
	Obs	**Fit**	**Obs**	**Fit**	**Obs**	**Fit**
ρ_{nw}	0.05	0.04	0.06	-0.01	0.03	0.15
ρ_{ne}	-0.36	-0.31	-0.13	-0.06	0.36	0.29
ρ_{se}	-0.15	-0.11	0.19	0.25	0.20	0.35
ρ_{sw}	0.13	0.14	0.24	-0.03	0.15	-0.03

5.1.2 Resulting Spatial Wind Field

Using the 4 parameters V_{max}, p_c, RMW and R35, the axi-symmetric wind field around the eye can be determined by using the Holland2010 spatial wind field model. In reality, the spatial wind field however is not axi-symmetric and should therefore be corrected by using the forward speed of the storm as was mentioned earlier. Applying the theories of Lin and Chavas (2012) and J. A. Zhang and Uhlhorn (2012), it was assumed that the synthetic cyclones have a wind inflow angle of 22.6° and show asymmetry because of an addition of 0.55 times the forward speed rotated over 20° to the axi-symmetric wind field. Therefore

the total spatial wind field is a combination of the axi-symmetric wind field as determined with the Holland2010 model and the corrections for wind inflow angle and asymmetry.

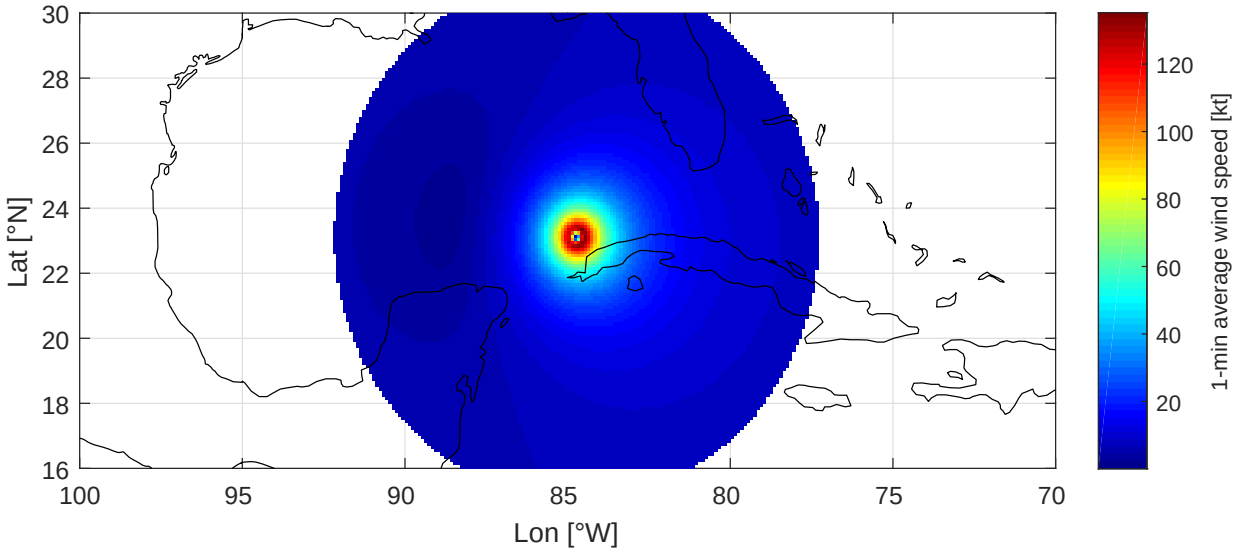

Figure 5.7 – Example of a resulting spatial wind field around the TC eye

These concepts are applied to the synthetic events by first computing the maximum sustained wind speed relative to the forward motion (V_{rel}) by subtracting $0.55 \times c$ with a rotation of 20° from V_{max}. V_{rel} is subsequently used as input for the Holland2010 model to compute the axi-symmetric wind field around the eye. The symmetric wind field is then corrected again with the forward speed to account for asymmetry and finally corrected for the wind inflow angle by applying a rotation of 22.6° to the obtained wind speed vectors around the eye. Additional details about the grid size determination and application of the spatial wind field model are given in Appendix C.1. Figure 5.7 gives an example of a spatial wind field model applied to a synthetic event.

5.2 Resulting Extreme Wind Speed Maps

The simulated set of synthetic TCs can, together with the spatial wind field model as explained in the previous section, be used to determine wind speed maps for specific return periods for any location of interest, in this study the GoM by taking the following steps:

1. First all synthetic tracks that at one point during its lifetime entered the buffer zone around the GoM are selected, and cut off outside of a rectangle drawn around this buffer zone as can be seen in Figure 5.8. The exact size of this polygon is of little importance but it is there to allow events just outside of the buffer zone to also affect the GoM.

2. Next, for all the tracks inside this polygon, the spatial wind field is computed on a spiderweb grid. Since only the buffer zone is of interest, a computational grid is drawn around the buffer zone in which the spiderweb values are transformed back to a rectangular grid resulting in a spatial wind field per hour per storm on a $0.1° \times 0.1°$ grid.

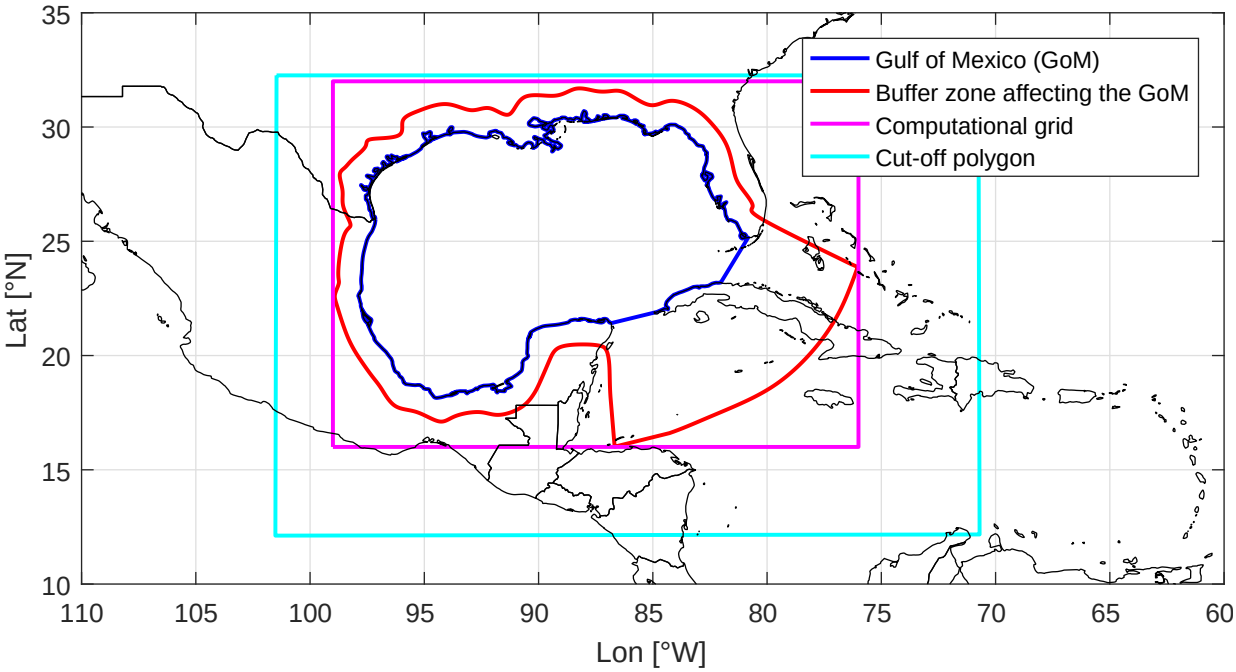

Figure 5.8 – Overview of the boundary definitions for the different computational domains

3. To finally determine wind speed maps for specific return periods, these spatial wind fields per time step are transformed to the maximum 1-minute average wind speeds per grid cell per storm, yielding only one value for wind speed per grid cell per storm instead of every hour. By doing this for every storm, each cell now contains a time series with one value per storm. Return periods up to approximately $1/10^{\text{th}}$ of the length can be obtained directly from the time series, although because of the many random processes in the procedure it is advised to use a lower fraction. This is done by constructing the Empirical Cumulative Distribution Function (ECDF) of the maxima, determining the probability of exceedance for the return period of interest by assuming a Poisson process for cyclone occurrence and adjusting for the number of events per year as is shown by the relation in equation 5.6 (Vickery et al., 2000) and inverting through the ECDF. In this equation F represents the ECDF, λ the number of maxima per year and T the return period of interest.

$$(1 - F) = \frac{1}{\lambda T} \tag{5.6}$$

This has a very similar outcome as selecting the 50^{th} highest value when interested in the 100 year Return Value (RV) for a data set spanning 5000 years. The resulting 100 years return period wind speed map is shown in Figure 5.9. Various maps for different return periods can be found in Appendix C.2.

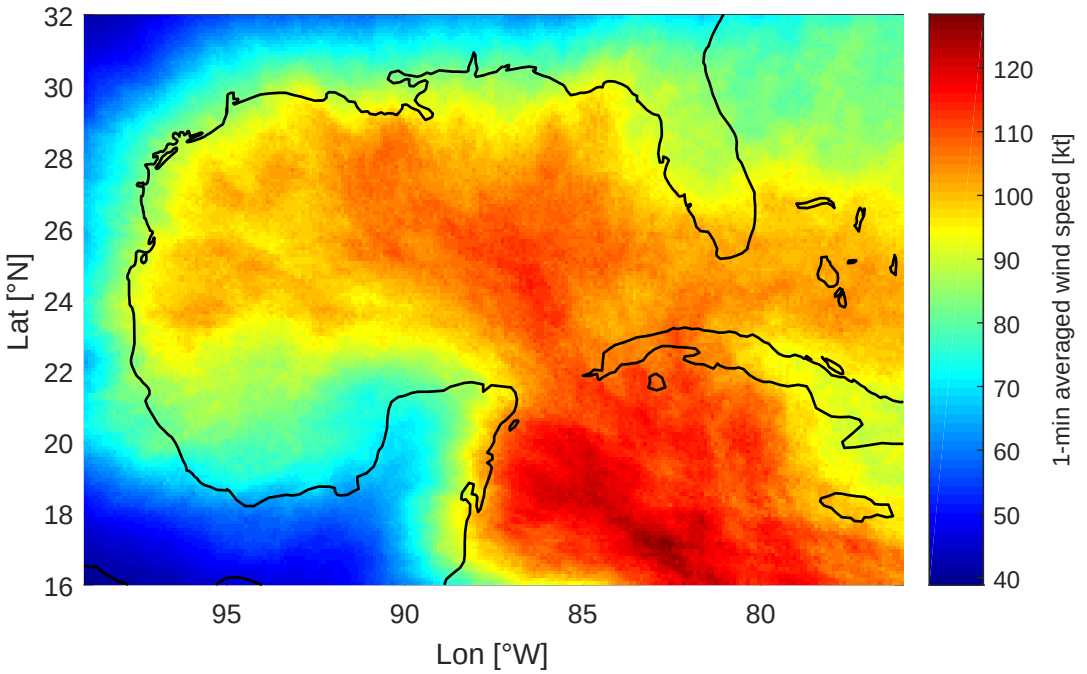

Figure 5.9 – 1 minute averaged wind speed map of the 100 year return value of the Gulf of Mexico as determined by TCWiSE with 5000 years of synthetic events based on historical cyclone track data from 1886-2015

5.3 Validation of Extreme Wind Speeds

An important reason for doing this case study in the GoM is that the region has a relatively high occurrence of TCs and that these have also been recorded up to 130 years ago. Because of this, there should be enough historical data to apply classical EVA and compare the results to the obtained extreme wind speeds from the synthetic TCs to validate the estimates. Validation of the wind speeds is done on the extremes and not on the spatial wind field of particular historical events. This is done as the applied Holland2010 wind field model is an already validated model by itself and therefore there is no additional value in validating whether this model matches historical measurements. Moreover, the aim of this study is not to be able to replicate historical wind fields, but to make reliable estimates for extreme values. Also, the assumptions made for wind inflow angles and asymmetry corrections are based on averages of many observations, and will therefore not always be a good representation of single events, but taken over many years of synthetic events, they will result in correct estimates for higher RVs. An elaborate description of the classical EVA performed on the historical data can be found in Appendix B.

5.3.1 Comparison of Return Values Obtained by EVA on Historical Data and Return Values Obtained Directly from the Synthetic TCs

The resulting estimates of V_{max} for return periods up to 200 years based on EVA on the historical data, together with the RVs obtained directly from the synthetic data and the 95% confidence intervals for both estimates, are plotted in Figure 5.10 for the 12 control

locations. In Figure C.7 in Appendix C.3 the simulated RVs are plotted versus the historical RVs. The first thing that can be seen is the great resemblance between the historical and

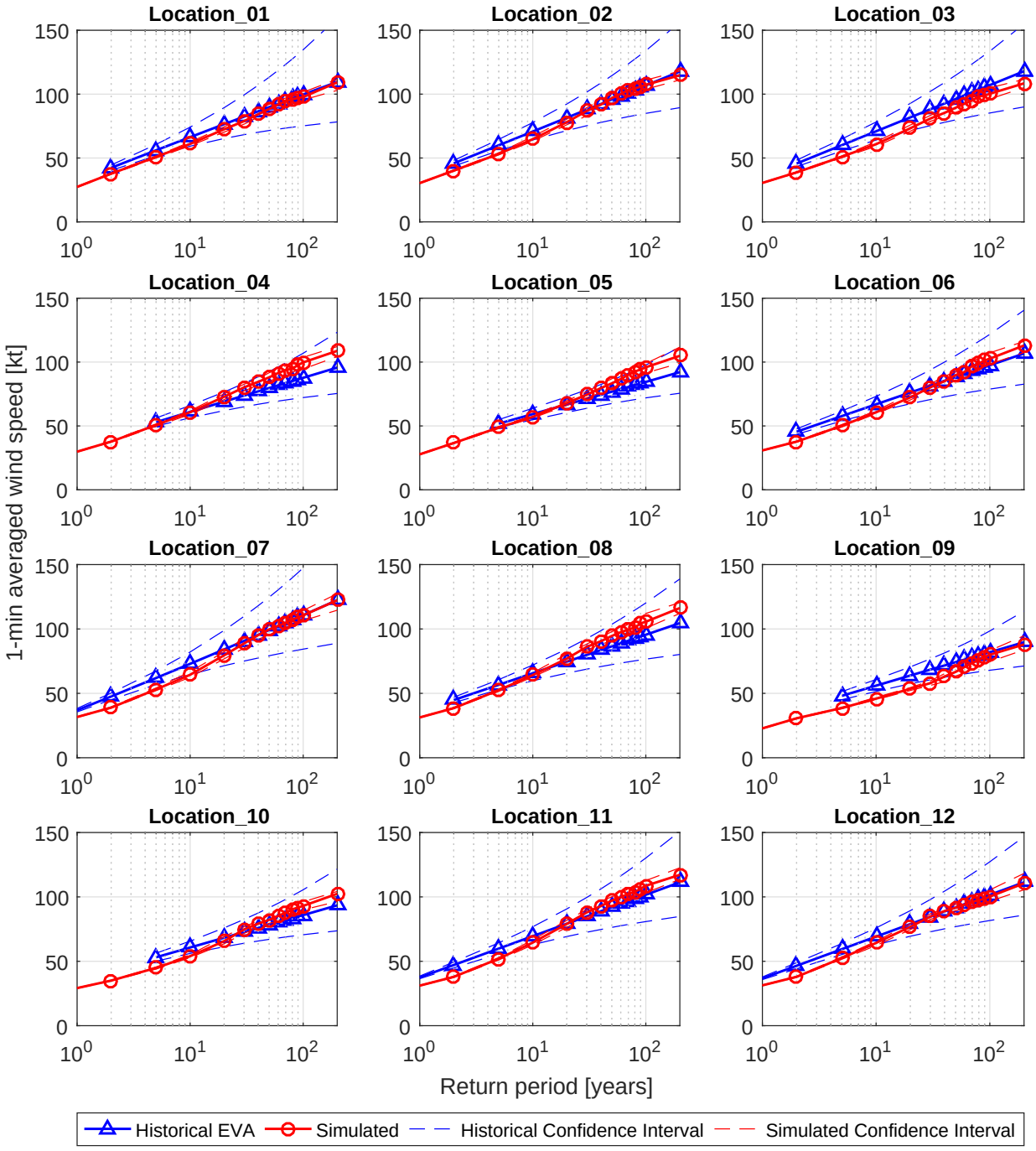

Figure 5.10 – Return values up to 200 years of 1-minute averaged wind speeds obtained from EVA on the historical data, together with the return values directly obtained from the simulated data including the 95% confidence intervals for both estimates

synthetic estimates. There appears to be no evident bias in the synthetic estimates from visual inspection. At several locations the EVA estimates are slightly higher than the synthetic ones and at other locations it is the other way around. For instance locations 1,2

and 3 all show simulated RVs which are all slightly lower than the historical RVs. Other locations such as 4 and 5 tend to have similar estimates for return periods up to 20 years after which the RVs for the simulated events slightly increase. The other locations show a slight underestimation of lower return period values and equal or higher simulated RVs for periods greater than 30 years.

As the number of years of the historical data is only 130 compared to 5000 years for the synthetic data, the confidence intervals for the EVA are much larger than those of the synthetic data. Also, as the shape parameter of the fitted GPD in the EVA for the lower and higher confidence bounds become respectively negative and positive, the confidence interval becomes much larger for greater return periods. Therefore most of the simulated estimates lie within the confidence intervals of the historical estimates, especially for greater return periods which indicates that the observed differences could be a result of fitting the GPD rather than actual discrepancies as a result of the functionality of the tool.

To quantify the accuracy of the synthetic estimates, use is made of the Normalised Mean Square Error (NMSE). In Section 5.1.1.1 the RMSE was used as a measure of goodness of fit for the fitted probability distributions to the historical data of the central pressure. In this case however, the use of the NMSE is more informative in comparing the quality of the estimates at each location as for some locations all wind speeds are larger than at other locations, which would by definition lead to larger absolute errors. By first normalising the errors this effect is adjusted for and the different scores per location can be compared. The NMSE is given by:

$$NMSE = \frac{1}{n}\sum_{i=1}^{n}\frac{(\hat{y}_i - y_i)^2}{\bar{\hat{y}}\bar{y}} \tag{5.7}$$

where $\hat{y}$ are the synthetic RVs, y the historical RVs, n the number of samples and the overbars indicate the mean over all samples. The values of the NMSE for each location sorted from low to high are given in Table 5.5.

Table 5.5 – NMSE for each location sorted from low to high

Locations	1	2	12	7	6	11	10	3	8	5	9	4
NMSE	1.3E-03	1.4E-03	2.0E-03	2.7E-03	3.4E-03	4.8E-03	6.0E-03	7.7E-03	8.5E-03	1.1E-02	1.1E-02	1.2E-02

From the NMSE it can be seen that locations 1,2 and 12 show the most agreement between the historical and synthetic estimates and locations 5,9 and 4 the least. Visually location 10 or 11 might appear to compare the worst, but other locations show a more consistent deviation from the historical estimates over multiple return periods whereas location 10 and 11 only deviate at the largest and smallest return periods.

During the validation of the generator tool in Section 4.2, a clear effect of the constant decay over land could be observed resulting in a higher probability of high wind speeds in the synthetic events which was visible at location 9 which is mostly affected by TCs that have just crossed land. The apparent overestimation of V_{max} within 200 km of the location did not result in an overestimation of higher return period values for sustained wind speed at the same location. This is remarkable as most of the higher RVs are slightly overestimated by the synthetic data, but not in location 9. It is difficult to say whether this is caused by the applied land decay function or not. Location 3 for instance also displays

slight underestimation and is hardly affected by TCs that have crossed land. Therefore the quality of the estimates of higher RVs based on the synthetic tracks do not seem to be influenced significantly by the crossing of land.

A common pattern in several locations is the increase in RVs for the greatest return periods for the synthetic data compared to the historical data. This increased difference does not necessarily mean that the synthetic estimate is incorrect or less reliable. The EVAs performed on the historical also contain a level of uncertainty as shown by the confidence interval. The GPDs were forced to have shape factors close to zero by altering the threshold to a level where this was achieved. By doing this, in some locations the threshold was relatively high and in others relatively low. This can be seen for instance at location 9 where historical estimates are only made for return periods greater than or equal to 5 years. This indicates that the threshold was close to this value as the GPD is not able to estimate return periods for values below the threshold. Therefore in some locations the fit might be more accurate for lower return periods and in other locations the fit might be slightly better for higher return periods. This is partly covered by the confidence interval but not entirely, as the interval as is shown is only valid for the statistical uncertainty of the fit of the GPD on the data above the computed threshold, but not on the selection of the threshold itself, which also introduces some uncertainty to the EVA estimates for the RVs.

Another factor that might influence the reliability of the EVA on the historical data is the limited amount of severe TCs that might have passed that location. The method of simulating synthetic events was invented because of the fact that TCs are relatively rare events and only cause severe effects very locally. It is assumed in this study, because of the fact that there are 130 years of historical cyclone data in the GoM, that the number of historical events are sufficient for predicting extremes solely with EVA while this has not been proven. Other studies have shown the inadequacy of EVA for TC conditions, although those were always based on significantly less data. To check if this might have been of influence, the number of historical events that have passed within 200 km of every control location are determined and shown in Table 5.6.

Table 5.6 – Number of historical TC occurrences within 200 km of each control location

Location	1	2	3	4	5	6	7	8	9	10	11	12
# Occurrences	66	102	97	91	64	86	101	96	75	67	96	93

Depending on the size of each event, an event within 200 km of a location will either severely or moderately affect the location. Only for very weak or small events 200 km is beyond the range of influence and therefore this distance is used here to quantify the occurrence at a location. Locations 1, 5 and 10 have had a slightly less than average occurrence rate with less than 70 occurrences in 130 years and locations 2 and 7 have had a slightly higher than average occurrence rate with more than 100 occurrences within 200 km the past 130 years. Location 1 shows a near perfect match for the RV estimates for the historical and synthetic data, thus the fact that it had less than average occurrence does not seem to have influenced the quality of the EVA at this location. The NMSE and number of occurrences at the 12 control locations have a correlation coefficient of -0.25 which would

imply that a higher occurrence rate lead to a slightly lower NMSE and therefore better fit. However, because of the limited number of locations, the correlation coefficient is not high enough in absolute terms to conclude that the correlation is statistically significant as this should be higher than 0.632 for a 2-tailed distribution with 12 observations, assuming a Gaussian distribution for the occurrences per location, for a 5% significance level as can be obtained from the table of critical values for Pearson correlation (Kendall et al., 1939). Therefore there is not enough evidence to establish a relation between the number of occurrences and goodness of fit of the historical and synthetic RVs.

The estimates based on the synthetic events are also quantitatively analysed to see if the estimates contain any bias or not. This is done separately per return period instead of for all the estimates together to better observe difference in bias for different return periods. Bias for a specific return period is computed as:

$$Bias_{RP} = \frac{1}{k}\sum_{k=1}^{12}\frac{\hat{y}_k - y_k}{y_k} \tag{5.8}$$

where k represents the location number. The computed bias per return period is shown in Table 5.7.

Table 5.7 – Return period in years together with the bias for each return period as a percentage and in kt

Return Period	5	10	20	30	40	50	60	70	80	90	100	200
Bias [%]	-11.7	-8.4	-3.6	-0.4	0.9	1.9	2.6	3.4	3.5	3.8	3.9	3.8
Bias [kt]	-6.6	-5.6	-2.7	-0.4	0.7	1.6	2.2	2.9	3.1	3.3	3.5	3.6

From the values it can be seen that averaged over the 12 control locations, the lower return periods of 5, 10 and 20 years show a slight negative bias, which means a slight underestimation of the estimates based on the synthetic data compared to the estimates based on the historical data. The estimates for 30 and 40 years show almost no bias and the RVs for return periods greater than 40 years show a constant but slight overestimation of the RVs and thus a positive bias. Since the bias at the smallest return periods is around 10%, and this is present at every location, it can be stated that the tool has a slight negative bias for return periods below 10 years. For periods greater than 10 years the bias is quite small, and also inconsistent at every location which means no evident bias can be established. Moreover, for greater return periods the confidence interval of the EVA is much larger which could also be the cause of the small bias. Therefore it cannot be established for return periods greater than 10 years that the synthetic RVs contain any bias and it seems more likely that the negative and positive biases are caused by the method of fitting the GPD to the historical data. The fact that there is a small bias for lower RVs would not affect the quality of the tool as for design purposes more interest lies in RVs greater than 10 years.

The fact that there is no clear bias across the entire basin implies that there are no crude errors in either the modelling scheme of the cyclone generation component, or in the applied spatial wind field model of TCWiSE. For the cyclone generation component this

was already expected after its own validation, but that validation only looked at entire CDFs of the synthetic versus the historical data, while the purpose of producing synthetic data is to get more information about the extremes. Since also for the extremes, the tool is capable of producing estimates which are in line with the expectations based on historical data, it can be concluded that at least for areas with a relatively frequent occurrence of TCs such as the GoM, TCWiSE does not contain any bias and is reliable in estimating extreme RVs.

6 Input Reduction

This chapter aims to test the reliability of Tropical Cyclone Wind Statistical Estimation Tool (TCWiSE) to determine extreme cyclone wind conditions in regions with rare cyclone occurrence. The historical data which was used as input for the generation of the synthetic tracks is gradually reduced in order to find the minimum amount of data required to make reliable estimates of extreme conditions. First the assumptions made are explained, together with the method of Input Reduction (IR). Afterwards the results are shown and discussed.

6.1 Methodology

In Section 5.3 it has been verified that for 130 years of historical Tropical Cyclone (TC) data in the Gulf of Mexico (GoM), the proposed method is capable of making reliable estimates for extreme wind speeds. The objective of this study however is to make reliable estimates for extreme conditions in regions with relatively low TC occurrence, which is not the case for the GoM. Unfortunately it is not possible to validate the accuracy of the method when it is applied at a different location with less historical occurrence, as the available data would be insufficient to make reliable estimates of extreme conditions with classical Extreme Value Analysis (EVA). Therefore, to replicate a situation in which less data is available, the number of historical data that has been used for predicting extremes are reduced, in order to observe the effects this has on the reliability of the tool.

6.1.1 Assumptions & Considerations

Several complications arise when doing this which require various assumptions that all have to be clarified and justified. To avoid inconsistencies in data availability for the various required parameters, the most correct method would be to identify the historical tracks for which all required data (the track coordinates, V_{max}, p_c, Radius of Maximum Winds (RMW) and Radius of 35kt Wind Speeds (R35)) is available, and determine all relations based on this data alone. Then use only this data to generate synthetic tracks, and regard these as the tracks generated based on all historical data. Subsequently, apply IR by reducing the complete tracks to a certain percentage, redefine all relations based on the reduced input, and again generate the synthetic tracks based on the new found relations and input. The complete tracks were identified by combining the three different data sources which were also used to obtain the track and size data. Many of the tracks however contained incomplete size data, and could therefore not be used. Of the 1054 initial tracks only 79 remained, and barely any of these entered the GoM as can be seen in Figure 6.1. This most

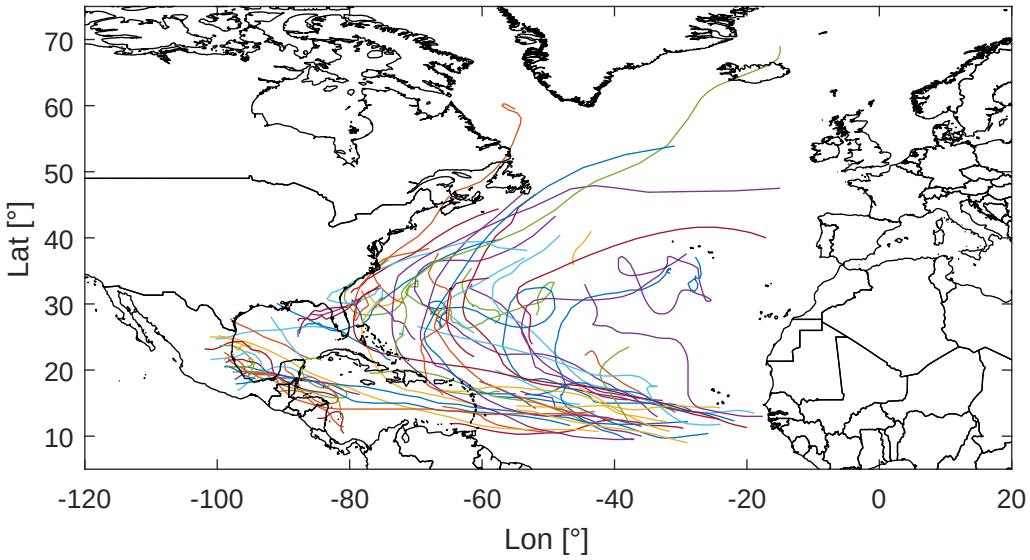

Figure 6.1 – Historic tracks for which all data being V_{max}, p_c, RMW and R35 is complete

likely has to do with missing size data near the Caribbean islands which causes tracks that are heading towards the GoM to miss data. Therefore even before generating synthetic events based on this data, it was already clear that using these tracks would not result in accurate estimates for extreme conditions and therefore this method was not applied.

As this method is thus not an option, the next difficulty lies in the decision of which input data has to be reduced and which not. The case study is performed with 130 years of data and a total of 1054 historical cyclone tracks in the entire Atlantic Basin (ATL). As the objective of this study is to apply this method in data scarce regions, instead of 1054 tracks, only a fraction of that would be available as input for the tool. For convenience, the hypothetical case of input reduction to 10% is discussed, resulting in around 105 historical tracks in an entire oceanic basin which could be a realistic scenario in data scarce areas.

Naturally, one would expect an input reduction to 10%, to apply to all the data and not only to specific segments, meaning that all historical data being tracks, intensity, central pressure and size all are reduced by selecting only 10% of the original data. Doing this however would not be comparable to the data availability in data scarce regions, and would lead to inconsistencies in data availability for two reasons:

1. The first reason is because the amount of available historical data for the different aspects of the applied method varies, which means not everything has been based on the full 130 years of historical data. Only the historical tracks and intensity data (c, θ, V_{max}) and the pressure (p_c) data consists of 130 years of complete data. This is not the case for the two parameters that describe the size (RMW and R35) of the events, as the relations upon which these parameters are determined, are constructed based on far less data than 130 years. As mentioned earlier, the sizes of TCs have only been accurately recorded since 2004, and only for several storms researchers have been able to define sizes up to 1988, although these values are not very accurate.

2. The second reason is the dependence on location which is different for each of these parameters and therefore also of influence for the amount of data available. For the

pressure, all data in the ATL was used to construct the parametric copula as no clear dependence on exact location within the ATL was visible in the data. However for both RMW and R35 only data within the GoM could be used to define a relation between V_{max} and both parameters respectively, as there was a very distinct difference between the values obtained throughout the entire ATL and only in the GoM.

These two factors were responsible for the fact that there is relatively little data for both RMW and R35, even without a reduction of the data. Reducing the input for RMW and R35 to 10% or less, would therefore result in very little data points, not enough to construct a proper relation between either and V_{max}. Moreover, doing this would not be in agreement with the amount of data available in regions with 10 times as less historical tracks available, as the used size data roughly spans only 10% to 20% of the timespan of the used track data, and therefore reducing the size data to 10% would be the equivalent of a time span reduction to 1% to 2%.

6.1.2 Description

From the above mentioned considerations it was concluded that, for the purpose of this study, the most viable method to perform IR is to only reduce the number of historical track and V_{max} data, but not the p_c, RMW and R35 data that was used to determine the joint distributions of V_{max} and the respective parameters.

To summarise:

- The reduction of the historical input in conclusion is done by selecting a certain percentage of the historical events, depending on the case, and use these to generate the synthetic tracks with their intensity V_{max}.

- The missing parameters, central pressure p_c, Radius of Maximum Winds (RMW) and Radius of 35kt Wind Speeds (R35), required to determine the spatial wind field are sampled from the same parametric copula and empirical joint distributions as were used when all data was available.

- The occurrence rate is kept identical. This means that, even though only a fraction of the original data is used, the same number of events are simulated per year as when all data was available.

For reduction to small fractions the selection of the historical events will be more important, as it is more likely that a smaller or larger fraction of the selected events will reach the GoM which is expected to have an impact on the extreme values. Nonetheless this selection method was chosen, as this is the fairest method of IR.

The occurrence rate is kept constant to be capable of determining the accuracy of the estimates of the extreme values for various return periods based on the reduced data, to the resulting estimates based on all data before any data reduction took place. Moreover, by simulating the same number of events as when all the data was used, discrepancies introduced by the process of random sampling the required parameters for the spatial wind field are also omitted. It would also not be possible to compare the results with estimates based on EVA done on the selected tracks, as EVA for TCs is not deemed accurate if little data is available because of the extremely local effects caused by each TC.

As a result, to be precise, this approach tests how reliable the tool is in areas with little overall observations, not necessarily a low occurrence rate, although one could argue whether there is any difference between the two. In both cases the same number of storms are used as input to generate synthetic events and therefore the stochastic variation in both is identical thus both resulting in synthetic events that belong to the same random process. The only difference would be the number of storms generated per year simulated.

6.1.3 Input Reduction Cases

To find a relation between the available amount of data and the accuracy of the tool, multiple cases of IR to different fractions are run. For each case, the same number of tracks as for the historical case will have to be generated as the occurrence rate is kept constant, resulting in approximately the same amount of storms ending up in the GoM for which the spatial wind field should be determined. This number might differ per set as the fraction of the generated events that enters the GoM is a function of a random process. Running a single set requires a significant amount of computational effort and therefore time, and thus a selection was made on which input fractions are run and on how many runs were done per selected input fraction.

The selected fractions and their characteristics are shown in Table 6.1. In the sets with the least amount of input a total of 53 historical tracks will be selected from the entire ATL of which approximately only 23 will enter the GoM. Ten different sets are run for each fraction. This is done to be able to correctly compare the variation in the different sets. Running a different number of sets for each fraction would yield a biased picture of the actual variation present which would make it difficult to compare the different fractions. Running more sets per fraction would be preferred as a sample size of 10 for each fraction is not that big, but as mentioned because of the fact that the whole process is quite time consuming, the number of sets that could be run was limited.

Table 6.1 – Information about the different sets ran with reduction of the input

Variable	IR Fraction			
	0.5	0.2	0.1	0.05
Number of input storms	527	211	105	53
Approximate number in the GoM	228	91	45	23
Number of sets	10	10	10	10
Number of storms generated per set	40538	40538	40538	40538

6.2 Results

The results of each set are compared with the results based on all data, which is seen as the reference case. Unlike for the validation of the extreme wind speed maps as in Section 5.3, where validation was only possible at several locations because of the computational effort of performing EVA at each grid cell, comparison of results can be done at every

grid cell, as both the reference case and IR cases have results at each grid cell. Only grid cells within the buffer zone drawn around the GoM as shown in Figure 5.8 are included in the results. The Return Values (RVs) are compared for specific return periods which are 2 years, 5 years, 10 to 100 years with 10 year intervals and 200 years. The focus will however be on the 100 year RV as this shows the clearest picture and makes it easier to discuss the results. Moreover, since the different RVs are not independent, doing this does not disregard the results of the other RVs. This is shown by the fact that the Normalised Mean Square Error (NMSE) over all return periods per grid cell, and the square error of the 100 year RV per grid cell have a Pearson's linear correlation coefficient of 0.91 with a large sample size as the domain has many grid cells and thus statistically significant. For a description of Pearson's linear correlation coefficient see equation 5.2. Thus stating that the two are not independent and conclusions that are made based on the 100 year RV also hold for other RVs. The 100 year RV maps of all 40 sets are shown in Figures 6.2 and 6.3.

First, the general trends that have been observed are discussed. Special attention is given to the effect of having more or less historical occurrences within the vicinity of an exact location, to the effect of the presence or absence of several high intensity events in the historical input and also to the difference in accuracy above land or water. Although wind speeds above land are not of interest for the purpose of this study, it can be useful to identify possible limitations introduced by the proximity of land. Afterwards, a more quantitative relation between the magnitude of the error and the number of historical data available is sought.

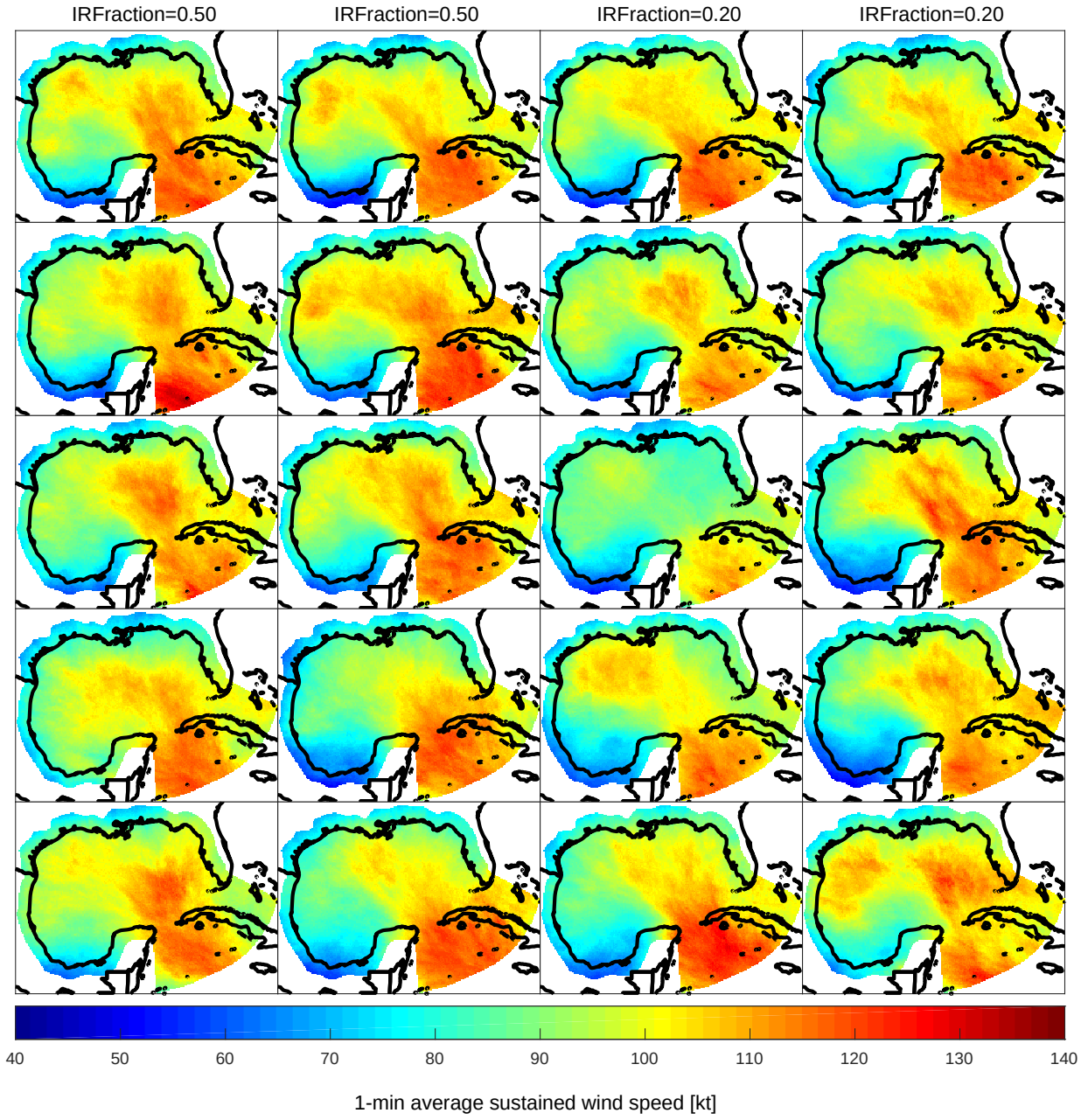

Figure 6.2 – 1-minute averaged wind speed maps of the 100 year RV of the Gulf of Mexico for all 10 sets each with 50% and 20% respectively of the original historical cyclone track data from 1886-2015

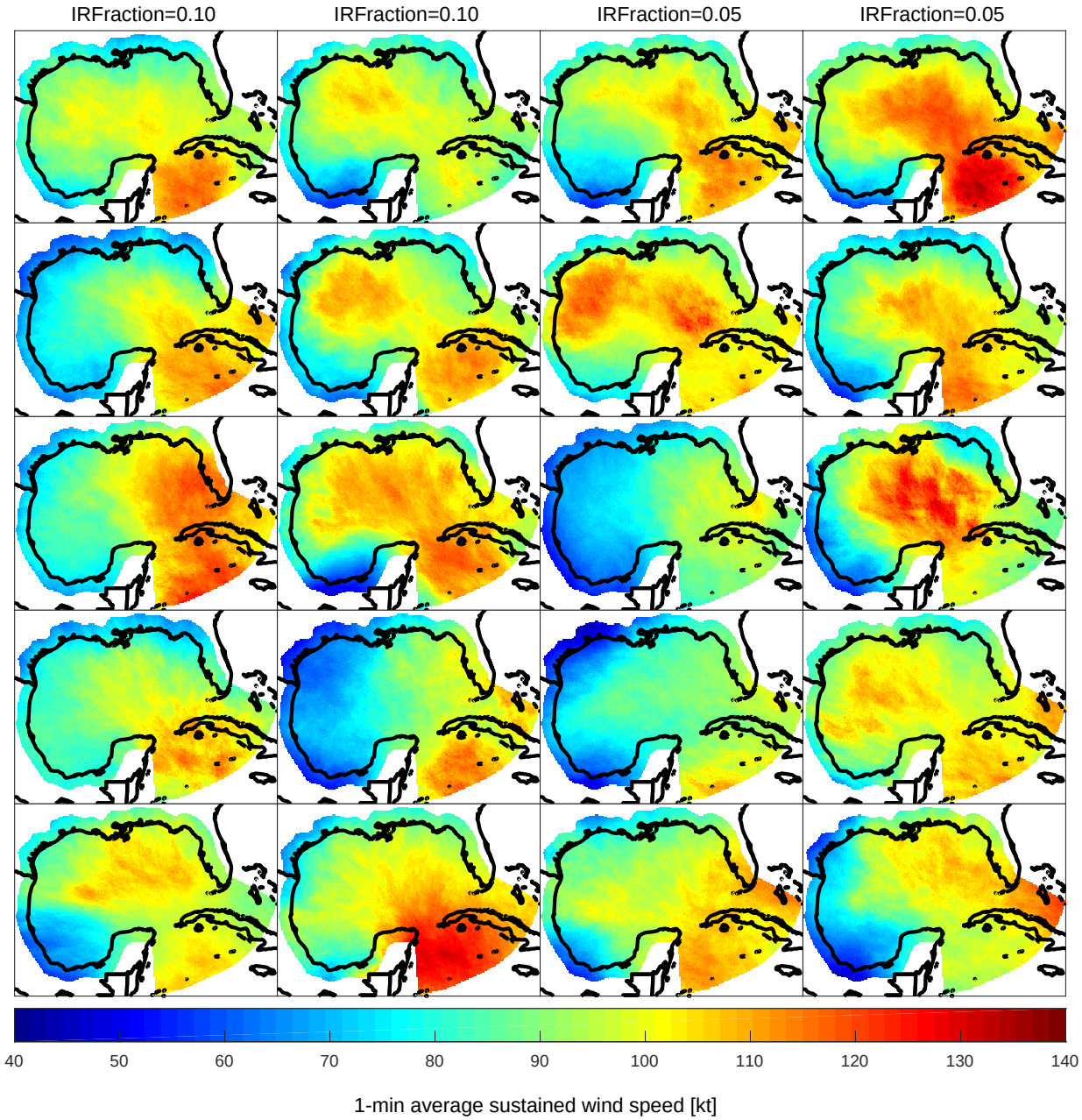

Figure 6.3 – 1-minute averaged wind speed maps of the 100 year RV of the Gulf of Mexico for all 10 sets each with 10% and 5% respectively of the original historical cyclone track data from 1886-2015

6.2.1 Observable Trends

The maps in Figures 6.2 and 6.3 show the results for each IR set, but are little informative without additional statistics. To get a better insight into the results for the different input fractions, the average of the mean, standard deviation and Coefficient of Variation (CV) of the 100 year RV over all grid cells above land and water, are shown in Table 6.2. The reduction fraction of 1 refers to the base case where all input was used. As only one set of 5000 years has been simulated for this case no standard deviation or CV is available. For more detail, in Appendix D in Figures D.1 and D.2, maps are shown of the average 100 year RV, the standard deviation and the average absolute error over the 10 sets per fraction respectively. Additionally Figure 6.4 shows a boxplot for each set of 5000 years with the normalised error per grid cell as a percentage of the results based on all input.

Table 6.2 – Average over all grid cells located above water and above land respectively, of the mean (μ) and standard deviation (σ) in kt and the Coefficient of Variation (CV) of the 100 year RVs per IR fraction, together with the number of historical events used as input.

IRFrac	1	0.50			0.20			0.10			0.05		
Parameter	μ	μ	σ	CV	μ	σ	CV	μ	σ	CV	μ	σ	CV
Water	99.5	99.5	3.6	0.04	97.5	6.1	0.06	98.0	7.5	0.08	93.2	9.9	0.11
Land	81.0	83.2	3.2	0.04	83.2	5.6	0.07	83.7	7.2	0.09	81.5	9.9	0.12
# Hist[1]	1054.0	527	-	-	211	-	-	105.0	-	-	53.0	-	-
# Dom[2]	456.0	229.9	7.4	0.03	94.7	7.9	0.08	46.3	5.0	0.11	22.2	3.5	0.16
# 200km[3]	81.0	41.2	11.7	0.28	16.8	6.0	0.36	8.3	3.4	0.41	3.8	2.2	0.57

[1] Hist represents the total number of historical events in the entire Atlantic Basin used as input for the generation of synthetic events
[2] Dom represents the total number of historical events that entered the GoM that were used as input for the generation of synthetic events
[3] 200km represents the average number of historical events within 200km of each grid cell that were used as input for the generation of synthetic events

The general trend that can be observed is that as the input reduces, the mean starts to deviate more from the reference case and the standard deviation starts to increase. This is visible from both Table 6.2 as from Figure 6.4 which clearly show an increased variation as the input decreases and also a deviation of the mean. This is moreover visible from the correlation between the observed error and the IR fraction as shown in Table 6.3. The table shows Pearson's linear correlation coefficient, unless otherwise stated, between various pairs of variables over all 40 sets. Table 6.4 shows correlations per IR fraction to avoid biases in the correlation. Whether these correlations are statistically significant depends on the sample size and the correlation. All computed correlations that are statistically significant to a level of 5% are highlighted in bold.

For each set the number of selected events that actually entered the GoM differed, and therefore some sets had less historical data within the GoM to serve as input for the tool. To check whether this had any influence, the notion of adjusted input reduction fraction is introduced, which is the input fraction of the entire set, slightly adjusted for whether a larger or smaller fraction than for all historical data has entered the GoM. A correlation

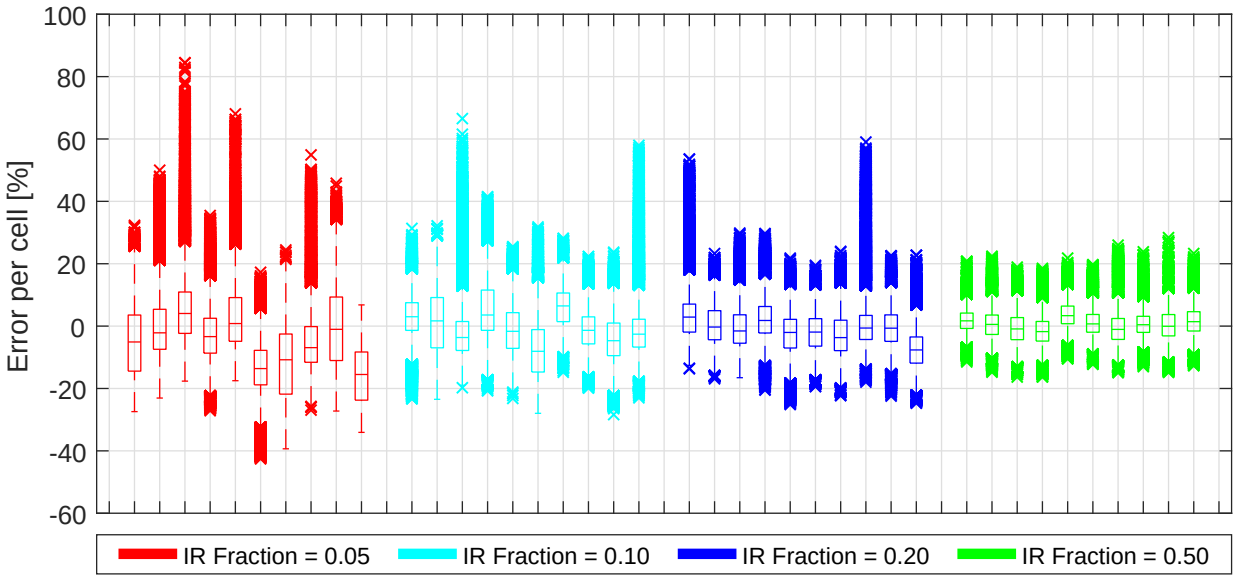

Figure 6.4 – Boxplot of the error per cell within the domain as a percentage of the estimate without IR, with a single boxplot per run set, separated by colour for each IR fraction. The middle line represents the median of the data, the edges of the box represent the 25th and 75th percentiles respectively and the whiskers represent the 99th percentiles. The markers represent all outliers beyond the 99th percentile.

coefficient of -0.62 between the Mean Square Error (MSE) per set and IR fraction was computed and between the adjusted IR fraction and MSE a coefficient of -0.64. This shows an increase in error for a reduction in input as is expected. The difference in correlation between the two is minimal, implying that the difference in fraction that went into the domain has a limited influence on the RVs.

From Figures 6.2 & 6.3 and the figures in Appendix D it can be observed that as less input is used to generate results, the level of detail in the maps is significantly reduced. Figures 6.2 & 6.3 show the 100 year RV maps for each of the 40 sets. For IR fractions of 0.50 one can still observe the intricate shape of the original map, however for lower fractions only a few sets show the same shape, others nothing like it. If the figures in Figure D.1 are compared to Figure 5.9, one can clearly see that the shape of the original map slowly starts to reduce to a much more uniform, rounded map as the input decreases. It should be noted that the map in Figure 5.9 is based on 1 set of data whereas the maps in Figure D.1 are averages over 10 different sets of input. Nonetheless they do show that the actual level of detail present in extreme wind speed maps is very dependent on the amount of historical data available. From Figure D.2 it can be observed that the standard deviation significantly increases as the input decreases. Per IR fraction the locations that show the highest standard deviation seem relatively random, showing no clear relation between specific locations and their characteristics.

Notable in Table 6.2 is the fact that for smaller input fractions the mean is always lower than the original mean, implying that the RVs are generally slightly underestimated as less data is available. This could be caused by many different factors which are investigated by looking at the correlation between different variables.

Two causes for a decrease, or negative bias, in the 100 year RV seem plausible, which

are that there is a strong correlation between the error and number of historical occurrences within the domain or near each grid cell, or that there is a strong correlation between the error and the intensity of the selected events. Both causes will be discussed separately, after which the effect of land on the accuracy of the estimations is discussed.

Table 6.3 – Pearson's linear correlation coefficient between pairs of variables per set unless otherwise specified resulting in a single observation per set. Numbers in bold are determined statistically significant to a level of 5%.

Correlated Variables		ρ
NMSE per Cell	RV 100 MSE	**0.91**
RV 100 MSE	IR Fraction	**-0.62**
RV 100 MSE	Adjusted IR Fraction	**-0.64**
RV 100 Bias	IR Fraction	0.28
RV 100 Bias	Adjusted IR Fraction	0.30
RV 100 MSE	Historical Occurrences in the GoM	**-0.64**
RV 100 MSE	Absolute Deviation of Historical Occurrence Fraction in the GoM	**0.41**
RV 100 Bias	Historical Occurrences in the GoM	0.30
RV 100 Bias	Absolute Deviation of Historical Occurrence Fraction in the GoM	-0.14
RV 100 MSE	Highest Observed V_{max} in the GoM	**-0.65**
RV 100 MSE	Average of the 2 Highest Observed V_{max} in the GoM	**-0.65**
RV 100 MSE	Average of the 5 Highest Observed V_{max} in the GoM	**-0.71**
RV 100 MSE	Average of the 10 Highest Observed V_{max} in the GoM	**-0.76**
RV 100 Bias	Highest Observed V_{max} in the GoM	**0.45**
RV 100 Bias	Average of the 2 Highest Observed V_{max} in the GoM	**0.38**
RV 100 Bias	Average of the 5 Highest Observed V_{max} in the GoM	**0.39**
RV 100 Bias	Average of the 10 Highest Observed V_{max} in the GoM	**0.41**

Table 6.4 – Pearson's linear correlation coefficient between pairs of variables over all sets or per input reduction fraction. Numbers in bold are determined statistically significant to a level of 5%.

Correlated Variables		Correlation per IRFrac			
		0.50	0.20	0.10	0.05
RV 100 MSE	Absolute Deviation of Historical Occurrence Fraction in the GoM	-0.26	0.04	0.56	-0.19
RV 100 MSE	Historical Occurrences in the GoM	-0.36	-0.46	-0.30	-0.38
RV 100 MSE Cell	Land / Water [1]	**0.02**	**0.02**	**0.03**	**-0.03**
RV 100 MSE Cell	Historical Occurrences within 200km per Cell	-0.01	**-0.12**	**-0.08**	**-0.24**
RV 100 MSE Cell	Absolute Deviation of Historical Occurrence Fraction within 200km per Cell	**0.06**	**-0.05**	**0.03**	**0.12**
RV 100 Bias	Absolute Deviation of Historical Occurrence Fraction in the GoM	-0.08	-0.18	-0.22	0.33
RV 100 Bias	Historical Occurrences in the GoM	0.06	0.31	0.50	0.64
RV 100 Bias Cell	Land / Water [1]	**0.25**	**0.26**	**0.23**	**0.24**
RV 100 Bias Cell	Historical Occurrences within 200km per Cell	**-0.07**	**0.08**	**0.06**	**0.17**
RV 100 Bias Cell	Absolute Deviation of Historical Occurrence Fraction within 200km per Cell	**0.09**	**0.09**	**0.09**	-0.02
RV 100 MSE	Highest Observed V_{max} in the GoM	-0.24	-0.34	0.02	-0.38
RV 100 MSE	Average of the 2 Highest Observed V_{max} in the GoM	-0.09	-0.22	0.11	-0.15
RV 100 MSE	Average of the 5 Highest Observed V_{max} in the GoM	-0.20	-0.33	0.33	-0.44
RV 100 MSE	Average of the 10 Highest Observed V_{max} in the GoM	-0.28	-0.56	0.49	-0.51
RV 100 Bias	Highest Observed V_{max} in the GoM	-0.57	0.27	0.44	0.34
RV 100 Bias	Average of the 2 Highest Observed V_{max} in the GoM	-0.63	0.27	0.25	0.16
RV 100 Bias	Average of the 5 Highest Observed V_{max} in the GoM	-0.50	0.26	0.28	0.44
RV 100 Bias	Average of the 10 Highest Observed V_{max} in the GoM	-0.18	0.35	0.21	0.53

[1] Instead of Pearson's correlation a Point Biserial correlation is used which describes the correlation between a continuous and a dichotomous variable

6.2.1.1 Effect of the Number of Historical Occurrences

When looking at historical occurrences, there are three occurrence statistics which are discerned from one another which all have different correlations with the observed error. Occurrence statistics per cell have a much larger sample size than occurrence per set, which makes the correlations based on them more statistically significant. Correlation coefficients for these statistics are computed both with the Mean Square Error of the 100 year RV (RV 100 MSE) and with the actual error (RV 100 Bias) to investigate the correlation both with the error in an absolute sense and with the bias of the error.

The total number of events that entered the domain for a given set: First correlations to the number of historical events within the domain are reviewed. Over all 40 sets as shown in Table 6.3, the correlation coefficient is -0.64 with the MSE and 0.3 with the bias. This clearly shows the effect of having more historical data. The more total data, the smaller the error and the higher the estimates. Also per IR fraction the MSE is negatively correlated with the number of historical occurrences both per set and per cell. Per set there is a stronger correlation, however it is less significant as the sample size is much smaller. The average bias per set is positively correlated to the number of historical occurrences for a small input fraction, although only statistically significant to 10%. Assuming that this correlation is not attributed to chance, this implies that when there is little data, a small increase in the number of occurrences over a larger area significantly increases the RV estimates of the synthetic data over the entire area.

The occurrence within the direct vicinity, 200 km, of a grid cell: The correlation of the MSE with the occurrences in the vicinity of a cell is strongest for the smallest IR fraction. this implies that the more historical occurrences there have been close to a grid cell, the better is the prediction of extreme wind speeds. This is also the fact for the correlation with the bias, which is negative for the largest input fraction, and positive for the smallest input fraction. This means, that when less overall data is available, having more data in the direct vicinity of the grid cell has a positive effect on the extreme wind speeds.

The deviation of the fraction of events that have entered the GoM from the number of events used as input in the Atlantic basin, compared to this fraction for all data without reduction of the input: From the correlations to the absolute deviation of the fraction of historical events within the domain or near a cell, it can be seen that there is little correlation, sometimes positive and sometimes negative, and in most cases not statistically significant. As for some fractions the coefficients are positive and for others negative, and all quite small, it can be concluded that it is important for the accuracy of the extreme wind speed estimates to have as much historical events in the vicinity as possible, regardless of whether the occurrence rate is close to the true occurrence rate.

6.2.1.2 Effect of Intensity of the Selected Historical Events

The other possible main cause for lower or less accurate estimates of extreme values could be the absence or presence of high intensity events in the domain among the selected events. To investigate this, the correlation coefficients between the MSE or bias and the magnitude

of V_{max} of the most intense event, and the average of V_{max} of the 2, 5 and 10 most intense events respectively for all sets together and per IR fraction have been computed and shown in Table 6.3. From the correlation coefficients between the MSE and the magnitude of the most intense events in the domain, which lie between -0.65 and -0.76, it can be noted that the absence of several high intensity events from the historical data has an impact on the obtained RVs. It should be noted that the number of historical events in the domain, and the value of the highest or average of the few highest historical observed values of V_{max} in the domain are heavily correlated, with a coefficient of 0.63 for the highest V_{max}, 0.71 for the average of the 2 highest, 0.79 for the average of the 5 highest and 0.88 for the average of the 10 highest. This makes it difficult to draw conclusions on what the effect of the highest V_{max} on the accuracy of the estimations is, as it could also be the effect of the number of historical events in the domain. Nonetheless, as the correlations are all slightly higher than the correlation between the number of occurrences and the error, and the fact that the correlation between the number occurrences, and highest values of V_{max} is not only 0.63, it can be concluded that high intensity events do have a clear positive impact on the accuracy of the estimations.

For the correlations per IR fraction none of the correlation coefficients between either the MSE or bias, and the intensity of the selected events in the domain are statistically significant. This does not necessarily mean they can not be used for interpretation of the results, but just that they are not conclusive as the sample size of 10 is quite small. For the IR fraction of 0.10 the correlations are positive while the others are negative. This would mean that the selection of high intensity events from the original data lead to an increase in error, which is counter intuitive as the distribution of maxima in the historical events are generally determining for the maxima of synthetic events. Because the coefficients are not statistically significant, it is assumed that the observed coefficients are a result of the small sample size, and not of the correlation present between the variables.

The correlations between the bias and the intensity of the selected events also display notable behaviour. When 50% of the input is used, selection of more intense historical events resulted in a decrease of the bias and thus of the synthetic estimates of the 100 year RV. Most likely this is the case since for a reduction to 50% of the data, still roughly 230 events reach the domain, leading to very small differences in the highest values of V_{max} and small differences in error which are most likely caused by other factors and not by the selection of high intensity events. For smaller IR fractions the difference between the top high intensity events becomes larger as well as the magnitude of the error, thus displaying a more evident correlation between those two variables with a smaller probability that the observed correlation is caused by other factors or by a small sample size.

6.2.1.3 Effect of whether Grid Cells are Located above Land or Water

If one compares the 100 year RV estimates of the grid cells located above land to those located above water in Table 6.2, one can see that for the land estimates the mean appears to increase slightly for the sets with less input, while the estimates over water noticeably decrease ass less input is provided. An explanation for this effect could be the land decay function that is applied. In the first case without reduction of the data, the decay over land is well represented in the historical data and therefore also in the local intensity changes. That, together with the linear decay as applied, resulted in rapid decay as happens in actual

events making landfall. As less data is used as input, a larger search area is required per grid cell to collect data, and therefore the very local decay at landfall is not always accurately represented in the Probability Density Functions (PDFs) for the change in sustained wind speed. In this case, only the linear decay function reduces the intensity of the synthetic events which explains the increase in the estimates for the 100 year RV for lower IR fractions. The reason for the fact that the average 100 year RV over land for the smallest IR fraction is slightly lower, most likely has to do with the fact that the estimates above water have also significantly reduced which naturally causes a reduction in the values above land as well.

To investigate if there is any difference in accuracy present between grid cells above land and grid cells above water, the correlation between the error and whether grid cells are located above land or water is computed. Since being above land or water is not a continuous but a dichotomous variable, Pearson's linear correlation can not be used and therefore the Point Biserial correlation is used which is suitable for determining correlation between one continuous variable and one dichotomous variable. This is done by defining being over land or water as a boolean variable, and assigning a 1 to all cells located above land and a 0 to all cells located above water. Subsequently the correlation is computed by (Linacre, 2008):

$$r_{pb} = \frac{M_1 - M_0}{s_n} \sqrt{\frac{n_1 n_0}{n^2}} \tag{6.1}$$

Where M_1 is the mean of all values given a 1, in this case the values above land, and M_0 the mean of all values given a 0, in this case all values above water. s_n is the standard deviations of all values above land and water, n_1, n_0 are the number of points above land and water respectively and n is the total number of points. The significance is determined by the statistic:

$$r_{pb} \sqrt{\frac{n_1 + n_0 - 2}{1 - r_{pb}^2}} \tag{6.2}$$

which is the same as an unpaired t-test which follows a student t distribution with $n - 2$ degrees of freedom when the null hypothesis that the correlation is zero is true (Linacre, 2008). From the correlation with the MSE it can be seen that there is a very small correlation between how well the RVs are estimated and whether a point is located above land or not. The correlation coefficients vary between -0.03 and 0.03 for the different IR fractions but are significant because of the great amount of data points, which implies there officially is some correlation, although in some cases positive and others negative. The correlation between the actual error or bias and land or water however is much stronger with a coefficient of about 0.25 for all IR fractions, which means that over land the bias with IR is generally more positive. This again has to do with the less severe land decay present as explained earlier.

6.2.2 Relation between reliability of the estimation of return values and the number of historical occurrences

So far a few conclusions were made based on the results which are:

1. More historical occurrences within the domain of interest leads to better estimates.

2. A deviation of the occurrence rate of number of storms entering the GoM does not influence the estimates.

3. Reduction of input generally leads to an underestimation of the RVs.

4. High intensity events are important in determining the RV estimates, especially when less input data is available.

5. Less input most likely leads to an underestimation of the decay of TCs above land, and thus to an overestimation of RVs above and very close to land.

These findings are quite general but also useful for understanding when the tool is applied in data sparse areas. Nonetheless they do not present any direct relation between the available historical data and the accuracy of RV estimates and therefore it was tried to do define a more quantitative relation by looking at the increase in error for the decrease in available data.

This is mainly done by studying the plots in Figure 6.5 and Figure 6.6, combined with the occurrence numbers in Table 6.2. As mentioned earlier, there are different occurrence rates that can be discerned and for this purpose the historical occurrence within the direct vicinity, in this case 200km is used, and the total number of events that have reached the GoM, which is a much larger area. To compare the area of the GoM with the area in the direct vicinity, the radius of the GoM would be approximately 750km, if the domain were described by a circle, which means the surface area is 14 times larger than that of the direct vicinity. For both cases a relation is for determining the accuracy in data scarce areas.

6.2.2.1 Relation Between the Reliability of the Estimates and the number of Historical Events in the Direct Vicinity of a Location

Figure 6.5 shows boxplots of the error per grid cell as a percentage of the estimate for that cell in the reference case of the 100 year RV, with separate boxplots for a small range of historical events within 200 km range of each grid cell. For each range of events a maximum of 4 boxplots are shown, one for each IR fraction. If less than 4 boxplots are shown for a certain number of events, it means that there were no observations in that range for the specific IR fraction. For the lowest number of occurrences, between 0 and 2, no green boxplot is shown as there were no grid cells for the IR fraction of 0.50 that had that few historical events within a 200km range. The same goes for more than 45 historical occurrences within 200km, as only for the IR fraction of 0.50 there were that many historical events within the vicinity, and not for the other fractions leading to the absence of boxplots for the other fractions. Each boxplot displays the error distribution of all grid cells in the domain from that IR fraction with a specific number of occurrences. The boxes show the median and the 25^{th} and 75^{th} percentiles respectively. The whiskers or dashed lines reach out to the 99^{th} percentiles. All markers signify the outliers beyond the 99^{th} percentile. In figure D.3 in the Appendix the figure is presented separately for each IR fraction, with lines displaying the median and specific percentiles instead of boxplots.

When more than 30 historical events have been observed within 200km distance from a grid cell, 99% of all estimates will have a maximum error of 10%. From 20 to 30 observations this increases to 20% and from 10 to 20 observations this increases to 25%. For less

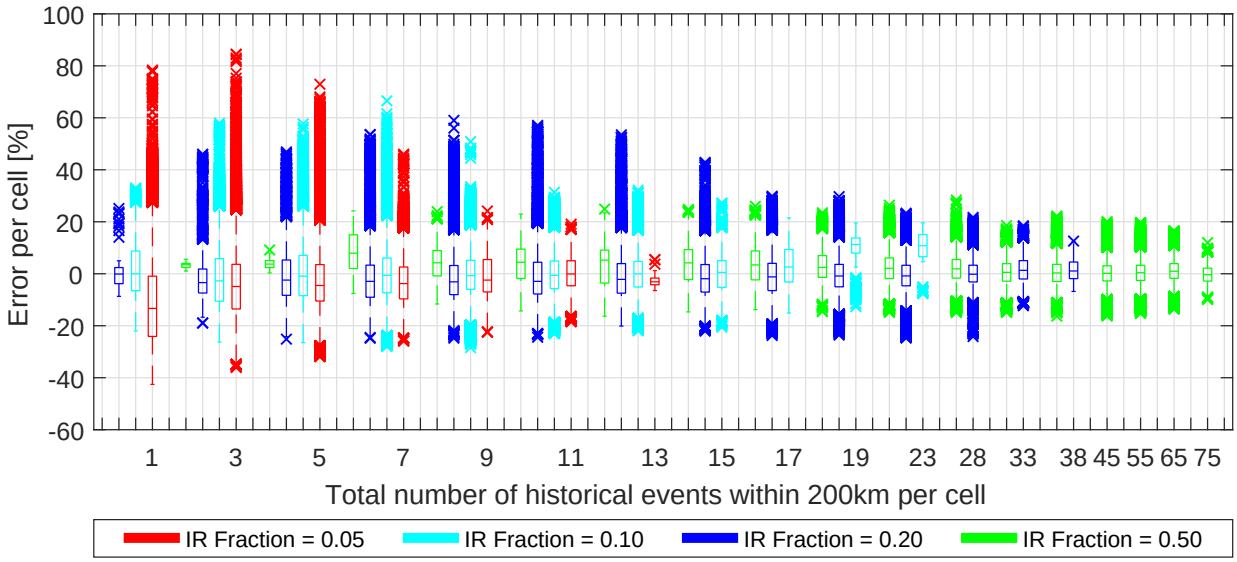

Figure 6.5 – Boxplot of the error per cell within the domain of the 100 year RVs versus the number of historical occurrences within 200 km of the cell, as a percentage of the estimate without IR, separated by colour for each IR fraction. The horizontal line represents the median of the data, the edges of the box represent the 25th and 75th percentiles respectively and the whiskers represent the 99th percentiles. The markers represent all outliers beyond the 99th percentile.

than 10 observations this increases to as much as 40%. Overall there is a trend of increasing error for less historical occurrences, but when one looks to the different IR fractions individually this relation is not as clear. For high occurrence rates for a specific IR fraction, i.e. approximately 70 for a fraction of 0.50, 35 for a fraction of 0.20, 20 for a fraction of 0.10 and 10 for a fraction of 0.05, the error is quite small, after which the error increases as the occurrence rate decreases until a certain maximum after which the error decreases again. The maximum error clearly increases for a reduction in total input, up to 80% difference for some cells with an IR fraction of 0.05 and only 0 to 4 historical occurrences in the vicinity. As these errors fall beyond the 99th percentile, they are considered to be outliers and not representative for errors that would be observed when this method is applied at other locations.

From these observations it is clear that besides a relation between the accuracy and the number of events in the direct vicinity, there also is a strong relation between the IR fraction and the error. Thus the following can be concluded for a relation between the number of historical events within 200 km of a location and the magnitude of the error of the extreme wind speed estimations:

- An exact quantitative relation between the magnitude of the error and the number of events within 200km of a grid cell, without involving other variables such as in this case the IR fraction, but in other cases most likely the number of events used as input for the tool or within a much larger range than 200 km from the location of interest, would have a very large variance.

- When more than 20 historical cyclones have been recorded within 200 km of a single location, the error will be no larger than 20% not considering outliers beyond the 99th percentile.

- When more than 10 historical cyclones have been recorded within 200 km of a single location, the error will be no larger than 25% not considering outliers beyond the 99th percentile.
- When less than 10 historical cyclones have been recorded within 200 km of a single location, and thus in data scarce regions, the error could be as large as an underestimation of 40%, or an overestimation of nearly 30% not considering outliers beyond the 99th percentile.

6.2.2.2 Relation Between the Reliability of the Estimates and the Number of Historical Events in the Gulf of Mexico

A more linear relation seems to be present between the average accuracy of the whole region and the number of events in the GoM. This can more clearly be seen from the boxplot in Figure 6.6 which shows the average error over all cells within the domain per set, divided per IR fraction. This means that every boxplot shown in the figure is made up of 10 data points, 1 for each set that has been run for that fraction. On the x-axis the IR fraction is shown, and not the number of events in the GoM, because of the limited variation in the number of occurrences caused by the limited number of reduction fractions that were run. In the figure a very clear trend is visible of reduction in accuracy for a reduction in input. From the previous figure it was clear that single cells could have a large deviation from the actual RV, but it was also visible that for every IR fraction many cells only had an error less than a couple percent.

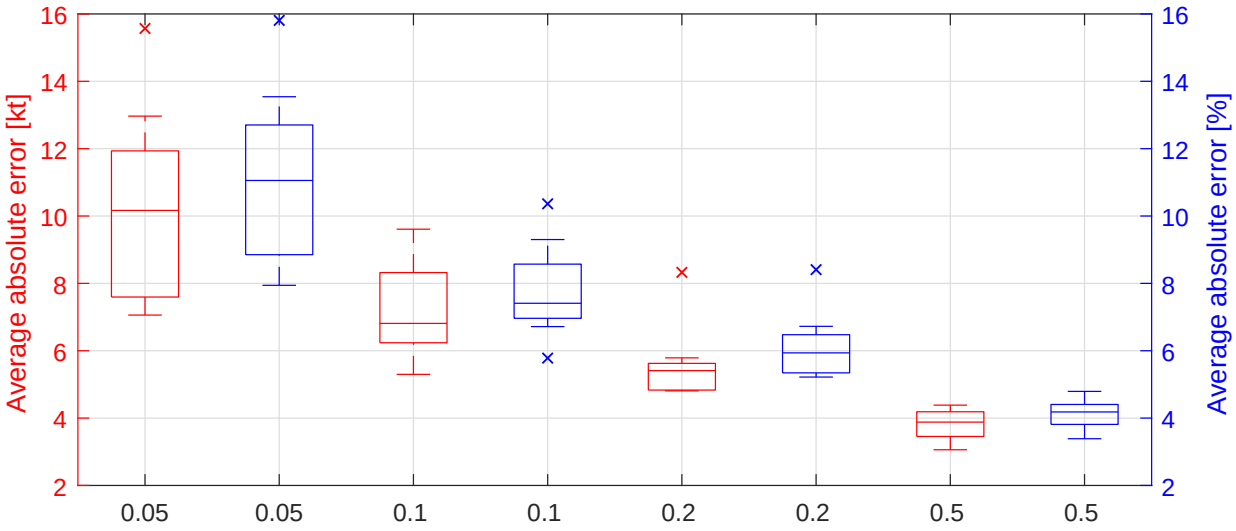

Figure 6.6 – Boxplot of the average absolute error over all grid cells per set in kt (red) and as a percentage of the estimate without IR (blue) within the domain of the 100 year RVs for each IR fraction. The horizontal line represents the median of the data, the edges of the blue box represent the 25th and 75th percentiles respectively and the black whiskers represent the 95th percentiles. The red markers represent all outliers beyond the 95th percentile.

By looking at the average absolute error over all grid cells, one gets a better idea about the magnitude of the error and thus the accuracy of the estimations over a larger area. If 50% of the input were used, which comes down to 456 events in the ATL of which

approximately 222 reached the GoM, the average error for all 10 sets remained less than 5% and 5kt. As this is still a large amount of data, this does not say anything about data scarce areas, but it does prove that the tool is capable of reproducing similar output for different input. For 20% or on average 95 events entering the GoM per set, the accuracy remains within 5% to 8% which reduces to 6% to 11% for 10% of the data or around 45 events entering the GoM and a total of 105 events used as historical input in the entire ATL. As for this amount of data on average around 8 events have directly affected a single location, i.e. came within 200 km, this is labelled as a data scarce region. An accuracy of 10% over a larger region therefore is quite a good result which could be very useful for determining design conditions in the region. Ordinary EVA for non cyclone winds or waves would have a similar accuracy.

If the input is reduced further, to a total of 53 events in the ATL and on average 22 events reaching the GoM per set, which comes down to an average of 3.8 within 200km of a single location, the accuracy rapidly decreases. The least accurate set had an average deviation of 16% from the original estimates and the most accurate a deviation of 7%. The trend in error versus amount of data shows that from this point on, if the data is further reduced, the error will rapidly increase. A deviation of only 7% on average is very usable for design purposes, but more than 16% on average over the entire domain becomes quite troublesome.

As only 4 different input reduction fractions were run there was little variation in the number of historical events that entered the GoM. Running more fractions would have provided enough data to be able directly link the error to the number of historical events over a larger area. This relation is most likely exponential, as can already be seen from Figure 6.6. The average error approximately multiplies with a factor of 1.5 for a reduction of the data by a factor 2. If the input would have been reduced further, the expectations are that the error would also increase significantly up to the point where the results would no longer be useful for design purposes.

7 Discussion

In this study the Tropical Cyclone Wind Statistical Estimation Tool (TCWiSE) has been developed to determine extreme Tropical Cyclone (TC) wind speeds and studied its accuracy in data scarce regions. Besides, recommendations are given on what kind of wave model to use in combination with the tool to determine extreme TC wave conditions. In this chapter the contributions to the literature and the application of the tool in other data scarce areas than investigated in the case study are discussed, together with the limitations of the tool.

7.1 Accuracy and Application of TCWiSE in Data Scarce Regions

In Chapter 6 the accuracy of the tool in data scarce areas was investigated by using a reduced amount of input, to simulate a situation in which less data is available. From this analysis several relations between variables were found such as a probable underestimation of extreme wind speeds when little data is available, and a slight overestimation very close to or above land. One of the objectives of this study was to define a relation between the number of historically observed events within the direct vicinity of a location, and the accuracy of estimates made by the tool for extreme wind speeds. From the results it was found that for less than 10 historically observed events within a range of 200 km of a location that at least once during their lifetime attained a maximum sustained wind speed of 50 kt, the 100 year return period could be underestimated by 40% or overestimated by nearly 30%, with outliers beyond the 99^{th} percentile to overestimations of 80% for several grid cells. However, it was also found that the total number of events used as input for the tool, or the number of historical observations in a much larger region surrounding a specific location, has more impact on the accuracy of the estimations than the number of observed events in the direct vicinity. When 45 events were observed in the entire Gulf of Mexico (GoM), the accuracy everywhere in the GoM, even if less than 5 events were observed in the direct vicinity, was within 20%.

These conclusions are only based on findings from the case study in the GoM, as the tool has only been applied and validated here, and not at other locations that actually suffer from rare cyclone occurrence. This was done as the obtained results at such locations could not be validated. Nevertheless, the investigation of the accuracy of this method in data scarce areas is a valuable contribution to the literature, as there have been no other studies where this has been done, and because of the necessity of an adequate method to determine extreme TC conditions in data scarce regions. As the tool has so far only been applied

in the GoM, the application of the tool at actual data scarce locations is discussed here together with the obstacles one would have to overcome when doing so.

In this study, while the input for the tracks and intensity was reduced to validate the accuracy, the same joint distributions to determine the central pressure and wind speed radii were used in the input reduction cases, as were used when all data was available. Doing so did not allow for uncertainty in the determination of the central pressure and wind radii to be represented in the accuracy as is determined for the tool. This is nevertheless not expected to have a large impact on the accuracy in data scarce regions. Central pressure data is not severely dependent on exact location, and therefore in regions with rare cyclone occurrence, central pressure data obtained from a larger area could be used to determine a joint distribution. As for size data, because of the greater dependency on location, data scarcity is a bigger issue for determining a joint distribution.

To deal with this issue, one approach would be to define global joint distributions between multiple parameters such as maximum sustained wind speeds, central pressure, Radius of Maximum Winds (RMW), Radius of 35kt Wind Speeds (R35) and possibly other wind radii, which also depend on the location in terms of longitude and latitude. Unlike the currently available relations between various parameters such as maximum sustained wind speed and central pressure, or central pressure and RMW, this relation should allow for variance in sampling as the observed relation between the variables are far from deterministic. The approach of using parametric copulas as done in this study for the joint distribution of the central pressure and maximum sustained wind speed is therefore seen as a valuable contribution to the literature in representing the variance between cyclone parameters. Further improving this by allowing for dependency between multiple variables, for example by the use of parametric vine copulas, is seen as the next step. Doing this would not entirely solve data scarcity for the parameters required for spatial wind field determination, but does provide a substantiated method for determining them.

In this study the tool has been tested to a minimum of 53 historical events used as input of which approximately 20 entered the GoM per case that has been run. There are areas where data scarcity is more severe than this. The most extreme example of this is in the South Atlantic where a single hurricane has been recorded to hit the coast of Brazil. Assuming size and pressure parameters could be determined with the use of globally defined relations as just described, this would still leave a big question mark for the intensity and track propagation and also for the occurrence rate. As the tool is based on statistics of historical events, having only a single record would result in the synthetic events behaving relatively similar to the observed event. While generating synthetic events in this case, difficulties arise when a generated event attains characteristics or a combination of characteristics not yet observed in the area. As in that case the tool has no historical data available to sample from, alternatives should be discovered in order to predict or estimate the behaviour in such cases. This is not only the case for Brazil, but in many other regions it is also likely that not for all possible combinations of cyclone parameters there is enough data to sample from.

One possibility would be the use of structured expert judgement to determine probability distributions for the cases of which no data is available. This is done by scoring a panel of experts, in this case on their capability to assess uncertainty regarding cyclone characteristics, and combining their judgement to determine the quantities of interest based

on their performance as uncertainty assessors. Another option would be the use of other numerical models that rely more on physics than statistics, to complement the tool in case there is not enough data to base predictions on historical statistics alone.

Without such improvements and adaptations, the tool is currently not seen as a reliable option to determine extreme conditions in the case of Brazil. At other data scarce regions it is advised to use all available data in the entire basin, and not only the events that affected the specific location of interest. An example of this is the Arabian Sea, where only 2 severe events have affected the 1000 km coastal stretch of Yemen, and another 2 the coastal stretch of Oman with similar length. Doing this would result in similar data availability as is tested in this study and therefore a similar level of accuracy can be expected.

7.2 Limitations of TCWiSE

TCWiSE can be divided in two main parts, the first being the generation of synthetic tracks with the coordinate of the eye, the heading, forward speed and maximum sustained wind speed with 6-hourly intervals, and the second being the determination of the spatial wind field around the eye by determining the missing parameters and applying an empirical spatial wind field model. The limitations in both these parts are discussed separately.

7.2.1 Generation of Synthetic Tracks

The generation of the synthetic tracks in the model was based on an already functioning tool by Rego et al. (2016). Many aspects have been changed but some were not changed which could affect the accuracy of the tool. The tool uses a Markov Model where the changes in track and intensity are solely depending on the values in the previous step. Another popular method is the auto-regressive model. In this study no comparison has been made between the two methods which leaves the question of which method would perform better. The tool uses the maximum sustained wind speed instead of central pressure as the parameter to represent the intensity of the synthetic events. Although the wind speed is generally more defining for the damage caused by a TC, many researchers that have used an Empirical Track Model (ETM) have instead used central pressure as the main intensity parameter. This is mainly done because of the more reliable and accurate measurements of historical pressure data compared to wind speed data. Nevertheless maximum sustained wind speed has been used in this study which might therefore introduce slight discrepancies.

A linear decay model for intensity when the events are located above land, instead of an exponential decay function is used in the tool. As was concluded from the results, when many data is available, the decay above land is represented well in the distribution functions for the intensity. However, when less historical data is available, grid cells have to obtain data from a larger area, resulting in a poorer representation of this decay close to and above land and therefore wind speed estimations very close to or above land are likely to be overestimated slightly.

Overall there are very few physical aspects present in the tool as everything is based on characteristics observed in history. If cyclone characteristics are expected to behave identically as over the last decades, this method proves accurate for the determination of extremes. However, with regard to global warming and climate changes, it remains

questionable whether this is the case. High Sea Surface Temperatures (SSTs) were identified as the main energy source feeding TCs. If SSTs continue to rise, possibly also the intensity and frequency of TCs will increase. An increase in cyclone occurrence was already visible in the historical data, but not applied in the tool as the cause for this rise is uncertain. In this study SSTs were only used to validate historical genesis locations, but have not been used for either the determination of cyclone genesis, its intensity or termination.

The tool uses a rather crude limit for the maximum sustained wind speed. This limit is based on historically observed wind speeds and the fact that there is a physical limit for maximum sustained wind speed which depends on physical factors such as SST and humidity. In other research by Emanuel (1988) this dependency on physical factors of the maximum intensity was implemented by introducing the notion of Relative Intensity (RI). This however had the downside that when synthetic events left warm water areas, their intensity drastically decreased while there have been historical events that maintained high wind speeds even over colder waters. Nonetheless some sort of dependency of intensity on the SST seems appropriate.

Another physical aspect that is absent in the tool is the presence of Coriolis. The Coriolis force is responsible for the spiralling nature of TCs and this force reduces to zero at the equator. Because of this, cyclones are unable to cross the equator or come too close to it. As the tool tends to overestimate events that approach the equator, changes in heading are only accepted if they turn synthetic events away from the equator when they come within 10 degrees of latitude of the equator. This is however an arbitrary statement and not directly linked to the underlying physics. Statements that would express the physical relation between the intensity or propagation direction and Coriolis would improve the accuracy of the tool near the equator.

From the validation of the synthetic tracks it was clear that the tool performed very well on larger spatial scales, in this case multiple grid cells or a couple hundred km, but had difficulties in replicating very local changes. This happens because of the necessity to obtain historical data from larger areas surrounding a grid cell. In data scarce regions this area becomes larger, as the density of historic data is less and the same amount of data is required to construct Probability Density Functions (PDFs) to sample the change in the variables. Therefore spatial detail in cyclone patterns or extreme intensities tend to spread out over a larger area. This effect increases for a reduction in input.

7.2.2 Determination Spatial Wind Field

To determine the spatial wind field around the eye, the tool has adopted the Holland2010 (Holland et al., 2010) empirical spatial wind field model combined with corrections to account for asymmetry by Lin and Chavas (2012) and for the inward spiralling nature of TCs by J. A. Zhang and Uhlhorn (2012).The use of the Holland2010 model was preferred over the older Holland1980 model because of the overestimation of wind speeds further away from the eye by the Holland1980 model. The spatial wind field model is an approximation of the actual wind field and only uses one additional wind radius. Historical events have shown deviation from this simplified representation of the wind field, as there have been recordings of events with multiple peaks further away from the eye. Wind fields of the synthetic events are therefore not as detailed as wind fields of historical events. However, as the extreme wind speeds for specific return periods are determined based on the wind

fields of thousands of synthetic events, this simplified representation will barely influence the estimates, although the exact influence is unknown.

To apply the spatial wind field model, besides the maximum sustained wind speed also the central pressure, RMW and R35 are required. Instead of using relations found in literature, a parametric Gumbel copula was used to determine the central pressure, and empirical joint distributions were used to determine the RMW and R35. This was done as the existing relations were considered to be too deterministic, while historically there has been plenty of variation around the determined relations. The parameters are determined with limited dependency. Central pressure has been determined being only dependent on the maximum sustained wind speed with data of the entire Atlantic basin. Both the RMW and R35 were determined only with data obtained in the GoM, where RMW was only dependent on the maximum sustained wind speed and R35 on both the RMW and the maximum sustained wind speed. By only using data from a certain area, dependence on location is also implied. In reality all theses parameters are dependent on one another although the exact level of dependency between all parameters has not been investigated in this study. Not taking into account the dependencies between all variables introduces slight discrepancies in the determination of the spatial wind field distribution around the eye, which in turn could affect estimates for extremes.

The method of using a parametric Gumbel copula to model the dependency between the maximum sustained wind speeds and the central pressure resulted in a continuous relation between the two which displayed the tail dependency between the variables in an accurate matter. For the other two variables empirical joint distributions have been used. A more comprehensive approach by applying multiple parametric copulas combined with a vine structure was deemed out of the scope of this study. The use of empirical joint distributions resulted in a discrete and not continuous relation between the variables which therefore also is responsible for slight discrepancies in the results.

8 Conclusions & Recommendations

In this chapter the final conclusions of this study are stated by answering the research questions. Subsequently recommendations for further research are given which either follow from the conclusions or have been derived from the limitations of the tool as discussed in Section 7.2.

8.1 Conclusions

Difficulties in determining extreme Tropical Cyclone (TC) conditions, whether these are rain, wind, wave or storm surge conditions, mostly come from the fact that severe adverse effects caused by TCs are very local. This is the case because the exact track, intensity and size of the storm determines to a large extent which area is affected the most and what the consequences are for the hydraulic conditions. Small variations in any of these parameters can greatly influence the conditions at any location. This is already the case in regions which suffer relatively often from TCs. In regions that do not suffer as regularly from TCs, data scarcity makes it even more difficult to anticipate adverse consequences. In these regions TCs are nevertheless often responsible for the most severe conditions, and the effects of such events should therefore be quantified in order to be able to prepare for such conditions. For extreme cyclone wave conditions specifically, there is an additional problem of feasibly determining extreme wave conditions from cyclone wind conditions.

This research presents the Tropical Cyclone Wind Statistical Estimation Tool (TC-WiSE) to determine extreme TC wind speeds and focused on the determination of its accuracy in data scarce regions. Moreover, a brief qualitative assessment of the available TC wave models has been performed in order to identify an adequate method to feasibly determine extreme TC wave conditions from TC wind conditions. In this study regions with rare TC occurrence are defined by having a historical record of less than 10 historical cyclone events in the direct vicinity of a location which in this study is taken as 200km, not including locations that have never been affected by any events in the region or locations far outside the tropics. In this case all historical cyclone events that have reached 1-minute averaged wind speeds of over 50 kt at least once during their lifetime, instead of the normal threshold of 64 kt, are used as historical events to increase the available amount of data.

To achieve the objective of this study several research questions and sub-questions have been formulated. These questions are answered below. For an elaborated discussion on the functionality and limitations of the tool the reader is referred to Chapter 7.

1. *What is an adequate method according to literature to:*

a. Deal with Tropical Cyclone data scarcity for the purpose of determining extreme wind conditions?

The simulation of synthetic cyclones by means of randomly sampling TC characteristics from probability distributions constructed with the characteristics of the historical cyclone events is determined as an adequate method to deal with data scarcity as explained in Section 2.3. This method offers an approach which models possible future cyclones while relating a probability to each of these events making it possible to determine extreme conditions for specific return periods.

b. Determine extreme Tropical Cyclone wave conditions from Tropical Cyclone wind data?

If there is significant computational capacity available, applying 1-dimensional, or low resolution 2-dimensional numerical wave models to a large number of synthetic TCs would be the preferable option in order to determine extreme TC wave conditions. In case computational power is a bottleneck, using empirical cyclone wave models, or using the determined extreme wind speeds together with assumptions for wind direction, would serve as the next best option in order to determine extreme wave conditions as explained in Section 2.2.2. However, in this study non of these methods have been tested and therefore this statement does come with uncertainty.

2. What are the main characteristics of the developed tool?

a. How accurate, in terms of % of the error, are wind speed estimates for the 100 year return period in regions with rare cyclone occurrence?

Define regions with rare cyclone occurrence as regions that have a historical record of less than 10 events within a 200 km radius, that at least once during their lifetime attained a maximum sustained wind speed of 50 kt. The results of this study show that the normalised error for the 99^{th} percentile could be up to an underestimation of 40% or an overestimation of 25%. Observations beyond the 99^{th} percentile are considered as outliers, but showed overestimations as much as 80%.

b. What is the minimum amount of historical cyclone data that is required in order to make estimations of the 100 year extreme wind speed with a maximum normalised error of 20%?

When more than 20 historical events have been recorded within a range of 200 km, a normalised error of less than 20% has been observed for all grid cells, considering observations beyond the 99^{th} percentile as outliers. However, when more historical events have been recorded in a larger area surrounding a location, not only in the direct vicinity, the accuracy increases. In this study when at least 45 historical events had been recorded inside the Gulf of Mexico (GoM), of which at least 10 in the direct vicinity of a location, a maximum normalised error of 20% was also observed, considering observations beyond the 99^{th} percentile as outliers.

c. Is there a direct relation between the number of historical occurrences within 200km and the accuracy of the estimations for the 100 year return period?

From the results it is clear that, in general, more historical occurrences in the direct vicinity of a location lead to higher accuracy in estimates of extreme values. However, the number of historical events in a larger area surrounding a single location is just as important, or maybe even more important for the accuracy of extreme value estimations.

Moreover, other variables, such as the number of high intensity events in the region, also have an impact on the accuracy of extreme value estimates. Therefore deriving a relation between the number of occurrences and the accuracy of extreme values, without involving other parameters, is possible but would come with large uncertainty.

d. Is there spatial variability in the accuracy of the estimation?

From the results it was clear that there is spatial variability present in the accuracy of the estimations. This is caused by several aspects. Firstly, cyclone wind speeds are overestimated above, and very close to land. In data scarce regions this effect becomes larger. As the density of historic data is less and the same amount of data is required to construct Probability Density Functions (PDFs) to sample the change in the variables, grid cells have to obtain their data from a larger area surrounding a cell. This results in an inadequate representation of the decay of cyclone wind speeds in probability distributions for change in intensity close to land. Secondly, areas with more historical occurrences in the direct vicinity show better estimates, even on small spatial scales in the order of 500 km to 1000 km.

8.2 Recommendations

Based on the conclusions and the limitations of the tool as discussed in Chapter 7 several recommendations are made for application, further research and improvement of the tool.

- When applying the tool in data scarce areas, it is advised to use all available data in the entire basin, and not only the events that affected the specific location of interest. Doing this would often result in similar data availability as is tested and therefore a similar level of accuracy can be expected.

- Increase the number of physical aspects present in the tool. With regard to global warming and climate change, cyclone occurrence and intensity might increase. By linking these parameters to physical parameters such as Sea Surface Temperature (SST) these changes can be taken into account. Addition of other physical processes such as Coriolis could also improve the tool.

- Develop global joint distributions between cyclone characteristics with interdependencies between all variables and with dependency on location that allow for variance in sampling. These distributions could be used in data scarce areas, to deal with data scarcity for these parameters in the region of interest.

- Allow for temporal variation in the number of synthetic events per year or month. When more physical aspects are used, temporal variation becomes more important as many physical aspects are season dependent. Allowing for temporal variation would also make it easier to allow for change in cyclone occurrence rate.

- Apply an exponential decay model to the cyclone intensity when located above land. Especially in data scarce areas, cyclone decay is not represented well enough in the tool and therefore exponential decay is more appropriate.

- Investigate the use of structured expert judgement to complement the tool. For several components such as future occurrence rate or behaviour of synthetic events for conditions do not have any historical observations, the use of experts could improve the performance of the tool.

- Investigate the use of numerical models to complement the tool in estimating quantities that do not have any historical observations. Similarly to expert judgement, numerical models that rely more on the physical aspects of TCs instead of the statistical aspects, could prove useful in improving the performance of the tool.

- Elaborate the input reduction study in order to improve the found relation between the accuracy of the tool and the amount of historical data. In this study only 4 different fractions with 10 sets for each fraction have been investigated at one location. An increase in the number of fractions and the number of sets is therefore recommended and possibly also the study at another location with frequent cyclone occurrence, possibly the Western North Pacific.

- To speed up the tool it could be written in another programming language than Matlab, such as Python.

References

Alves, J.-H. G., Tolman, H. L., & Chao, Y. Y. (2005). Hurricane-Generated Wind-Wave Research at NOAA/NCEP.

Anderson, T. (1984). An Introduction to Multivariate Statistical Analysis.

Batts, M. E., Cordes, M. R., Russel, L. R., Shaver, J. R., & simiu, E. (1980). Hurricane Wind Speeds in the United States. *Journal of the Structural Division*, *106*(10), 2001–2016.

Bowyer, P. J., & MacAfee, A. W. (2005). The Theory of Trapped-Fetch Waves with Tropical Cyclones— An Operational Perspective. *Weather and Forecasting*, *20*(3), 229–244.

Brabson, B. B., & Palutikof, J. P. (1999). Tests of the Generalized Pareto Distribution for Predicting Extreme Wind Speeds. *Journal of Applied Meteorology*, *39*, 1627–1640.

Brzeźniak, Z., & Zastawniak, T. (2000). *Basic Stochastic Processes: a course through exercises*. Springer Science & Business Media.

Calverley, M. J., Szabo, D., Cardone, V. J., Orelup, E. A., & Parsons, M. J. (2005). Wave Climate Study of the Caribbean Sea.

Camargo, S. J., Barnston, A. G., & Zebiak, S. E. (2005). A statistical assessment of tropical cyclone activity in atmospheric general circulation models. *Tellus A*, *57*(4), 589–604.

Chen, S. S., & Curcic, M. (2016). Ocean surface waves in Hurricane Ike (2008) and Superstorm Sandy (2012): Coupled model predictions and observations. *Ocean Modelling*, *103*, 161–176.

Chi, X., & Goodwin, B. (2012). A High-Dimensional, Multivariate Copula Approach to Modeling Multivariate Agricultural Price Relationships and Tail Dependencies.

Darling, R. (1991). Estimating Probabilites of Hurricane Wind Speeds Using a Large-Scale Empirical Model. *Journal of Climate*, *4*(10), 1035–1046.

Deltares. (2010). Orca Extreme Toolbox.

DeMaria, M., Knaff, J. A., & Kaplan, J. (2005). On the Decay of Tropical cyclone Winds Crossing Narrow Landmasses. *Journal of Applied Meteorology and Climatology*, *45*, 491-499.

DeMaria, M., Pennington, J., & Williams, K. (2015). The Tropical Cyclone Extended Best Track Dataset. http://rammb.cira.colostate.edu/research/tropical_cyclones/tc_extended_best_track_dataset/.

Dietrich, J. C., Westerink, J. J., Kennedy, A. B., Smith, J. M., Jensen, R. E., Zijlema, M., ... Cobell, Z. (2011). Hurricane Gustav (2008) Waves and Storm Surge: Hindcast, Synoptic Analysis, and Validation in Southern Louisiana. *Monthly Weather Review*, *139*, 2488–2522.

Emanuel, K. (1988). The Maximum Intensity of Hurricanes. *Journal of the Atmospheric Sciences*, *45*(7), 1143–1155.

Emanuel, K., Ravela, S., Vivant, E., & Risi, C. (2006). A Statistical Deterministic Approach to Hurricane Risk Assessment. *Bulletin of the American Meteorological Society (BAMS)*, *87*(3), 299–314.

Fearon, G. (2014). Extreme Wind Speeds for the South-West Indian Ocean Using Synthetic Tropical Cyclone Tracks.

Francis, M. (2011). Galileo's Pendulum. https://galileospendulum.org/2011/08/29/hurricanes-on-earth-hurricanes-on-jupiter/.

Genest, C., & Favre, A.-C. (2007). Everything You Always Wanted to Know about Copula Modeling but Were Afraid to Ask. *Journal of Hydrologic Engineering*, *12*(4), 346–368.

Georgiou, P. N. (1983). Design Wind Speeds In Tropical Cyclone-prone Regions. *Journal of Wind Engineering and Industrial Aerodynamics*, *13*(1-3), 139–152.

Georgiou, P. N., Davenport, A., & Vickery, B. (1983). Design Wind Speeds in Regions Dominated by Tropical Cyclones. *Journal of Wind Engineering and Industrial Aerodynamics*.

Graham, S., & Riebeek, H. (2006). Hurricanes: The Greates Storms on Earth. *NASA Earth Observatory*. http://earthobservatory.nasa.gov/Features/Hurricanes/.

Hasselmann, K., Barnett, T., Bouws, E., Carlson, H., Cartwright, D., Enke, K., ... Walden, H. (1973). Measurements of wind-wave growth and swell decay during the Joint North Sea Wave Project (JONSWAP). *Dtsch. Hydrogr. Z.*, *8*, 95.

Holland, G. J. (1980). An Analytic Model of the Wind and Pressure Profiles in Hurricanes. *Monthly Weather Review*, *108*(8), 1212–1218.

Holland, G. J., Belanger, J. I., & Fritz, A. (2010). A Revised Model for Radial Profiles of Hurricane Winds. *Monthly Weather Review*, *138*, 4393–4401.

Holthuijsen, L. H. (2007). *Waves in Oceanic and Coastal Waters*. Cambridge university press.

IBTrACS. (2014). International Best Track Archive for Climate Stewardship. https://www.ncdc.noaa.gov/ibtracs/.

International Research Institute, Columbia University. (2017). Climate Data Library. http://iridl.ldeo.columbia.edu/SOURCES/.NOAA/.NCEP/.EMC/.CMB/.GLOBAL/.Reyn_SmithOIv2/.climatology/.c7100/.sst/DATA/2/STEP/.

Jäger, W., & Morales-Nápoles, O. (2016). Joint Time Series Modelling of OceanWaves'

Significant Heights and Peak Periods with Vine-Copulas.

James, M., & Mason, L. (2005). Synthetic Tropical Cyclone Database. *Journal of waterway, port, coastal, and ocean engineering*, *131*(4), 181–192.

Kendall, M. G., Kendall, S. F. H., & Babington Smith, B. (1939). The Distribution of Spearman's Coefficient of Rank Correlation in a Universe in which all Rankings Occur an Equal Number of Times:. *Biometrika*, *30*(3/4), 251–273.

Laing, A. (2011). Introduction to Tropical Meteorology. http://www.goes-r.gov/users/comet/tropical/textbook_2nd_edition/navmenu.php_tab_9_page_1.0.0.htm.

Landsea, C., Franklin, J., & Beven, J. (2014). The revised Atlantic hurricane database (HURDAT2).

Leontaris, G., Morales-Nápoles, O., & Wolfert, A. (2016). Probabilistic Scheduling of Offshore Operations Using Copula Based Environmental Time Series - An Application for Cable Installation Management for Offshore Wind Farms. *Ocean Engineering*, *125*, 328–341.

Lin, N., & Chavas, D. (2012). On Hurricane Parametric Wind and Applications in Storm Surge Modeling. *Journal of Geophysical Research*, *117*(D9).

Linacre, J. (2008). he Expected Value of a Point-Biserial (or Similar) Correlation. *Rasch Measurement Transactions*, *22:1*, 1154.

Liu, B., Liu, H., Xie, L., Guan, C., & Zhao, D. (2011). A Coupled Atmosphere–Wave–Ocean Modeling System: Simulation of the Intensity of an Idealized Tropical Cyclone. *Monthly Weather Review*, *139*(1), 132–152.

Malilay, J. (1997). Tropical Cyclones. *The Public Health Consequences of Disasters by E.K. Noji*, *207*, 227.

Matsui, N., Compo, G. P., & Hartten, L. M. (2011). Estimating Tropical Cyclone Central Pressures for Reanalysis of Global Fields. *Monthly weather review*.

McAdie, C. J., Landsea, C. W., Neumann, C. J., David, J. E., & Blake, E. S. (2009). National Hurricane Center. Tropical Cyclones of the Noth Atlantic Ocean, 1851 – 2006. http://www.nhc.noaa.gov/outreach/history/.

Meza-Padilla, R., Appendini, C. M., & Pedrozo-Acuña, A. (2015). Hurricane-Indunced Waves and Storm Surge Modeling for the Mexican Coast. *Ocean Dynamics*, *65*(8), 1199–1211.

National Weather Service. (2017). Houston IAH Extremes, Normals, and Annual Summaries. http://www.weather.gov/hgx/climate_iah_normals_summary.

Nguyen, B. (2015). Long-Term Regional Simulation of Tropical Cyclones Using a Generalized Stochastic Empirical Storm Model, A Case Study in the North Pacific.

Nicholls, R. J., Mimura, N., & Topping, J. (1995). Climate Change in South and Southeast Asia: Some Implications for Coastal Areas. *Journal of Global Environmental Engineering*, *1*, 137–154.

NOAA. (2014). Frequently Asked Questions. *Hurricane Research Division*. http://www.aoml.noaa.gov/hrd/tcfaq/F1.html.

NOAA. (2016). Automated Tropical Cyclone Forecast (ATCF) "Archive Data Files / Text Files" . ftp://ftp.nhc.noaa.gov/atcf/archive/.

NOAA Hurricane Research Division. (2016a). Hurricanes in History. http://www.nhc.noaa.gov/outreach/history/.

NOAA Hurricane Research Division. (2016b). Record Number of Storms by Basin. http://www.aoml.noaa.gov/hrd/tcfaq/E10.html.

Patton, A. (2003). Andrew Patton's Matlab code page. http://public.econ.duke.edu/~ap172/code.html.

Powell, M., Soukop, G., Cocke, S., Gulati, S., Morisseau-Leroy, N., Hamid, S., ... Axe, L. (2005). State of Florida hurricane loss projection model: Atmospheric science component. *Journal of Wind Engineering and Industrial Aerodynamics*, *93*, 651–674.

Rego, J., & Minns, T. (2016). Mozambique - Coastal Flooding Hazard Assessment.

Rego, J., van Ormondt, M., & Vatvani, D. (2016). Cyclone Generator Methodology with a Focus on Southwest Indian Ocean.

Russel, L. B. (1968). Probability distributions for Texas gulf coast hurricane effects of engineering interest. PHD Thesis.

Samenow, J. (2017). Harvey marks the most extreme rain event in U.S. history. *The Washington Post*, *August 29*. https://www.washingtonpost.com/news/capital-weather-gang/wp/2017/08/29/harvey-marks-the-most-extreme-rain-event-in-u-s-history/?utm_term=.28b5c673dab4.

Scheff, S. W. (2016). *Fundamental Statistical Principles for the Neurobiologist*. Academic Press.

Schott, T., Landsea, C., Hafele, G., Lorens, J., Taylor, A., Thurm, H., ... Zaleski, W. (2012). The Saffir-Simpson Hurricane Wind Scale. *NOAA/National Weather Service [Internet]*, 1–4.

Scowcroft, G., Ginis, I., Knowlton, C., Yablonsky, R., Morin, H., & McIntire, D. (2015). Hurricanes: Science and Society. University of Rhode Island (URI) Graduate School of Oceanography (GSO) http://www.hurricanescience.org/science/science/hurricanelifecycle/.

Sklar, A. (1959). Fonctions de Réparition à n Dimensions et Leurs Marges 8. *Publications de l'institut statistique de l'Université de Paris*, 229–231.

Smith Warner International ltd., & Deltares. (2012). Regional Risk Reduction Initiative, Final Phase 3 Report.

The MathWorks, Inc. (2016). Matlab 2016a.

Tryggvason, V., Davenport, A., & Surry, D. (1976). Predicting wind-induced response in hurricane zones. *Journal of the Structural Division*, *122*, 2333–2350.

United Nations Development Programme. (2004). Reducing Disaster Risk: A Challenge for Future Development.

Vickery, P. J. (2005). Simple Empirical Models for Estimating the Increase in the Central Pressure of Tropical Cyclones after Landfall along the Coastline of the United States. *Journal of Applied Meteorology*, *44*(12), 1807–1826.

Vickery, P. J., Masters, F. J., Powell, M. D., & Wadhera, D. (2009). Hurricane hazard modeling: The past, present, and future. *Journal of Wind Engineering and Industrial Aerodynamics*, *97*(7), 392–405.

Vickery, P. J., Skerlj, P., & Twisdale, L. (2000). Simulation of Hurricane Risk in the US Using Empirical Track Model. *Journal of Structural Engineering*, *126*(10), 1222–1237.

Vickery, P. J., & Twisdale, L. A. (1995). Prediction of Hurricane Wind Speeds in the United States. *Journal of Structural Engineering*, *121*, 1691–1699.

Vickery, P. J., & Wadhera, D. (2008). Statistical Models of Holland Pressure Profile Parameter and Radius to Maximum winds of Hurricanes from Flight-Level Pressure and H*Wind Data. *Journal of Applied Meteorology and Climatology*, *47*, 2497–2517.

Washington Post. (2017). 60 Inches of Rain Fell from Hurricane Harvey in Texas, shattering U.S. Storm Record.

Wilson, B. W. (1957). Hurricane Wave Statistics for the Gulf of Mexico. *Coastal Engineering Proceedings*, *1*(6), 4.

Young, I. R. (1988). A Parametric Hurricane Wave Prediction. *Journal of Waterway, Port, Coastal, and Ocean Engineering*, *114*(5), 637–652.

Young, I. R., & Vinoth, J. (2013). An "Extended Fetch" Model for the Spatial Distribution of Tropical Cyclone Wind–Waves as Observed by Altimeter. *Ocean Engineering*, *70*, 14–24.

Zehnder, J. A. (2015). Tropical Cyclone. *Encyclopaedia Britannica*. https://www.britannica.com/science/tropical-cyclone.

Zhang, J. A., & Uhlhorn, E. W. (2012). Hurricane Sea Surface Inflow Angle and Observation-Based Parametric Model. *Monthly Weather Review*, *140*, 3587–3605.

Zhang, S., & Nishijima, K. (2012). Statistics-based investigation on typhoon transition modelling. Presented at The Seventh International Colloquium on Bluff Body Aerodynamics and Applications (BBAA7) Shanghai, China; September 2-6, 2012.

Appendix

A Holland's Spatial Wind Field Models

In parametric wind models, the wind is assumed to be a geostrophic flow which is expressed in the gradient wind speed V_g which is the wind speed at gradient height, usually between 500-2000m height, which is then transformed to a surface value at 10m height by atmospheric boundary layer notions (Vickery et al., 2009). The basis Holland used for his formulation is the gradient wind equation (Vickery et al., 2000):

$$\frac{1}{\rho_a}\frac{\partial p(R)}{\partial R} = \frac{V_g^2}{R} + fV_g \tag{A.1}$$

Where:

V_g	= Gradient wind speed	[m/s]
R	= radial distance from the centre of the eye	$[m]$
$p(r)$	= Pressure around the eye as a function of R	[hPa]
ρ_a	= Density of air	$[kg/m^3]$
$f = 2\Omega \sin \Psi$	= Coriolis parameter	$[rad/s]$
Ω	= Rotation rate of the earth	$7.2921 \cdot 10^{-5}$ $[rad/s]$
Ψ	= Latitude of the Tropical Cyclones (TCs) centre	$[Degrees]$

He then neglected the effect of Coriolis to show that this reduces to a direct relation between V_{gmax} and $\sqrt{\Delta p}$, with $\Delta p = p_n - p_c$ the central pressure deficit, and p_n and p_c the environmental and central pressure in hPa. However, actual measurements had shown variations of V_{gmax} for the same pressure deficit, and therefore Holland introduced additional parameters A and B (B is generally referred to as the Holland parameter) to express the radial pressure around the eye as (Holland, 1980):

$$p(r) = p_c + \Delta p \exp\left[-\frac{A}{R^B}\right] \tag{A.2}$$

Where:

A = Location parameter	[-]
B = Pressure profile factor	[-]

The effect of changing the parameters A and B is clearly observed in Figure A.1

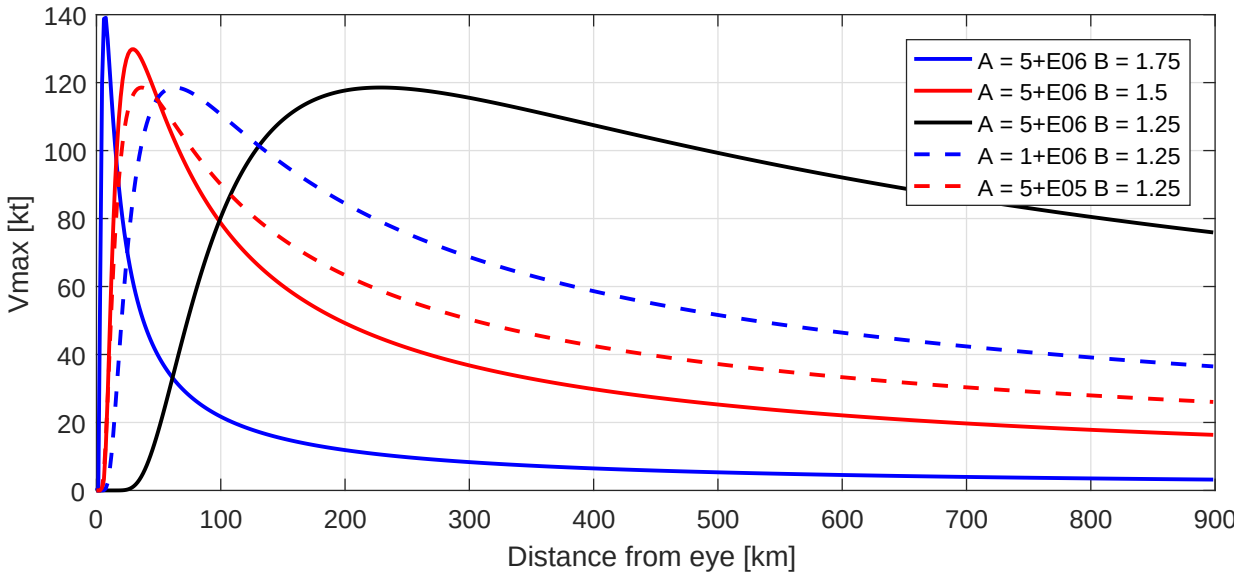

Figure A.1 – Effect of the parameters A and B on the spatial wind profile

By combining this with the gradient wind equations, Holland (1980) expressed the radial wind profile as:

$$V_g = \sqrt{\frac{AB\Delta p \exp\left(-\frac{A}{R^B}\right)}{\rho_a R^B} + R^2 f^2/4 - Rf/2} \tag{A.3}$$

In the region of maximum winds the the air is in cyclostrophic balance because the Coriolis force is small in comparison to the pressure gradient and centrifugal forces (Holland, 1980). These winds are given by:

$$V_g = \sqrt{\frac{AB\Delta p \exp\left(-\frac{A}{R^B}\right)}{\rho_a R^B}} \tag{A.4}$$

By setting $dV_g/dR = 0$ the radius of max winds is $R_{max} = A^{1/B}$. This leads to an expression of max wind speed of:

$$V_{max} = \sqrt{\frac{B\Delta p}{\rho_a e}} \tag{A.5}$$

Now parameters A and B can be described in terms of observable quantities by:

$$A = R_{max}^B \tag{A.6}$$

$$B = \frac{\rho_a e V_{max}^2}{\Delta p} \tag{A.7}$$

Therefore by knowing the observable quantities V_{max}, Δp and R_{max} one could determine the spatial wind field around the eye by first computing parameters A and B by filling in equations A.6 and A.7 and subsequently filling in equation A.4.

This Holland1980 model was later revised to incorporate additional wind observations at some radius within the hurricane circulation (Holland et al., 2010). This Holland2010 model allowed for better fitting of the wind profile to observations and also removed the

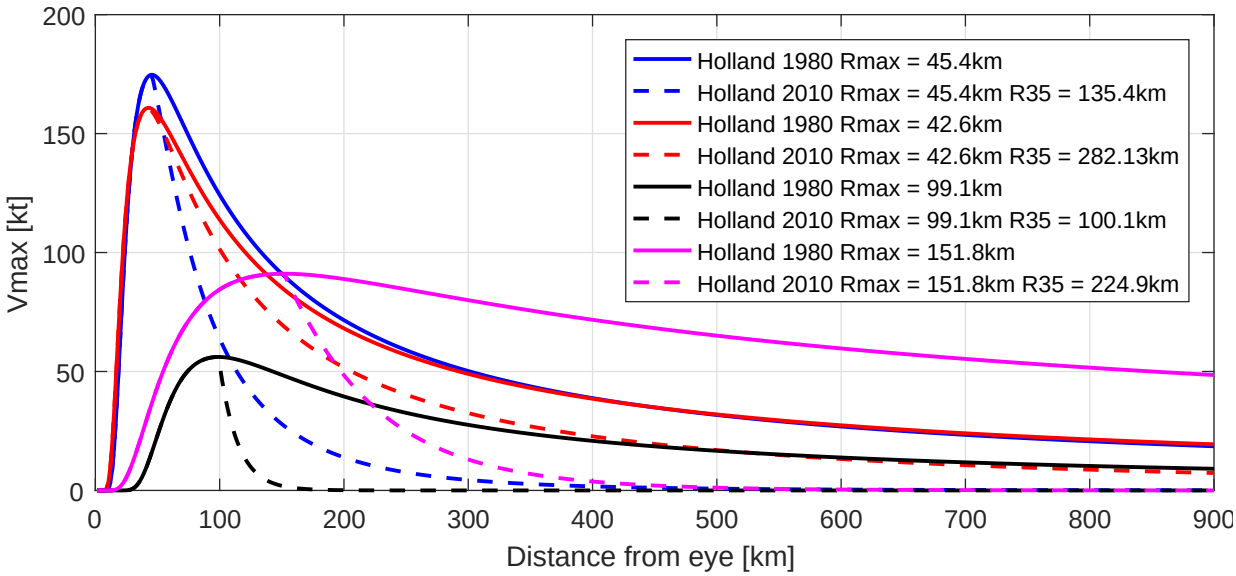

Figure A.2 – Visualisation of the over prediction of wind speeds at distances further than RMW from the eye by the Holland1980 model compared to the Holland2010 model based on historical events

general over-prediction of wind speeds at a larger distance from the eye which were the result of fitting a profile to the Radius of Maximum Winds (RMW) as can be seen in Figure A.2. In the new model equation A.4 is slightly altered and rewritten in the form of:

$$V_s = \left\{ \frac{b_s \Delta p_s \left(\frac{R_{maxs}}{R}\right)^{b_s}}{\rho_{as} e \left(\frac{R_{max}}{R}\right)^{b_s}} \right\}^x \tag{A.8}$$

The intermediate step of first calculating the gradient level flow and then reducing this field to the surface is now eliminated. The inclusion of the variable exponent x instead of the constant 0.5 accommodates both the maximum wind assessments and data in the outer circulation. The subscript s refers to the surface values and b_s is related to the original Holland B parameter by:

$$b_s = B g_s^x \tag{A.9}$$

Where g_s is the reduction factor for gradient winds. If x is kept at 0.5 and $b_s = B$ the equation is identical to equation A.4. If the maximum surface winds and pressure deficit are reliably determined, b_s can still be estimated as B. Exponent x can be determined by assuming a linear variation of x with radius and adjusting the profile using least squares to observed winds at various radii resulting in the following expression for x:

$$\begin{aligned} x &= 0.5 && R \leq R_{max} \\ x &= 0.5 + (R - R_{max}) \frac{x_n - 0.5}{R_n - R_{max}} && R > R_{max} \end{aligned} \tag{A.10}$$

Where x_n is the adjusted exponent fitted with least squares to the observations at radius R_n.

B Extreme Value Analysis

Extreme wave conditions are generally determined based on Extreme Value Analysis (EVA), this goes for extreme wind, rain, storm surge and wave data. As an example the determination extreme wave conditions specifically are described. Wave conditions are usually stated in terms of significant wave height (H_s) and peak period (T_p), where H_s represents the average of the one third highest waves in a wave time series representing a certain wave state and T_p is the wave period with the highest energy (Holthuijsen, 2007). In EVA an extrapolation to higher return period wave heights is done by fitting a probability distribution to the maxima of the historical data and computing the wave height for the fitted distribution for return periods not yet observed. These maxima can be either the highest value from every year creating an Annual Maxima Series (AMS), or Peak over Threshold (PoT) excesses where all values above a certain predefined threshold are considered to be maxima. Subsequently an Empirical Cumulative Distribution Function (ECDF) is constructed from these maxima to which several probability distributions are fitted of which the best fitting one is selected. These distributions are generally the Gumbel, Weibull or Generalised Extreme Value (GEV) distribution when considering AMS or the Generalised Pareto Distribution (GPD) when considering PoT excesses (Holthuijsen, 2007).

B.1 Extreme Value Analysis on the Historical Data

Since the historical data set spans 130 years, using an AMS would be possible as in theory there should be enough data points to fit a distribution. However, not all historical tracks will pass every location of the of $0.1^\circ \times 0.1^\circ$ grid and therefore it is quite possible that at several locations there will not be any data for several years. Moreover, it is very possible that a single year coincidentally contains two very severe events, and using an AMS would ignore the lesser of these two as it only takes one per year. For these reasons it was opted to apply the PoT method which uses all values over a specific threshold.

Per storm only the maximum observed wind speed per grid cell is stored and therefore the time series of all storms over these 130 years is actually a time series of maxima. These maxima are assumed to be Independent and Identically Distributed (IID)) and therefore, unlike for the usual PoT application, no minimum peak width is required and all values in the time series are considered peaks, even though the previous or next value in the time series might be higher.

The PoT excesses are fitted with a GPD of which the Cumulative Distribution Function (CDF) is defined by:

$$F(x, \alpha; \kappa) = 1 - [1 - (\kappa/\alpha)(x - \xi)]^{1/\kappa} \tag{B.1}$$

Where $\xi \leq x \leq \xi + \alpha/\kappa$ for $\kappa > 0$, and $\xi \leq x \leq \infty$ for $\kappa \leq 0$ where ξ is the threshold parameter, κ the shape parameter and α the scale parameter (Brabson & Palutikof, 1999). For the special case when $\kappa = 0$, the CDF reduces to:

$$F(x;\alpha) = 1 - \exp\left[-(x-\xi)/\alpha\right] \tag{B.2}$$

If one is interested in determining return values for specific return periods, one can solve for the quantile x_T for the return period T by solving:

$$x_T = \xi + \alpha/\kappa[1 - (\lambda T)^{-\kappa}] \tag{B.3}$$

with the definition of λ as the average number of peak excesses over the threshold per year. The threshold is determined separately per grid cell instead of one constant level for the entire basin. The threshold is identified by finding the threshold where the variation in the shape parameter of the GPD is minimal and the shape parameter is close to zero. This is done for two reasons. Firstly, as the extreme quantiles of wind speed generally display a shape parameter close to zero, one could make the assumption that this is also the case for cyclone conditions, although this is not certain. Secondly, since EVA is done for every grid cell it is impossible to visually check whether the shape parameter is determined correctly for every cell, and therefore this assumption leads to the most reliable estimates for the wind speed maps as a whole.

The shape and scale parameters are estimated with the Probability Weighted Moments (PWM) method and not with Maximum Likelihood Estimation (MLE) as based on visual inspection of several fits, PWM performed better. Both the determination of the optimal threshold and fitting the scale and shape parameter is done with the Orca Toolbox for extremes (Deltares, 2010) in MATLAB (The MathWorks, Inc, 2016).

To apply EVA on the historical data, first the spatial wind field maps for all historical events should be modelled. The size of historical events has only been recorded in the last couple of years, and therefore the same method as for the synthetic tracks is applied where both p_c, Radius of Maximum Winds (RMW) and Radius of 35kt Wind Speeds (R35) are sampled for each historical event. By applying the same method as for the synthetic data, any contingencies introduced by the method should be represented in the historical data as well and therefore not influence the value of the validation.

The size of the events can significantly influence the extreme wind speed estimates as in the historical case there are only 130 years of data. This means that the estimates for higher Return Values (RVs) are more sensitive to extremes. Whether such an extreme is measured at a specific location is very dependent on the size of the event as this determines whether it crosses, or passes by the location. To show the effect that the sizes of the historical events can have on the RVs, two maps of the 10 year return period wind speeds, obtained by EVA on identical historical track and V_{max} data, with different samples for p_c, RMW and R35, are subtracted from each other as shown in Figure B.1. This results in a wind speed map displaying the difference between two estimates.

In most locations the difference in wind speed between the two estimates lies within plus and minus 5 kt but there are locations where the estimates differ as much as 30 kt, which is unacceptable as using one of these two estimates to validate the synthetic data would lead to different conclusions than when the other estimates would have been used. Therefore it was opted to try and reduce the randomness by sampling 20 sets of p_c, RMW

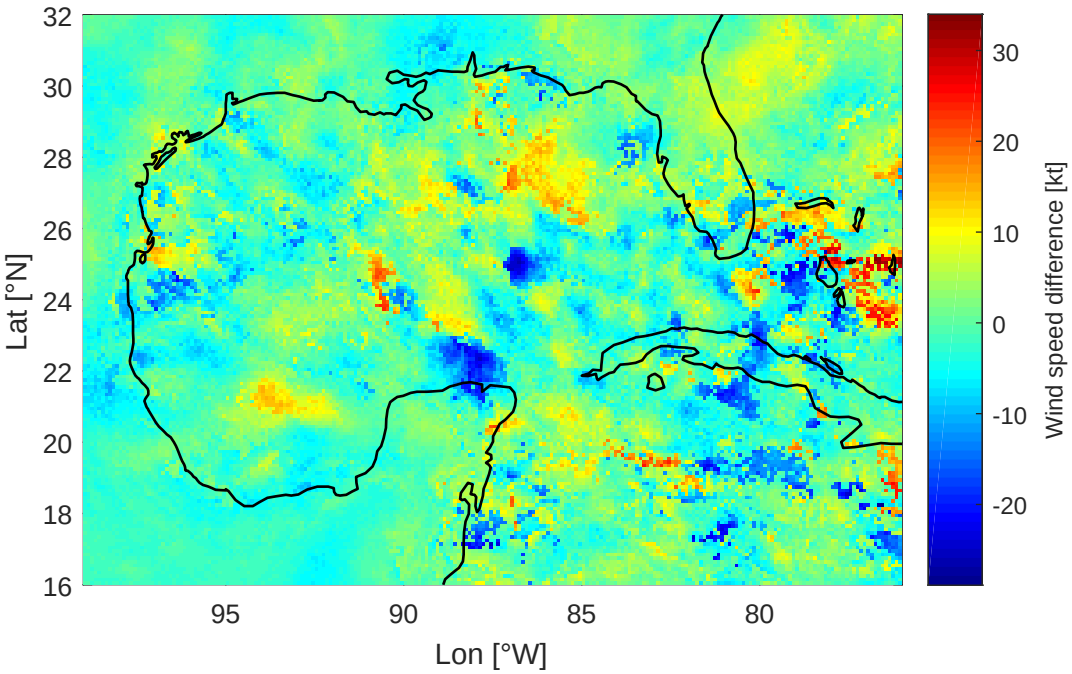

Figure B.1 – Diference in wind speed between 2 estimates for the 100 years return period sustained wind speed by EVA on the same historical data with different samples for p_c, RMW and R35

and R35 for the historical tracks and applying EVA on each of those 20 sets at 12 control locations, the same as were used for the validation of the track generator tool as shown in Figure 4.7, and take the average. This was done as making entire wind speed maps with EVA for such a large data set was too computationally expensive for the duration of this study. The confidence bounds were determined by computing the coefficients α and β for all RVs of interest for each subset i at each location k so that:

$$Lc_{i,k} = \alpha_{i,k} \cdot RV_{i,k} \tag{B.4}$$

$$Hc_{i,k} = \beta_{i,k} \cdot RV_{i,k} \tag{B.5}$$

where Lc and H_c are the lower and higher confidence bounds respectively. Subsequently these coefficients are averaged over all subsets to obtain the average coefficient for each RV of interest at every location. By multiplying these with the average best estimate for the RV of interest one obtains the lower and upper confidence bound per RV per location:

$$Lc_k = \overline{\alpha_k} \cdot \overline{RV_k} \tag{B.6}$$

$$Hc_k = \overline{\beta_k} \cdot \overline{RV_k} \tag{B.7}$$

In Figure B.2 this is done at control location 1 for 5 different samples together with the average of these 5 sets. Every subset can clearly be discerned from one another showing the effect the sizes can have on the estimates. At the 200 year RV the minimum and maximum estimate are approximately 15 kt apart and the average naturally lies somewhere in the middle, thus justifying the choice for this method.

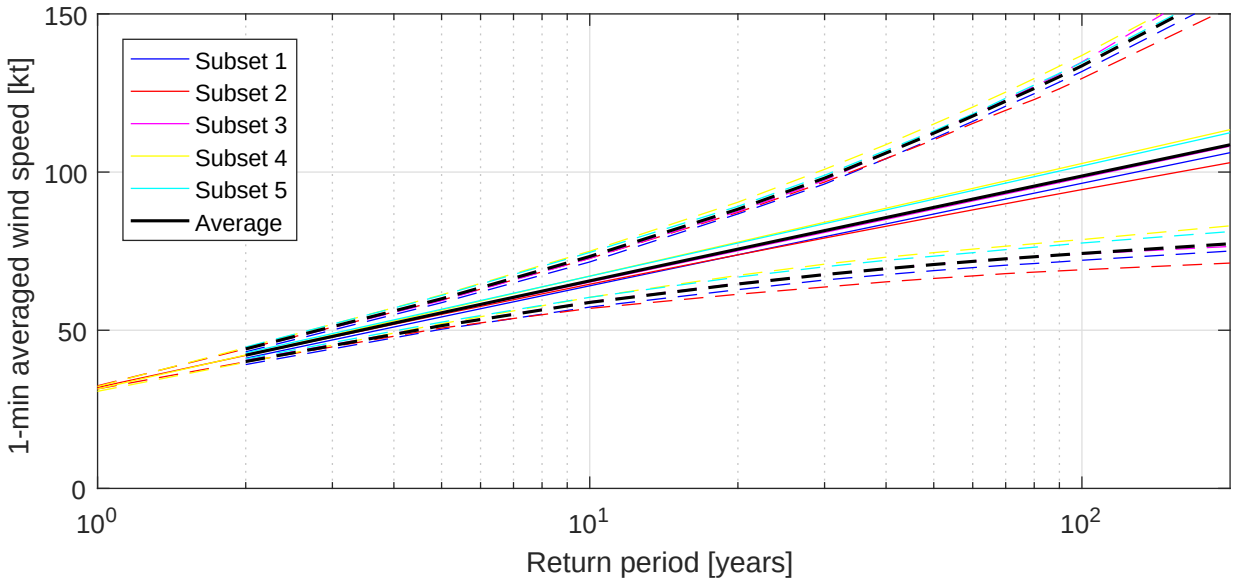

Figure B.2 – EVA to determine V_{max} at control location 1 for 5 identical sets of historical track data with different samples for p_c, RMW and R35, together with EVA on the average of these 5 sets and the 95% confidence intervals

C Extreme Wind Speed Maps

In this Appendix extra detail is given on the determination of the extreme wind speed maps, together with additional wind speed maps for various return periods.

C.1 Application of the Spatial Wind Field Model

The synthetic Tropical Cyclones (TCs) as obtained from the track generation are computed with a 6 hour interval. Since the forward speed of TCs can be more than 40 km/h, a six hour interval could lead to a distance travelled of over 240 km. To obtain smooth wind speed maps it is therefore required to interpolate to at least 1 hour intervals. This should be done before computing the spatial wind field instead of first computing the spatial wind field at each 6 hour step, and then interpolating the values obtained at each grid cell. This has to do with the translatory and rotating nature of TCs which would otherwise result in incorrect estimations.

Spatial wind fields are best determined on a spiderweb grid, which is a circular grid around a specific point with discrete bins for heading and distance from the eye. As close to the eye velocities can increase and reduce significantly over a very short distance, a fine grid spacing is required to resolve for these rapid changes. Therefore a bin width of 1.5 km is used up to a maximum of 900 km from the eye together with 36 radial bins each of 10°. To further use the obtained data, they are transformed from a spiderweb grid to a regular rectangular grid.

Unfortunately the computational effort of using a rectangular grid of the same detail as the spiderweb grid is immense, and therefore the scale is reduced to grid cells of $0.1^\circ \times 0.1^\circ$ to make the computation feasible. This transformation is done by locating the four corners of a cell from the spiderweb grid around a point of the rectangular grid, and taking the weighted average of those 4 corners based on distance from the grid point. An example of a spatial wind field for a randomly selected synthetic TC is shown in Figure 5.7 and a close-up of the eye together with the velocity vectors in Figure C.1 which clearly shows the asymmetry in the wind field and the effect of applying a wind inflow angle.

This approach unfortunately introduces slight errors for very small storms (Radius of Maximum Winds (RMW)$<\sim$15 km) as spiderweb cells that contain the value of V_{max} might not be located directly around a grid point of the rectangular grid, and are therefore not used for the wind speed determination of that cell. For most storms this affects the outcome less than 0.5%, but there are storms that are severely impacted by this effect leading to deviations as high as 10%. Errors this high will be of influence in the estimation of extreme values and therefore a solution was sought that would not drastically increase

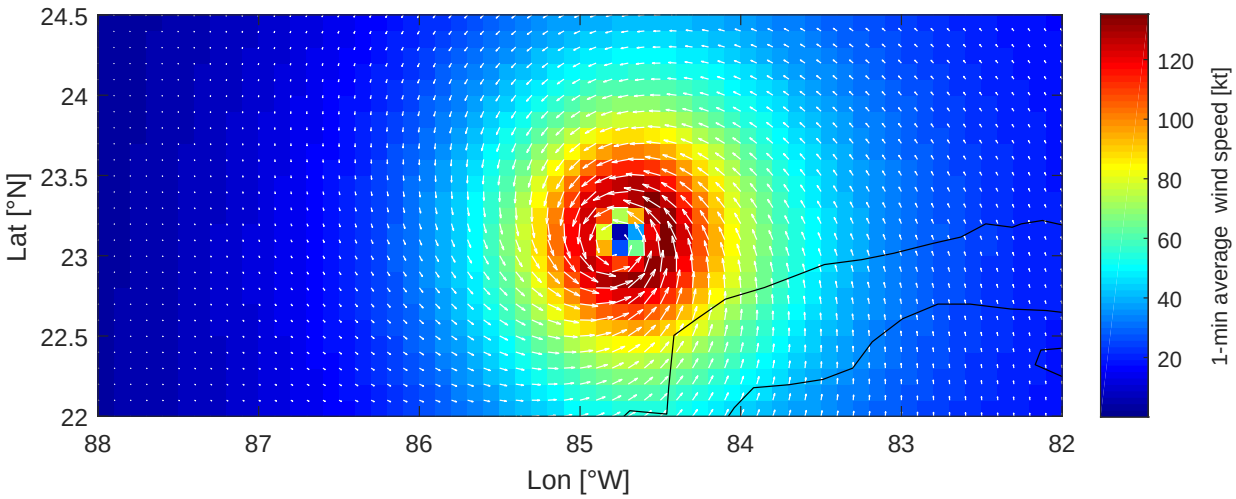

Figure C.1 – Color plot together with the velocity vectors of the maximum sustained wind speed around the TC eye

the computational effort.

Using a finer grid spacing for the entire basin would quadratically increase the computational effort, and applying other methods such as locating the maximum values of the spiderweb grid within a cell of the rectangular grid, would drastically increase the effort as well as this would require cell by cell operations. Therefore it was opted to only compute the spatial wind field on a finer grid of $0.025° \times 0.025°$ if the RMW was less than 15km and if V_{max} was greater than 40kt. This finer grid was then transformed back to the coarser grid by taking the maximum of each cell of the finer grid that was located within a cell of the coarser grid. By doing this the error introduced in the maximum sustained wind speed by the grid size was severely reduced. For example the TC in Figure C.2, one of the smallest

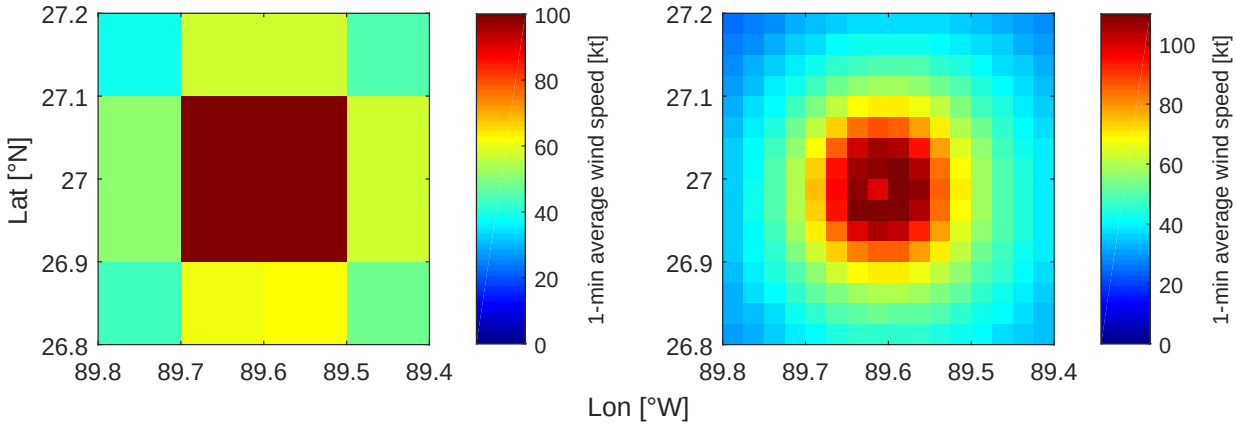

Figure C.2 – Comparison of a color plot of the sustained wind speed around the eye of the same TC for a coarser grid on the left and a finer grid on the right

synthetic TCs with an RMW of 5km and a V_{max} of 111kt, is shown, transformed from a spiderweb grid to both a coarse and a fine grid. The differences can clearly be spotted as in the coarser grid there is no reduction in wind speed at the location of the eye and the maximum observed speed is less than 100kt, whereas for the finer grid this is 110kt.

The finer grid still shows an error of slightly less than 2%, but since this is the worst case scenario and already much better than the 10% observed for the coarser grid, this deviation is accepted for the purpose of this study. In future situations if more computational power and memory is available, an even finer grid for every storm over the whole computational domain would be preferred.

C.2 Return Period Wind Speed Maps

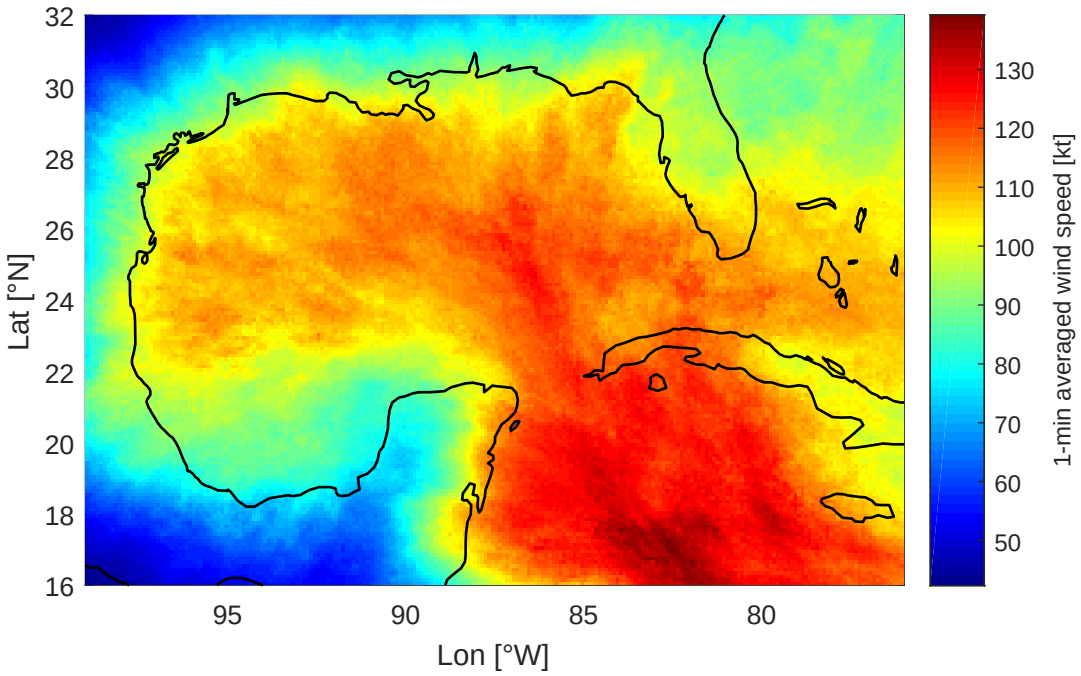

Figure C.3 – 1-min averaged wind speed map of the 200 year RV of the Gulf of Mexico as determined by TCWiSE with 5000 years of synthetic events based on historical cyclone track data from 1886-2015

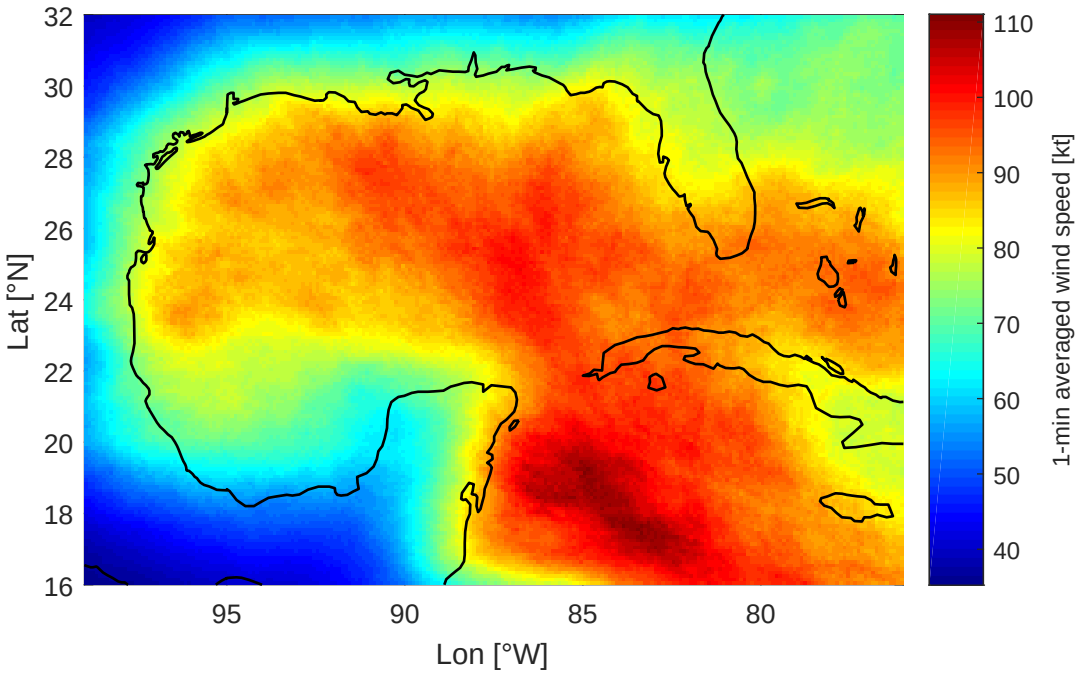

Figure C.4 – 1-min averaged wind speed map of the 50 year RV of the Gulf of Mexico as determined by TCWiSE with 5000 years of synthetic events based on historical cyclone track data from 1886-2015

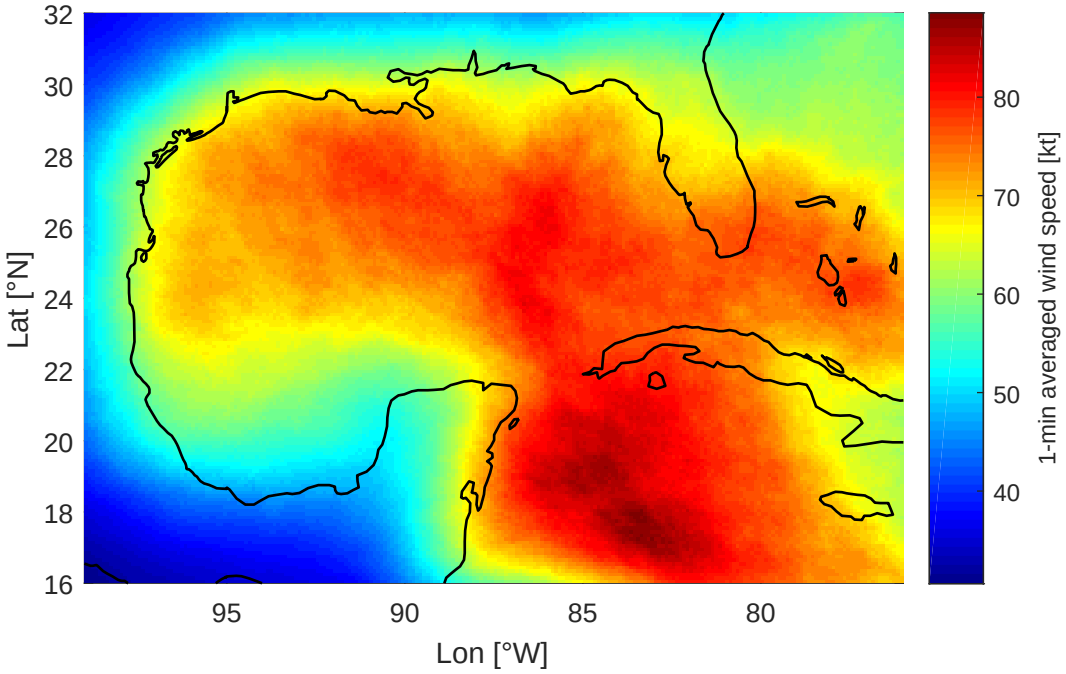

Figure C.5 – 1-min averaged wind speed map of the 20 year RV of the Gulf of Mexico as determined by TCWiSE with 5000 years of synthetic events based on historical cyclone track data from 1886-2015

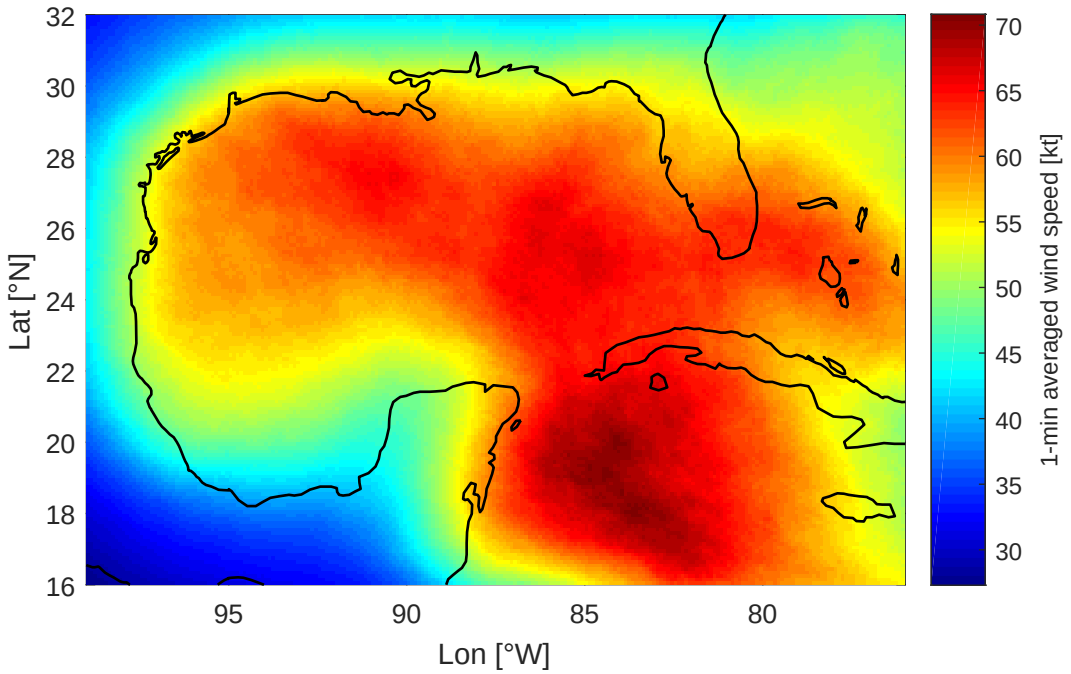

Figure C.6 – 1-min averaged wind speed map of the 10 year RV of the Gulf of Mexico as determined by TCWiSE with 5000 years of synthetic events based on historical cyclone track data from 1886-2015

C.3 Extreme Wind Speed Validation

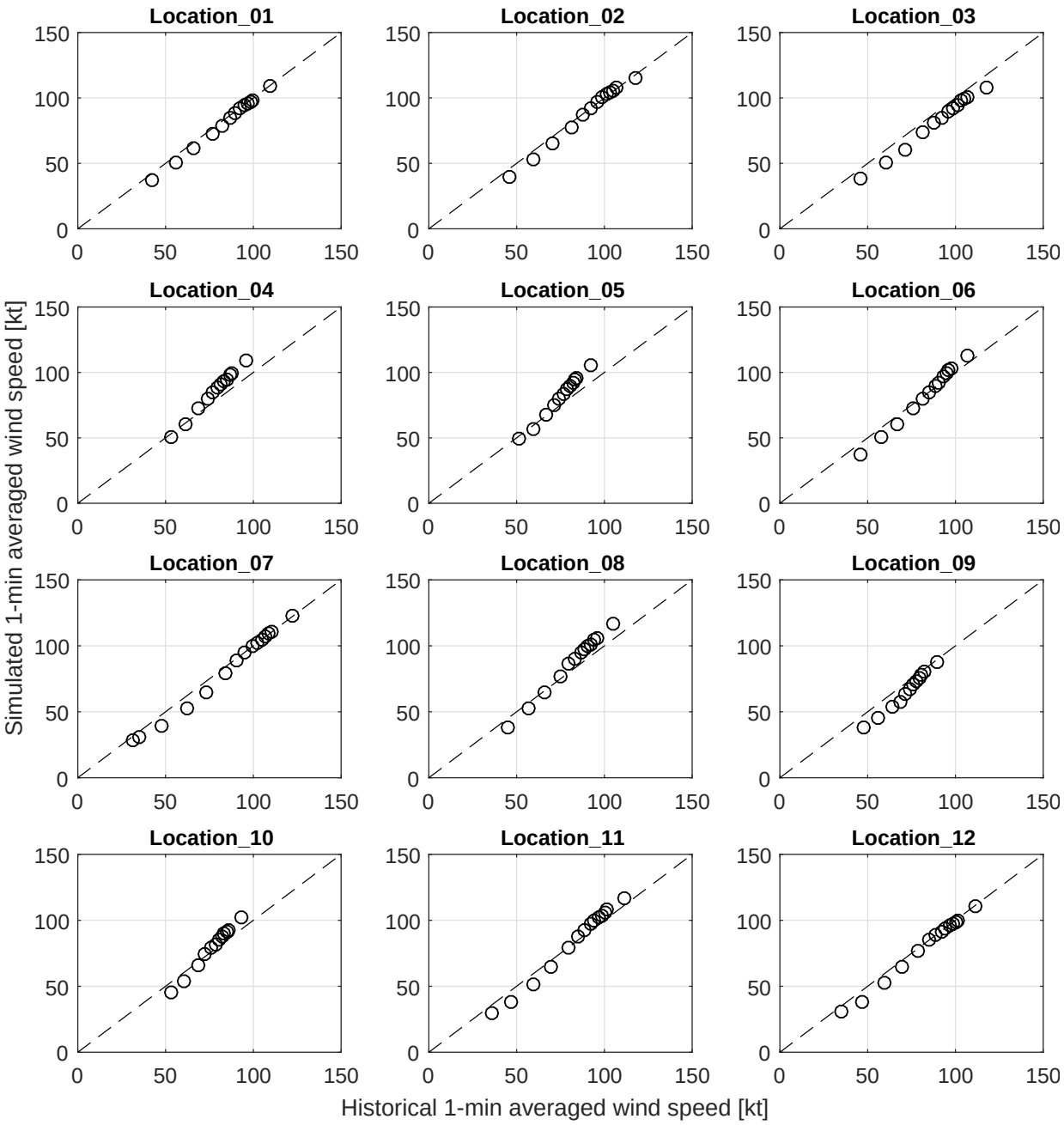

Figure C.7 – Return values up to 200 years of 1-minute averaged wind speeds directly obtained from the simulated data plotted against return values obtained from Extreme Value Analysis (EVA) on the historical data,

D | Input Reduction Figures

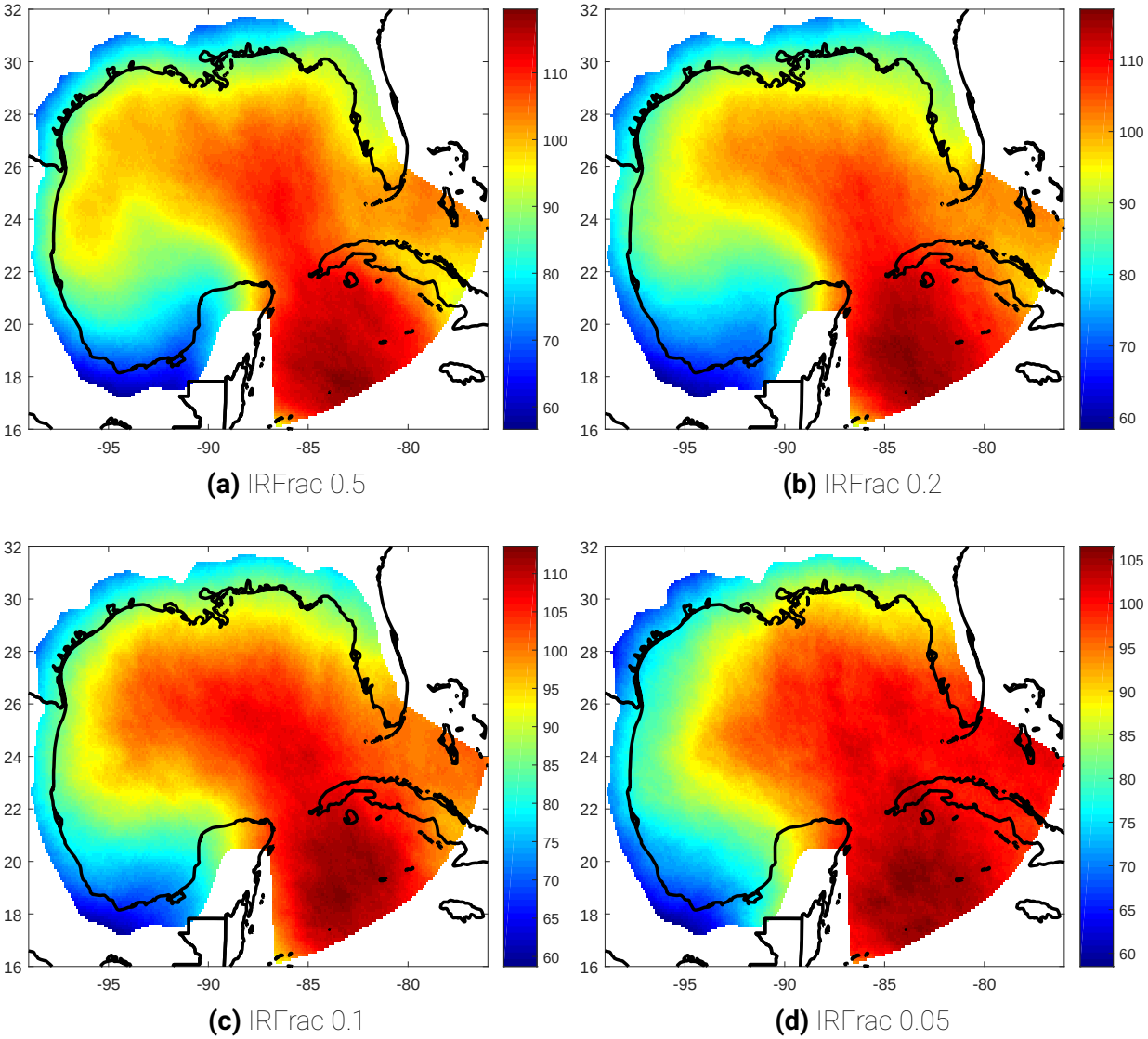

(a) IRFrac 0.5 **(b)** IRFrac 0.2

(c) IRFrac 0.1 **(d)** IRFrac 0.05

Figure D.1 – Mean μ [kt] over 10 sets per IR fraction of the 1-minute averaged wind speed 100 year Return Value (RV)

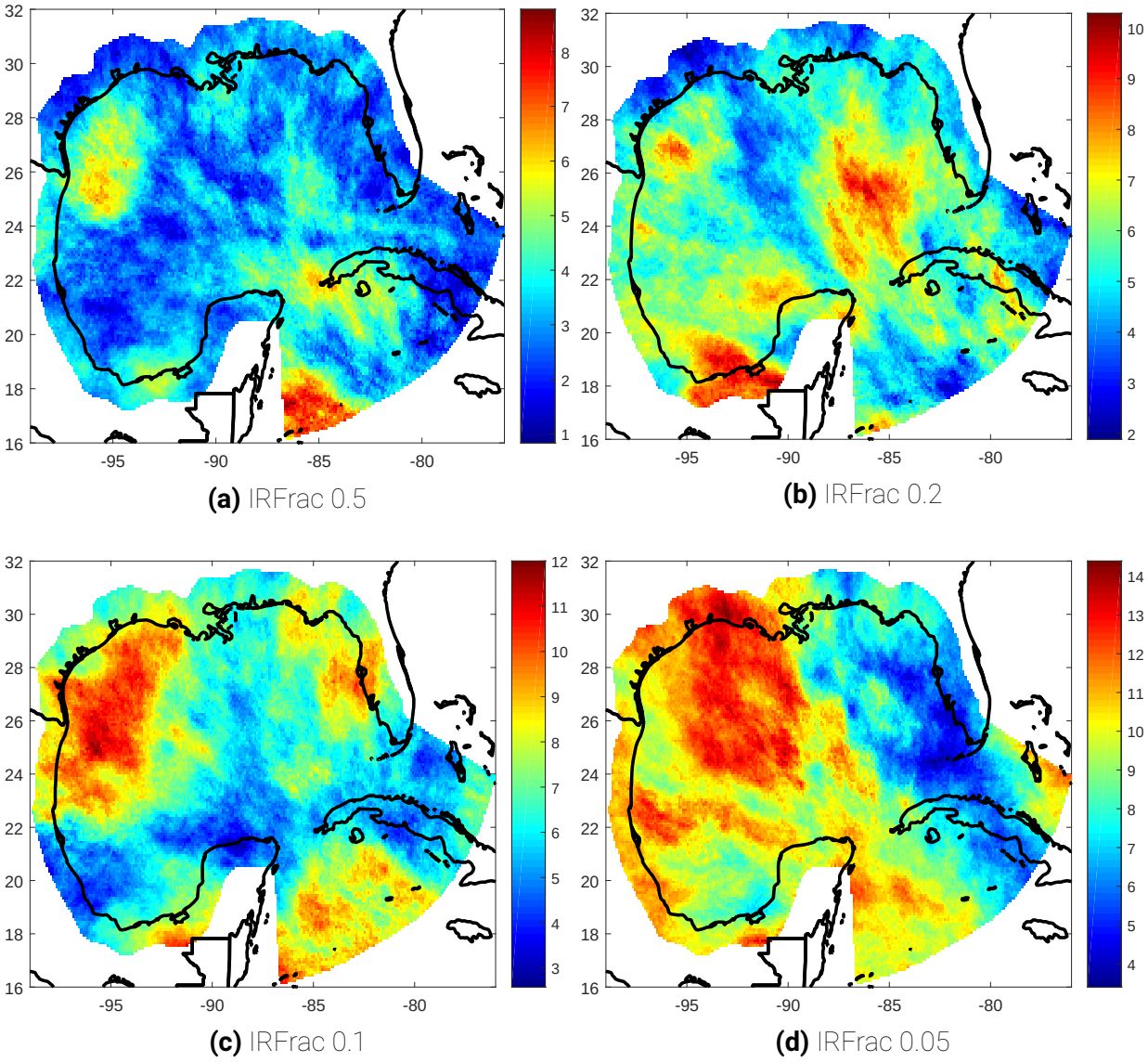

(a) IRFrac 0.5 **(b)** IRFrac 0.2

(c) IRFrac 0.1 **(d)** IRFrac 0.05

Figure D.2 – Standard deviation σ [kt] over 10 sets per IR fraction of the 1-minute averaged wind speed 100 year RV

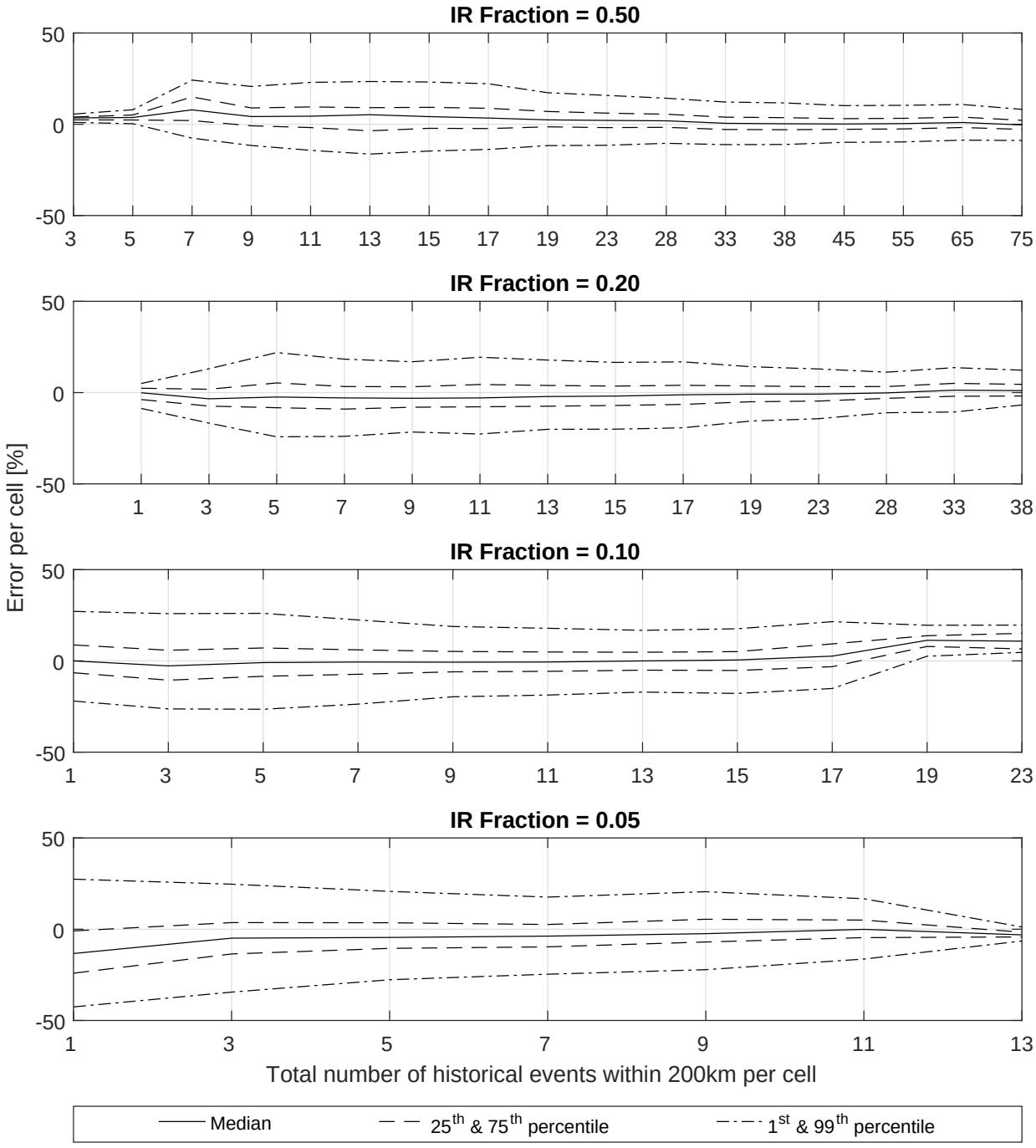

Figure D.3 – Separate plots for each input reduction fraction of the median, 1st, 25th, 75th and 99th percentile of the error per cell within the domain of the 100 year RVs, versus the number of historical occurrences within 200 km of the cell, as a percentage of the estimate without Input Reduction (IR)